

**MATHEMATICAL MODELLING OF 1,6-HEXANEDIOL
DIACRYLATE PHOTOPOLYMERIZATION WITH
SPATIAL GRADIENTS AND FILM SHRINKAGE**

by

Alaa El Halabi

A thesis submitted to the Department of Chemical Engineering

In conformity with the requirements for the degree of Master of Applied Science

Queen's University

Kingston, Ontario, Canada

(January, 2025)

Copyright © Alaa El Halabi, 2025

Abstract

Two dynamic models are proposed for the photopolymerization of 1,6-hexanediol diacrylate (HDDA) with bifunctional initiator bis-acylphosphine oxide (BAPO) in the presence of oxygen. The first accounts for spatial variations due to monomer and oxygen diffusion, while the second addresses spatial variations and film shrinkage. These partial-differential-equation (PDE) models predict overall vinyl-group conversion as well as time- and spatially-varying concentrations of monomer, initiator, oxygen, pendant vinyl groups and seven types of radicals. Measured diffusion coefficients for monomer, oxygen and initiator, provided by Canon Production Printing, are used in the models. Parameter estimation is performed using overall vinyl-group conversion data from Canon Production Printing, which were obtained using Fourier Transform Infrared (FTIR) spectroscopy for a range of operating conditions of film thicknesses ($8 - 17 \mu\text{m}$), BAPO levels ($1 - 4 \text{ wt}\%$) and light intensities ($200 - 6000 \text{ W}/\text{m}^2$). The first model, which accounts for spatial variations but ignores shrinkage, gives reliable predictions for runs with high BAPO levels ($4 \text{ wt}\%$) and light intensities ($\geq 5000 \text{ W}/\text{m}^2$). Model predictions are not accurate for runs conducted using low BAPO levels ($1 \text{ wt}\%$), indicating that some model parameters may be inaccurate.

As predicted by the second model, shrinkage has a noticeable influence on the model predictions, where a $\sim 9\%$ discrepancy is observed between predictions of overall vinyl-group conversions obtained from the models with and without shrinkage. Prediction discrepancies are larger for simulated experiments involving thin films ($8 \mu\text{m}$) or low light intensities ($1200 \text{ W}/\text{m}^2$). In future, it will be important to re-estimate the kinetic parameters, using the shrinkage model, so that accurate model predictions can be obtained over a wide range of operating conditions.

Co-Authorship

The material in Chapter 2 has been published in the *AIChE Journal* with co-authors K. Abdi, A.D.D. Vo, A. Ebrahimzadeh, J. van den Hoek, L. van der Velden, R. Willemse, M. van der Linden, P. Iedema and K. B. McAuley. The material in Chapter 3 has been submitted to *Macromolecular Reaction Engineering* for publication with co-authors K. Abdi, A.D.D. Vo, P. Iedema and K. B. McAuley. The original drafts of both manuscripts of chapter 2 and 3 were written by me and edited by the co-authors. The corresponding calculations, simulations and equations were formulated by me under the supervision of Dr. Kim McAuley. Dr. Kim McAuley also helped edit and revise this thesis and provided technical suggestions.

Acknowledgements

I would like to begin by expressing my deepest gratitude to my supervisor, Dr. Kim McAuley, for her exceptional guidance, support, and invaluable mentorship throughout my graduate studies. Her supervision has been instrumental not only in my academic development but also in supporting me through one of the most challenging periods of my life. When I faced significant health issues during my academic journey, Dr. McAuley's understanding and compassion helped me navigate that difficult time, allowing me to continue my work with confidence and resilience. Her encouragement and the numerous opportunities she has provided have been pivotal in shaping both my academic and professional growth. I cannot thank her enough for her kindness, inspiration, and unwavering support.

I would like to acknowledge the Chemical Engineering Department at Queen's University, the Natural Sciences and Engineering Research Council of Canada (NSERC) and Technisch Industriële Procesbeheersing (TIPb) for financial support. I would also like to thank Canon Production Printing for providing experimental data for Chapter 2. I thank Dr. Piet Iedema from the University of Amsterdam and TIPb for his technical advice and support for the work in this thesis.

I would like to thank all the faculty and staff at the Department of Chemical Engineering at Queen's University as well as my colleagues for making my time at Queen's enjoyable.

I would like to thank my parents, Nisrine and Khaled, and my brothers, Wael and Rayan, for the love and support they provided me while being far away from home. I would also like to thank all my friends in Kingston and abroad for their support and encouragement during my journey at Queen's.

Table of Contents

Abstract.....	i
Co-Authorship.....	ii
Acknowledgements.....	iii
Table of Contents	iv
List of Figures.....	viii
List of Tables.....	xi
List of Abbreviations.....	xii
Chapter 1 - Introduction.....	1
Chapter 2 - Accounting for spatial variations during photopolymerization of 1,6-hexane-diol diacrylate in the presence of oxygen.....	6
2.1 Summary.....	6
2.2 Introduction.....	7
2.3 Experimental Data and Statistical Analysis	10
2.3.1 Measurement of the diffusion coefficient of oxygen in HDDA	10
2.3.2 Measurement of self-diffusion coefficient for HDDA and diffusion coefficient of BAPO in HDDA.....	12
2.3.3 Measurement of overall vinyl-group conversion in HDDA polymer films.....	13
2.4 Model Development.....	14

2.4.1 Reaction mechanism	14
2.4.2 Model equations.....	16
2.5 Parameter Estimation and Simulation Results.....	18
2.5.1 Parameter estimation.....	18
2.5.2 Simulation results and model assessment.....	20
2.6 Conclusion	26
Chapter 3 - Modeling of 1,6-hexane-diol Diacrylate Photopolymerization with Spatial Gradients and Film Shrinkage.....	29
3.1 Summary.....	29
3.2 Introduction.....	30
3.3 Reaction Mechanism and Modeling Assumptions.....	32
3.4 Model Development.....	36
3.4.1 Definition of the dimensionless spatial coordinate w	36
3.4.2 Deriving the relationship between w and z	38
3.4.3 Material balance PDE for HDDA monomer.....	41
3.5 Simulation Results and Model Assessment	42
3.6 Conclusions.....	49
3.7 Acknowledgements.....	50
Chapter 4 – Summary, Conclusions and Recommendations	51
References.....	54

Appendix A	60
A1 Custom-built Oxygen Measurement Enclosure	60
A2 DOSY NMR.....	61
A3 Film Thickness Measurements.....	62
A4 Data Collection	63
A5 Reaction scheme	63
A6 List of reactions, assumptions, PDEs and their initial and boundary conditions.....	65
A7 Derivation of two PDEs	79
A7.1 Deriving PDE for initiator shown in Equation (2.2) in Chapter 2	79
A7.2 Deriving PDE for oxygen shown in Equation (2.4) in Chapter 2	80
A8 Diffusivities of monomer and initiator.....	81
A9 Parameter estimates from Abdi's model	82
A10 Additional Simulation Results and Plots.....	83
Appendix B	87
B1 List of Reactions and Assumptions	87
B2 List of Algebraic Equations and PDEs.....	92
B3 Detailed derivation of model PDEs.....	103
B3.1 Relationship between \mathbf{z} and \mathbf{w}	103
B3.2 Material Balance on Monomer PDE:.....	107
B3.3 Material Balance PDE for $\mathbf{R} = \bullet$ Radical End Group.....	115

B3.4 Material Balance on Oxygen PDE	118
B4 Detailed Algebraic Modifications Required to Solve the PDEs using MATLAB “pdepe”	122

List of Figures

Chapter 1

Fig. 1.1: HDDA monomer and BAPO initiator chemical structures 2

Fig. 1.2: Printer setup vs experimental setup at Canon Production Printing 3

Chapter 2

Fig. 2.1: Measured oxygen concentration (\blacktriangle) and model predictions (—) using Equation (1) .. 12

Fig. 2.2: Decomposition of a) initiator molecules at one of the two weak carbon-phosphorus bonds and b) subsequent decomposition of the remaining carbon-phosphorous bond in *I* [15, 16]..... 15

Fig. 2.3: Measured diffusivities * of a) initiator, b) monomer and c) oxygen along with predicted diffusivities as a function of monomer conversion. (----) predictions using initial parameter guesses for free-volume parameters *AI*, *AM* and *AO2* in Table 2.2, (—) predictions using estimated free-volume parameters obtained in the current study. 18

Fig. 2.4: Model predictions (curved lines) and the corresponding FTIR measured values for the experiments of those runs. 22

Fig. 2.5: Model predictions of a) two validation runs for experiments with thick film (12 μm) and high BAPO level (4 wt%) using light intensities of — 2000 W/m^2 and — 3006 W/m^2 , and an additional validation run b) — using a thicker film (18 μm), high BAPO level (4 wt%) and low light intensity of 1198 W/m^2 23

Fig. 2.6: Oxygen concentration levels with respect to time at different film depths 25

Fig. 2.7: Vinyl group concentration levels with respect to time at different film depths 26

Chapter 3

Fig. 3.1: Decomposition of a) initiator molecules and b) remaining carbon-phosphorous bonds in $I\sim$. Adapted from [15].	34
Fig. 3.2: Formation of different macroradicals: a) regular radical ends $R = \bullet$, b) cyclized radical ends $C \bullet$, c) branch-point radical ends $B \bullet$, d) tertiary radical ends $T \bullet$ and e) peroxidic radicals $O \bullet$. Adapted from [16].....	35
Fig. 3.3: Relationship between spatial coordinate z and transformed coordinate w at time 0.	38
Fig. 3.4: Phenomena leading to shrinkage and swelling of a thin segment of the film	41
Fig. 3.5: Position z vs time for (—) the top surface of the film where $w = 0$, (---) $w = 0.2$, (--) $w = 0.5$, and (---) the bottom surface of the film $w = 1$. This simulation was conducted for a thick film ($18 \mu m$), using high light intensity ($6000 W/m^2$) and a high BAPO level ($4 wt\%$).....	43
Fig. 3.6: Position z vs time for (—) the top surface of the film where $w = 0$, (---) $w = 0.2$, (--) $w = 0.5$, and (---) the bottom surface of the film $w = 1$. This simulation was conducted for a thick film ($18 \mu m$), using high light intensity ($6000 W/m^2$) and a low BAPO level ($1 wt\%$).....	44
Fig. 3.7: Oxygen concentration vs time for (—) the top surface of the film where $w = 0$, (---) $w = 0.2$, (--) $w = 0.5$, and (---) the bottom surface of the film $w = 1$. This simulation was conducted for a thick film ($18 \mu m$), using high light intensity ($6000 W/m^2$) and a high BAPO level ($4 wt\%$).....	45
Fig. 3.8: Monomer concentration vs time for (—) the top surface of the film where $w = 0$, (---) $w = 0.2$, (--) $w = 0.5$, and (---) the bottom surface of the film $w = 1$. This simulation was conducted for a thick film ($18 \mu m$), using high light intensity ($6000 W/m^2$) and a high BAPO level ($4 wt\%$).....	46
Fig. 3.9: Plot of shrinkage run (—) and no shrinkage run (--) with high thickness ($18 \mu m$) vs shrinkage run (—) and no shrinkage run (--) with low thickness ($8 \mu m$).....	47

Fig. 3.10: Plot of shrinkage run (—) and no shrinkage run (---) with high light intensity (6000 W/m^2) vs shrinkage run (—) and no shrinkage run (---) with low light intensity (1200 W/m^2) 48

Fig. 3.11: Plot of shrinkage run (—) and no shrinkage run (---) with a high BAPO level (4 wt%) vs shrinkage run (—) and no shrinkage run (---) with a low BAPO level (1 wt%) 48

Appendix A

Fig. A.1: Oxygen Sensor Schematic 60

Fig. A.2: 1D-dosy at 10% gradient strength with 1% BAPO in HDDA..... 61

Fig. A.3: Calculation of the layer thickness using NIR spectra. the clear interference pattern in the NIR spectrum is shown on the left; A schematic presentation of the interference pattern and the angles is shown on the right..... 62

Fig. A.4: Formation of different macroradicals: a) regular radical ends $R \bullet$, b) cyclized radical ends $C \bullet$, c) crosslinking radical ends $B \bullet$, d) tertiary radical ends $T \bullet$ [15, 16]..... 64

Fig. A.5. Initiator concentration vs depth at different times, with diffusivity both turned off (Dashed lines) and on (Solid lines) 81

Fig. A.6. Monomer concentration vs depth at different times, with diffusivity both turned off (Dashed lines) and on (Solid lines)..... 82

Fig. A.7. Low BAPO (1 wt%) level plots 85

Fig. A.8. Thickness plots..... 86

Appendix B

Fig. B.1: Schematic diagram of reactions and diffusion for a thin segment of height Δz and scaled height Δw during a short period of time Δt 107

List of Tables

Chapter 2

Table 2.1: List of experimentally obtained parameters..... 19

Table 2.2: List of estimated parameters 20

Appendix A

Table A.1: Initial and boundary conditions for solving Fick’s second law [63]. 61

Table A.2: Model Assumptions [15, 16] 66

Table A.3: List of reactions of the photopolymerization of HDDA in the presence of oxygen.... 70

Table A.4: List of Algebraic Equations..... 73

Table A.5: Material balances for chemical species and end-groups developed by Vo et al. [16].

These equations are solved along with Equations 2, 3 and 4 using PDEPE solver in MATLAB. 74

Table A.6: list of initial and boundary conditions for the equations in Table A.5 and the PDEs in Equations 2, 3 and 4..... 77

Table A.7: List of parameters and their estimates obtained from Abdi’s model [15] 82

Appendix B

Table B.1: List of reactions of the photopolymerization of HDDA [17] 87

Table B.2: Model Assumptions [15-17]..... 89

Table B.3: List of algebraic equations [15-17] 92

Table B.4: List of model PDEs along with their initial and boundary conditions 94

Table B.5: List of restructured PDEs for MATALB’s PDE solver “pdepe”. 123

List of Abbreviations

Abbreviation

BAPO	Bis-acylphosphine oxide
HDDA	1,6-Hexanediol diacrylate
SSH	Stationary state hypothesis

Symbols

A_C	Free-volume parameter for the cyclization reaction
A_b	Free-volume parameter for the crosslinking reactions
A_{bb}	Free-volume parameter for the backbiting reactions
A_f	Free-volume parameter for the initiator efficiency
$A_{in,j}$	Free-volume parameter for the initiation reactions ($j = IM, IV_p, \tilde{I}M, \text{ and } \tilde{I}V_p$)
A_p	Free-volume parameter for propagation reactions
$A_{t_{in,j}}$	Free-volume parameters for termination reactions involving initiator radicals ($j = II, \tilde{I}\tilde{I}, \text{ and } I_pI_p$)
A_{HDDA}	Free-volume parameter of HDDA Monomer
A_{BAPO}	Free-volume parameter of initiator BAPO
A_{O_2}	Free-volume parameter of dissolved oxygen
B^{\rightarrow}	Linear magnetic field gradient
B^{\bullet}	Radicals at the crosslinking points
c	Speed of light
C^{\bullet}	Cyclized radical ends

D_j	Diffusion coefficient in HDDA for species HDDA ($j = \text{HDDA}$), BAPO ($j = \text{BAPO}$), and oxygen ($j = O_2$)
f	Efficiency for decomposition of the initiator molecules
f_0	Efficiency for decomposition of the initiator molecules at the start of the polymerization
\tilde{f}	Efficiency for decomposition of carbon-phosphorous bonds \tilde{I} attached to polymer chains (\tilde{I})
h	Planck's constant
H_s^{cp}	Henry's coefficient
\tilde{I}	Carbon-phosphorous bonds attached to polymer molecules
I^\bullet	Carbon-centered initiator radicals
\tilde{I}^\bullet	Phosphorous-centered initiator radicals
I_P^\bullet	Phosphorous-centered initiator radicals generated from decomposition of \tilde{I}
$I_{l,0}$	Light intensity at the top surface of the film
\bar{I}_l	Average light intensity within the film
J	Objective function
$k_{b,j}$	Rate coefficient for crosslinking reactions involving R^\bullet ($j = R$), C^\bullet ($j = C$), B^\bullet ($j = B$), and T^\bullet ($j = T$)
k_{b,j_0}	Rate coefficient for crosslinking reactions when they are kinetically-controlled
$k_{bb,j}$	Rate coefficient for backbiting reaction involving R^\bullet ($j = R$) and C^\bullet ($j = C$)
k_{bb0}	Rate coefficient for the backbiting reactions k_{bb} when they are kinetically-controlled

k_C	Rate coefficient for cyclization
k_{C0}	Rate coefficient for cyclization when it is kinetically-controlled
k_d	Rate coefficient for decomposition of initiator
$k_{\tilde{d}}$	Rate coefficient for decomposition of \tilde{I}
$k_{in,IM}$	Initiation rate coefficient for initiation reaction involving a carbon-centered radical I^\bullet and a monomer
$k_{in,\tilde{I}M}$	Initiation rate coefficient for initiation reaction involving a phosphorous-centered radical \tilde{I}^\bullet and a monomer
k_{in,I_pM}	Initiation rate coefficient for initiation reaction involving a phosphorous-centered radical I_p^\bullet and a monomer
k_{in,IV_p}	Initiation rate coefficient for initiation reaction involving a carbon-centered radical I^\bullet and a pendant vinyl group
$k_{in,\tilde{I}V_p}$	Initiation rate coefficient for initiation reaction involving a phosphorous-centered radical \tilde{I}^\bullet and a pendant vinyl group
k_{in,I_pV_p}	Initiation rate coefficient for initiation reaction involving a phosphorous-centered radical I_p^\bullet and a pendant vinyl
$k_{in,j0}$	Initiation rate coefficient involving different species when the corresponding reaction is kinetically-controlled ($j = IM, \tilde{I}M, I_pM, IV_p, \tilde{I}V_p$, and I_pV_p)
$k_{O_2,j}$	Oxygen incorporation rate coefficient involving different species when the corresponding reaction is kinetically-controlled ($j = I, \tilde{I}, I_p, R, B, C$ and T)
$k_{p,j}$	Rate coefficient for the propagation involving R^\bullet ($j = R$), C^\bullet ($j = C$), B^\bullet ($j = B$), O^\bullet ($j = O$), and T^\bullet ($j = T$)

k_{p,j_0}	Rate coefficient for the propagation reactions when they are kinetically controlled
$k_{t,jj}$	Self-termination rate coefficient for reactions involving large macromolecules j ($j = RR, CC, BB, OO$, and TT)
k_{t,jj_0}	Rate coefficients for termination reactions $k_{t,jj}$ when they are kinetically-controlled
$k_{t,ij}$	Cross-termination rate coefficients involving the radicals of type i ($i = I, \tilde{I}, I_p, R, C, B, O$, and T) and j ($j = I, \tilde{I}, I_p, R, C, B, O$, and T)
$k_{t_{in},jj}$	Self-termination rate coefficient for reactions involving initiator radicals ($j = I, \tilde{I}$, and I_p)
k_{t_{in},jj_0}	Self-termination rate coefficient for reactions involving initiator radicals when they are kinetically-controlled
M	Monomer
M_{HDDA}	Molecular weight of HDDA of 226 g/mol
N_{X_v}	Number of measured values for overall-vinyl-group conversions
N_{X_M}	Number of measured values for monomer conversions
O^\bullet	Peroxidic radical end
P_{O_2}	Partial pressure of oxygen in air
Q	The accumulated rate of consumption of monomer
R_X	The rate of consumption of species X
t_{exp}	Time duration of light exposure
$v_{f,0}$	Free volume fraction before polymerization starts (i.e., $X_M = 0$)
$v_{f,1}$	Free volume fraction when all monomer is consumed (i.e., $X_M = 1.0$)

v_f	Free volume fraction
$v_{fc,b}$	Critical free volume parameter for crosslinking reactions
$v_{fc,bb}$	Critical free-volume fraction for backbiting reactions
$v_{fc,in,j}$	Critical free-volume fraction for the j^{th} initiation reaction ($j = IM, IV_P, \tilde{I}M, \tilde{I}V_P, I_P M$ and $I_P V_P$)
$v_{fc,p}$	Critical free-volume fraction for propagation reactions
$v_{fc,tm,jj}$	Critical free volume parameters for termination reactions involving initiator radicals ($j = I, \tilde{I}$, and I_P).
V_P	Pendant Vinyl group
w	Dimensionless spatial coordinate
X_M	Monomer conversion
$X_{M,i}$	Monomer conversion prediction corresponding to the i^{th} measurement
$X_{M_{meas},i}$	Measurement for the monomer conversion at condition corresponding to the i^{th} measurement
$X_{V,i}$	Overall vinyl-group conversion prediction corresponding to the i^{th} conversion data
$X_{V_{meas},i}$	Value of the i^{th} overall-vinyl group conversion measurement
z	Distance from the top surface of the film
z_f	Film thickness

Greek symbols

σ_V^2	Measurement variance for the vinyl group conversions
σ_M^2	Measurement variance for the monomer conversions

ρ_{HDDA}	Monomer density of 1,010 kg/m^3
ρ_{pol}	Polymer density of 1,261 kg/m^3
δ	Encoding step time
Δ	Diffusion step time
λ	Light wavelength
ϕ	Quantum yield of initiator
ϵ	Extinction coefficient

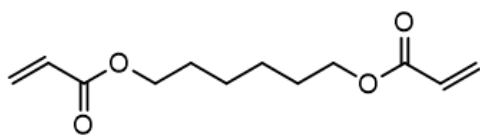
Chapter 1

Introduction

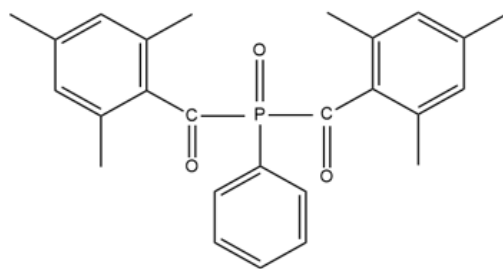
Free radical photopolymerization is a chemical process where light, typically ultra-violet (UV) light, is used to initiate the formation of radicals, which then propagate to form long polymer chains. This process has a fast-curing time so that polymerization reactions are completed in a few seconds [1, 2]. A variety of different recipes and light intensities can be used to obtain polymer films and 3D objects with the desired final properties [3, 4]. For example, combinations of monovinyl and divinyl monomers can be used to form crosslinked polymer networks [5]. Free radical photopolymerization is used in a variety of applications including dental resins and fillings [1, 6, 7], contact lenses [8, 9], protective surface coatings [10, 11], tissue engineering [12] and 3D printing [13, 14].

The photopolymerization considered in the current thesis involves homopolymerization of 1,6-hexanediol diacrylate (HDDA) (See Fig. 1.1), which is a divinyl monomer that was considered in previous experimental and mathematical modelling studies involving our research group at Queen's University [15-17]. All the experiments were performed at Canon Production Printing in Venlo, the Netherlands, where research scientists mix pigments with HDDA and other monomers, along with the free-radical photoinitiators to form ink mixtures used for highspeed printing. HDDA is an important monomer because of its ability to form a highly crosslinked polymer that holds the pigment particles in place and acts as a protective layer to the printed material. This thesis is concerned with developing two fundamental models that predict overall vinyl-group conversion during the photopolymerization of HDDA using the bifunctional initiator bisacylphosphine oxide

(BAPO) (See Fig. 1.1). It also involves parameter estimation using data obtained from Canon Production Printing [17]. Fig. 1.2a shows how a poster moves under a UV light source during highspeed printing so that the amount of light that is absorbed depends on the printing speed and on the light intensity. Fig 1.2b shows the experimental setup at Canon Production Printing that was used to generate the data reported in this thesis. Using this setup, the HDDA polymer film is not moving, and the UV light is turned on and then off to induce photopolymerization. During the experiments, real time Fourier Transform Infrared Spectroscopy (FTIR) is used to monitor overall vinyl group conversion [18]. Our collaborators at Canon also performed other experiments, described in Chapter 2, to obtain the diffusivities of oxygen, initiator, and HDDA monomer within HDDA films [17, 19]. These measured diffusivities are used in the models developed in the current thesis.



HDDA monomer
(1,6-Hexanediol Diacrylate)



BAPO initiator
(Bis-acylphosphine Oxide)

Fig. 1.1: HDDA monomer and BAPO initiator chemical structures

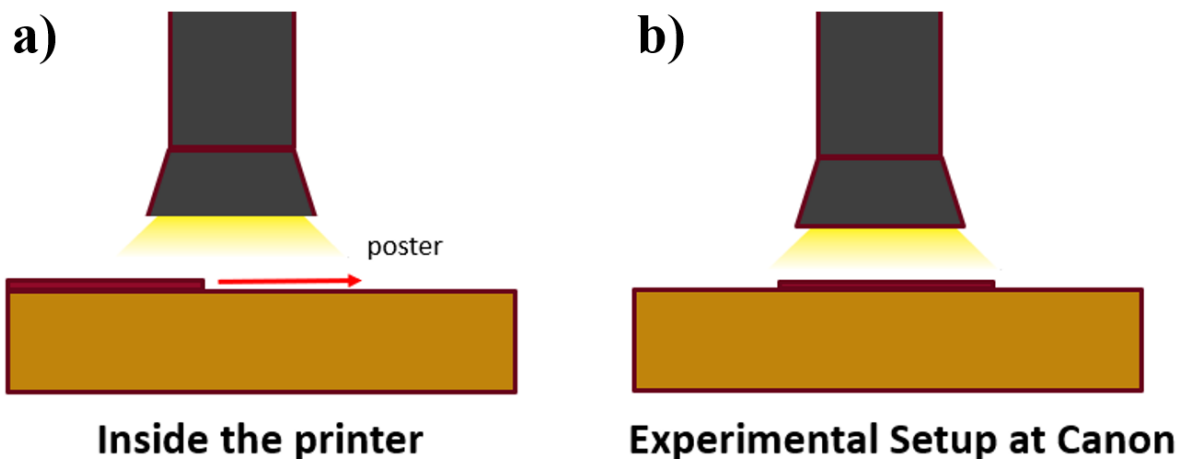


Fig. 1.2: Printer setup vs experimental setup at Canon Production Printing

Fundamental models are helpful for designing, scaling up and optimizing chemical processes [20-23]. These models, sometimes called mechanistic or first-principles models, are derived based on scientific principles such as conservation of mass, energy, and momentum. Hence, material and energy balances are often used to develop model equations that describe underlying reaction kinetics, transport phenomena, and thermodynamic behaviour of chemical reaction systems. Fundamental models are useful for simulating new situations where no data are available. Fundamental models involving chemical reactions usually contain unknown kinetic parameters that require estimation from experimental data. Accurate parameter values are required so that accurate model predictions can be obtained.

In past years, several models were developed to describe the photopolymerization of HDDA [15, 16, 18, 24, 25]. Earlier models used a simplified reaction scheme that assumes similar kinetics for vinyl groups on HDDA monomer and pendant vinyl groups on polymer chains, while ignoring other side reactions [18, 25]. Abdi et al. developed a more comprehensive model that uses separate rate constants for propagation and crosslinking reactions, and accounts for side reactions (i.e., cyclization and backbiting) [15]. Vo et al. extended Abdi's model to account for oxygen inhibition

[16]. These models account for the influence of light intensity and initiator concentration and how they affect vinyl-group conversion [15-18, 25]. In this thesis, two new models are introduced that build upon previous work: the first accounts for spatial variations within the depth of the film (Only in the z direction) due to monomer and oxygen diffusion, while the second also addresses film shrinkage. The objectives of the research in this thesis are to:

- i.* Develop a mathematical model that accounts for spatial variation within the depth of the film during HDDA photopolymerization in the presence of oxygen
- ii.* Estimate oxygen-related kinetic parameters and diffusion-related parameters using experimental data obtained from Canon Production Printing
- iii.* Derive a mathematical model that accounts for film shrinkage during the photopolymerization of HDDA and then formulate the resulting PDEs and ODEs so they can be solved using MATLAB's pdepe solver
- iv.* Conduct simulations to learn about oxygen and monomer concentration gradients within HDDA polymer films and how they influence vinyl-group conversion
- v.* Determine whether shrinkage has a noticeable influence on predictions of vinyl-group conversion within HDDA polymer films during photopolymerization
- vi.* Account for the upward motion of the polymer caused by the downward diffusion of HDDA monomer, a phenomenon that has been ignored in models that don't account for shrinkage.

The resulting models will provide valuable information to scientists at Canon Production Printing who design printing processes and ink recipes. The new methods for formulating polymerization models with shrinkage should be helpful for other types of photopolymerization systems.

The remainder of this thesis is organized as follows. In Chapter 2 a mathematical model for the photopolymerization of HDDA that accounts for spatial gradients is proposed. Chapter 2 has been published in *AIChE Journal*. In Chapter 3, an extension of the model to account for film shrinkage using coordinate transformation is proposed. Chapter 3 has been submitted for publication in *Macromolecular Reaction Engineering*. Chapter 4 contains conclusions and recommendations. Finally, Appendices A and B contain supplementary information for Chapters 2 and 3, respectively, including all the detailed modeling assumptions and derivations.

Chapter 2

Accounting for spatial variations during photopolymerization of 1,6-hexanediol diacrylate in the presence of oxygen*

Department of Chemical Engineering, Queen's University, Kingston, ON, Canada

2.1 Summary

A dynamic model is proposed for photopolymerization of 1,6-hexanediol diacrylate (HDDA) with bifunctional initiator bis-acylphosphine oxide (BAPO) in the presence of oxygen. This partial-differential-equation (PDE) model predicts time- and spatially-varying vinyl-group conversion as well as concentrations of monomer, initiator, oxygen, and seven types of radicals. Experiments to obtain diffusivities of oxygen, BAPO and HDDA are reported. Oxygen-related parameters are estimated using real-time Fourier-transform infrared (FTIR) conversion data. FTIR experiments were conducted using a range of film thicknesses ($8 - 17 \mu\text{m}$), BAPO levels ($1 - 4 \text{ wt}\%$) and light intensities ($200 - 6000 \text{ W/m}^2$). The model predicts qualitative trends. Conversion predictions for runs with high intensities ($\geq 5000 \text{ W/m}^2$) and high BAPO ($4 \text{ wt}\%$) are accurate with a root-mean-squared error (RMSE) of 0.04. Larger RMSE (0.13) for runs with lower intensities and BAPO indicates that improved parameter estimates are required. Parameter estimates will be updated using in future using a model that accounts for shrinkage during polymerization.

* El Halabi, A., K. Abdi, A. D. D. Vo, A. Ebrahimzadeh, J. F. van den Hoek, L. van der Velden, R. Willemse, M. van der Linden, P. Iedema, and K. B. McAuley (2023). "Accounting for spatial variations during photopolymerization of 1, 6-hexanediol diacrylate in the presence of oxygen." *AICHE Journal*, **70**, paper e18490.

2.2 Introduction

Free-radical photopolymerization has been increasing in popularity, especially in the production of films, coatings, and a variety of optical, dental, and microelectronic applications [26]. This article focuses on modeling the photopolymerization of the divinyl monomer 1,6-hexanediol diacrylate (HDDA), which forms a cross-linked network of polymer chains. The HDDA photopolymerization process involves a complex set of chemical reactions, especially when a bifunctional photo-initiator such as bis-acylphosphine oxide (BAPO) is used [15]. Several mathematical models have been developed to provide insights into the photopolymerization kinetics of HDDA [16] and other acrylate [27] and methacrylate monomers [28]. These models have been used to study the influences of experimental factors such as film thickness, light intensity, initiator concentration and oxygen content. For example, Iedema et al. developed an early model to describe the photopolymerization of HDDA in an oxygen-free environment [18]. This model provided predictions of vinyl-group conversion vs. time for HDDA photopolymerization experiments with different light intensities, using a simplified kinetic scheme with only one type of polymeric free radical and one type of vinyl group [18]. The most comprehensive oxygen-free kinetic model for HDDA photopolymerization accounts for initiation, propagation, crosslinking, backbiting, cyclization, and termination reactions, resulting in four different types of free-radical end groups on the polymer chains and two types of vinyl groups [15]. Abdi et al. used conversion vs. time data and weighted least squares (WLS) parameter estimation to fit 30 kinetic parameters in this model, while accounting for diffusionally-limited rate constants and free-volume effects [15]. Recent studies reveal that these effects are important in other free-radical acrylate [29] and methacrylate [30] polymerization systems. The experiments used for parameter estimation were conducted using a range of different film thicknesses, light intensities, and initial BAPO

concentrations [15]. Abdi's model produces reliable predictions of vinyl-group conversions but is unable to account for oxygen [15].

Oxygen presents an important complication during photopolymerization processes that are in contact with air. Oxygen diffuses into the monomer/polymer mixture and reacts with initiator radicals and carbon-centered polymeric radicals to form peroxy radicals which are much less reactive, thereby inhibiting the polymerization [31]. Several early models were developed to account for oxygen inhibition in photopolymerization processes involving HDDA [25] and methacrylate monomers [32]. One of the earliest was developed by Decker et al. to study oxygen inhibition during the photopolymerization of multi-acrylate systems [33]. O'Brien et al. worked on modeling oxygen effects on photopolymerization kinetics while accounting for oxygen, initiator and monomer mass-transfer effects [34]. Goodner and Bowman also accounted for simultaneous mass transfer and polymerization, using a free-volume approach to predict changes in diffusivities and rate constants as the polymerization proceeds [5]. Andrzejewska et al. developed a model to study the influence of oxygen on termination kinetics, accounting for two kinds of radicals with different propensities to diffuse and react [35]. All these models provided new insights into the influence of oxygen inhibition on photopolymerization processes; however, they relied on highly simplified reaction schemes that might result in inaccurate model predictions for new experiments.

Recently, Vo et al. proposed a more comprehensive model to describe oxygen inhibition during HDDA photopolymerization, which builds on the detailed kinetic scheme of Abdi et al. and accounts for formation and consumption of peroxy radicals [16]. Vo's model includes 5 additional parameters, on top of Abdi's 30 parameters, which she estimated using data from 8 experimental runs conducted in the presence of oxygen. Vo's model produces reliable conversion vs. time

predictions for thin films (up to 12 μm) and relatively low light intensities (up to 1000 W/m^2), but underpredicts overall vinyl-group conversion in thicker films and when higher light intensities are used. Vo et al. suggested that these discrepancies in model predictions arise because their model does not account explicitly for spatial gradients in oxygen and other species in the film as the photopolymerization progresses [16].

The influence of oxygen-induced spatial concentration gradients during photopolymerization of HDDA and other acrylate monomers has been explored by several research groups [34]. In thicker films ($\sim 100 \mu\text{m}$), Goodner and Bowman [5] predicted that a thin layer at the top surface has lower monomer conversion due to ongoing oxygen diffusion into the film as polymerization proceeds. However, with thinner films ($\sim 10 \mu\text{m}$), the oxygen diffuses through the entire depth of the film, impeding conversion to various extents at different depths [25]. As such, oxygen inhibition may cause polymer films to have varying mechanical properties over their thicknesses [36]. The model of Iedema et al. provides reliable fits for conversion vs. time data in thin films with low oxygen levels, but overpredicts conversion in an oxygen-rich environment. Difficulties in predicting experimental data over a wider range of conditions may be due to the simplified reaction mechanism and inaccurate parameter values used in Iedema's model [25]. The aim of the current modeling research is to develop an improved model using the comprehensive reaction scheme of Vo et al. with explicit modeling of diffusion within the HDDA polymeric film [16]. A further objective is to provide new diffusivity data for oxygen, BAPO and HDDA so that improved estimates can be obtained for model parameters related to mass-transfer and oxygen inhibition. The resulting improved HDDA photopolymerization model will be helpful for selecting appropriate recipes and operating conditions to achieve high-quality rapid printing processes.

The remainder of the article is organized as follows. First, new experimental results and statistical analysis are discussed. Second, an updated model is proposed which relies on Vo's reaction mechanism, but explicitly accounts for oxygen, initiator, and monomer concentration gradients in the film. This updated model, which relies on an assumption of constant film thickness, uses partial differential equations (PDEs) to describe concentrations of reacting species and functional groups, which vary with time and position in the film. Six oxygen-related and diffusion-related parameters are then estimated based on conversion versus time data from thirty-two experimental runs. The predictive ability of the model is assessed using additional data not utilized for parameter estimation. Finally, recommendations are made regarding a future model that will account for changes in density and film thickness during the photopolymerization process.

2.3 Experimental Data and Statistical Analysis

2.3.1 Measurement of the diffusion coefficient of oxygen in HDDA

Pure HDDA films with a thickness of 1.5 *mm* were used to determine the oxygen solubility and oxygen diffusion coefficient in HDDA monomer. The film was first exposed to a nitrogen gas flow for approximately 90 minutes so that all atmospheric oxygen was purged from the system. After 90 minutes, air was fed to the chamber where the HDDA film is located. Oxygen concentration at the bottom of the film was measured using an optical oxygen sensor in a custom-built enclosure, which is shown schematically in Fig. A.1, in Appendix A. Note that oxygen measurements at the bottom of the film are only available for the oxygen diffusion experiments. No measurements of oxygen concentrations are available during photopolymerization experiments.

A plot of the oxygen concentration vs time is shown in Fig. 2.1. The data shown in Fig. 2.1 are responses from two replicate runs. Whiskers on the error bars correspond to one standard deviation, which was computed from a pooled variance estimate. The curve shown in Fig. 2.1 is a plot of:

$$[O_2]_{z=z_f} = H_s^{cp} P_{O_2} \left(1 - \frac{4}{\pi} \sum_{n=odd}^{\infty} \frac{(-1)^{\frac{n-1}{2}}}{n} e^{-\frac{(\frac{n\pi}{2})^2 D_{O_2} t}{z_f^2}} \right) \quad (2.1)$$

which is the analytical solution of the oxygen material balance PDE, $\frac{\partial [O_2]}{\partial t} = D_{O_2} \frac{\partial^2 [O_2]}{\partial z^2}$ using the initial condition and boundary conditions provided in Table A.1, in Appendix A. The boundary condition at $z = 0$ corresponds to an assumption of equilibrium between oxygen in the air and dissolved oxygen at the film surface. The Henry's law coefficient $H_s^{cp} = 1.18 \times 10^{-7} \frac{mol}{L Pa}$ and the oxygen diffusion coefficient $D_{O_2} = 3.48 \times 10^{-9} \frac{m^2}{s}$ were obtained from the data in Fig. 2.1 using least squares regression. The diffusivity of oxygen and other species depends on the free volume of the system which goes down as polymerization proceeds. Therefore, as monomer conversion increases, the diffusivity of oxygen is expected to drop.

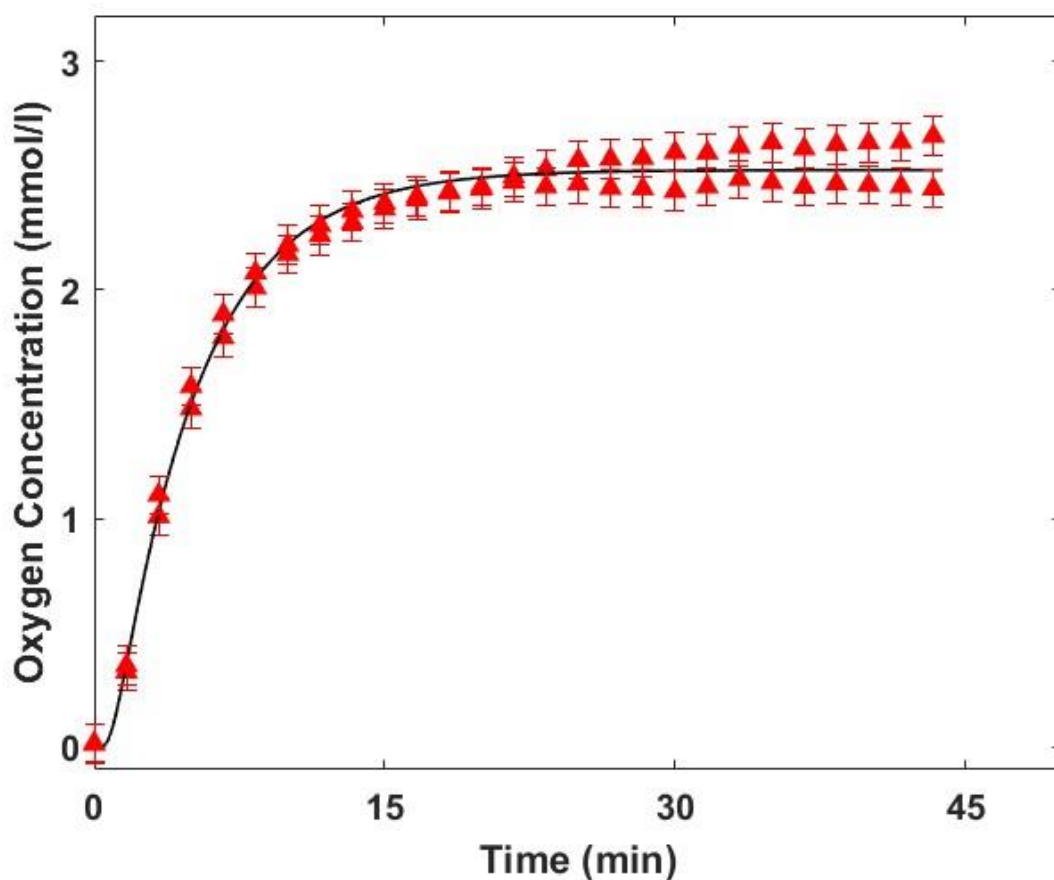


Fig. 2.1: Measured oxygen concentration (\blacktriangle) and model predictions (—) using Equation (1)

2.3.2 Measurement of self-diffusion coefficient for HDDA and diffusion coefficient of BAPO in HDDA

Diffusion coefficients of HDDA and BAPO (The structure of BAPO is shown in Fig. 2.2a) were measured using diffusion-ordered NMR spectroscopy (DOSY). DOSY NMR works by analyzing the results of a pulsed field gradient spin echo experiment to obtain the diffusion coefficients of individual signals in a spectrum [37]. In the experimental setup, a solution containing 1 wt% BAPO was placed in a 400 MHz NMR spectrometer (magnetic field B_0) and exposed to a linear

magnetic field gradient (B^{\rightarrow}) which spatially encodes the HDDA and BAPO molecules. After a diffusion delay the molecules are similarly decoded. The diffusion coefficient can then be calculated from the signal attenuation of each molecule. An encoding/decoding step with duration $\delta = 3000 \mu\text{s}$ and a diffusion step with duration $\Delta = 0.2 \text{ s}$ were used to obtain NMR peaks, which resulted in calculated diffusion coefficients $D_{\text{HDDA}} = 1.59 \times 10^{-10} \frac{\text{m}^2}{\text{s}}$ and $D_{\text{BAPO}} = 8.78 \times 10^{-11} \frac{\text{m}^2}{\text{s}}$. Additional details about the DOSY NMR measurements are provided in Appendix A.

2.3.3 Measurement of overall vinyl-group conversion in HDDA polymer films

Overall vinyl-group conversion vs. time data were collected using Fourier-transform infrared reflection (FTIR) spectroscopy. The setup of the experiments used to obtain these data consists of a pure HDDA film with added BAPO initiator and Tego Rad 2250 surfactant (2 wt%). Tego Rad 2250 surfactant is used so that HDDA monomer spreads well over the attenuated total reflectance (ATR) crystal. These films were exposed to the air so that the initial oxygen concentration was uniform throughout. The experiments are divided into two sets. The first data set arises from 12 experimental runs that had a film thickness of $\sim 12 \mu\text{m}$, an initial BAPO concentration of 4 wt%, and light intensities ranging from 200 W/m^2 to 6000 W/m^2 . The second data set arose from an attempted factorial design involving three factors with two or three replicates for every combination, leading to 23 experimental runs. The factors film thickness (8 or $16 \mu\text{m}$), initial BAPO concentration (1 or 4 wt%), and light intensity (1000 or 5000 W/m^2). Details about how film thickness was determined are provided in Appendix A. All experiments were conducted in the presence of atmospheric oxygen during polymerization. Thirty-two out of the 35 experimental runs are used for estimating the model parameters in this study, while the remaining 3 are saved for model validation. Details about the photopolymerization method and data collection are provided

in Appendix A. Note that, Vo et al. used 8 out of the 35 runs for parameter estimation in their previous modelling study (i.e., runs involving thin films with relatively low light intensities). The additional 27 runs used in the current study contain new information.

2.4 Model Development

2.4.1 Reaction mechanism

The current modeling study relies on the reaction mechanism of Abdi et al. and the extension proposed by Vo et al. to account for oxygen inhibition [16]. A detailed list of reactions is provided in Table A.3 in Appendix A. The first step in the mechanism is light-induced decomposition of one of the carbon-phosphorus bonds of the BAPO initiator (see Fig. 2.2). Decomposition of BAPO results in two types of radicals, a carbon-centered I^\bullet radical and a phosphorous-centered \tilde{I}^\bullet radical. The phosphorous-centered radical has a remaining carbon-phosphorous bond that can be decomposed in a later reaction to produce I_p^\bullet (see Fig. 2.2b). Initiator radicals can react with vinyl groups on the HDDA monomer generating R^{\bullet} . This macroradical end group R^{\bullet} has a free radical and an unreacted vinyl group (see Fig. A.4b). We assume that the life of R^{\bullet} is too short for the vinyl groups in R^{\bullet} to be consumed by crosslinking before the corresponding free radical reacts (assumption 4 and assumption 7 in Table A.2 in Appendix A).

The end group R^{\bullet} can propagate with HDDA monomer. Diagrams showing this reaction and other reactions involving free-radical end groups are provided in Fig. A.4 in Appendix A. When this propagation reaction happens, the vinyl group from the R^{\bullet} whose radical is consumed becomes a pendant vinyl group V_p . End groups of type R^{\bullet} can also undergo cyclization reactions to produce the cyclic radical C^\bullet . Free radical end groups such as R^{\bullet} and C^\bullet can also participate in crosslinking reactions by propagating with pendant vinyl groups V_p to produce a crosslinking radical B^\bullet .

Backbiting reactions produce a tertiary radical T^\bullet . Radical end groups can react with oxygen to produce peroxidic radical end groups O^\bullet as shown in Scheme 2.1 where reactant $\sim\sim\sim\bullet$ can be any polymeric radical of type R^\bullet , C^\bullet , B^\bullet , T^\bullet or O^\bullet in the reacting mixture. Peroxidic radicals undergo slow propagation, crosslinking, and back-biting reactions. Finally, peroxidic radicals can terminate with other radicals in the reaction mixture. Consumption of R^\bullet , C^\bullet , B^\bullet and T^\bullet radicals via termination with O^\bullet radicals lead to an important reduction in the rate of consumption of vinyl groups.

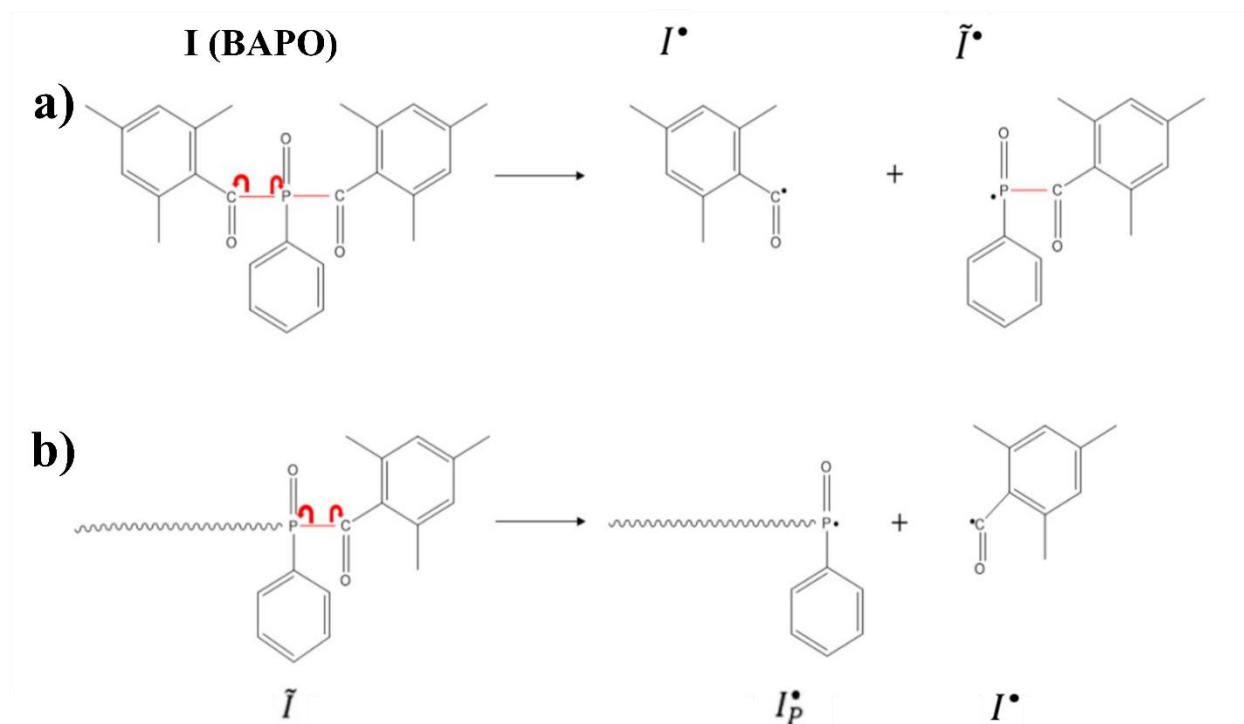


Fig. 2.2: Decomposition of a) initiator molecules at one of the two weak carbon-phosphorus bonds and b) subsequent decomposition of the remaining carbon-phosphorus bond in \tilde{I} [15, 16]



Scheme 2.1: Formation of peroxidic radicals from other radical end groups [16]. The peroxy end group shown within the ellipse is referred to as O^\bullet in the complete reaction mechanism shown in Table A.3 in Appendix A.

2.4.2 Model equations

The proposed model accounts for spatial variation in concentrations of chemical species and end groups, leading to 13 partial differential equations (PDEs). Three of these PDEs, which are related to oxygen and diffusion effects, are described in detail below. A material balance on the initiator is:

$$\frac{\partial [I]}{\partial t} = \frac{\partial}{\partial z} \left(D_I \frac{\partial [I]}{\partial z} \right) - 2k_d [I] \quad (2.2)$$

where $[I]$ is the initiator concentration in mol/L , t is the time in s , and z is the distance from the top surface of the film in m . The first term on the right-hand side accounts for initiator diffusion within the film. The second term in Equation (2.2) accounts for light-induced initiator consumption. The factor 2 appears because BAPO is a bifunctional initiator that can decompose at two different locations [38]. The initiator decomposition rate constant k_d depends on light intensity which decreases gradually with the film depth z (See Equations 4.1 and 4.2 in Table A.4 in Appendix A) [25].

Diffusion terms also appear in the material balances for HDDA and oxygen:

$$\begin{aligned} \frac{\partial [M]}{\partial t} = & \frac{\partial}{\partial z} \left(D_M \frac{\partial [M]}{\partial z} \right) - 2k_{in,IM} [I^\bullet][M] - 2k_{in,\tilde{I}M} [\tilde{I}^\bullet][M] - 2k_{in,I_P M} [I_P^\bullet][M] - \\ & 2k_{p,R} [R^\bullet][M] - 2k_{p,B} [B^\bullet][M] - 2k_{p,C} [C^\bullet][M] - 2k_{p,T} [T^\bullet][M] - \\ & 2k_{p,O} [O^\bullet][M] \end{aligned} \quad (2.3)$$

$$\begin{aligned}
\frac{\partial[O_2]}{\partial t} = & \frac{\partial}{\partial z} \left(D_{O_2} \frac{\partial[O_2]}{\partial z} \right) - k_{O_2,R}[O_2][R^{\bullet}] - k_{O_2,B}[O_2][B^{\bullet}] - k_{O_2,C}[O_2][C^{\bullet}] - \\
& k_{O_2,T}[O_2][T^{\bullet}] - k_{O_2,I}[O_2][I^{\bullet}] - k_{O_2,\tilde{I}}[O_2][\tilde{I}^{\bullet}] - k_{O_2,I_P}[O_2][I_P^{\bullet}] + \\
& \frac{1}{2} k_{t,OO}[O^{\bullet}][O^{\bullet}]
\end{aligned} \tag{2.4}$$

The diffusivities D_I , D_M and D_{O_2} in Equations (2.2), (2.3) and (2.4) depend on the local free volume within the polyHDDA film:

$$D_X = D_{X_HDDA} \exp \left[-A_X \left(\frac{1}{v_f} - \frac{1}{v_{f0}} \right) \right] \quad X = I, M, O_2 \tag{2.5}$$

where D_{X_HDDA} is the measured diffusivity of species X within HDDA monomer. As polymerization proceeds D_I , D_M and D_{O_2} decrease due to decreasing free volume within the film. In Equation (2.5), A_I , A_M and A_{O_2} are adjustable parameters, v_{f0} is the free volume of HDDA monomer and v_f is the local time-varying free volume within the reacting polyHDDA film. Table A.4 in Appendix A contains Equation 4.3 which is used to compute v_f as a function of monomer conversion. Other algebraic equations that are used to calculate variables that appear in the PDEs are also provided in this table. The other ten material balance equations that appear in the model are the same as the ordinary differential equations developed by Vo et al. and are provided in Table A.5 in Appendix A. Initial and boundary conditions for Equations (2.2) to (2.4) and the other model PDEs are provided in Table A.6 in Appendix A.

Fig. 2.3 shows the measured initial diffusivities of the initiator, monomer and oxygen along with the corresponding predicted diffusivities, which decrease as monomer conversion increases. Dashed curves in Fig. 2.3 correspond to predicted diffusivities computed using initial guesses for free volume parameters A_I , A_M and A_{O_2} obtained from the study of Vo et al [16]. The solid curves

correspond to predictions obtained using parameter values estimated in the current study (see Table 2.2). Details about how the parameter estimates were obtained are provided below. Using the estimated value of A_M , the predicted diffusivity of monomer decreases by orders of magnitude as polymerization proceeds. The predicted diffusivities of initiator and O_2 also decrease substantially. It makes sense that D_{O_2} is less influenced by monomer conversion than D_M is because monomer molecules are much larger than O_2 . Notice from the ordinate in Fig. 2.3a that the diffusivity of initiator is much lower than that of monomer and O_2 , which makes sense, because initiator molecules are larger.

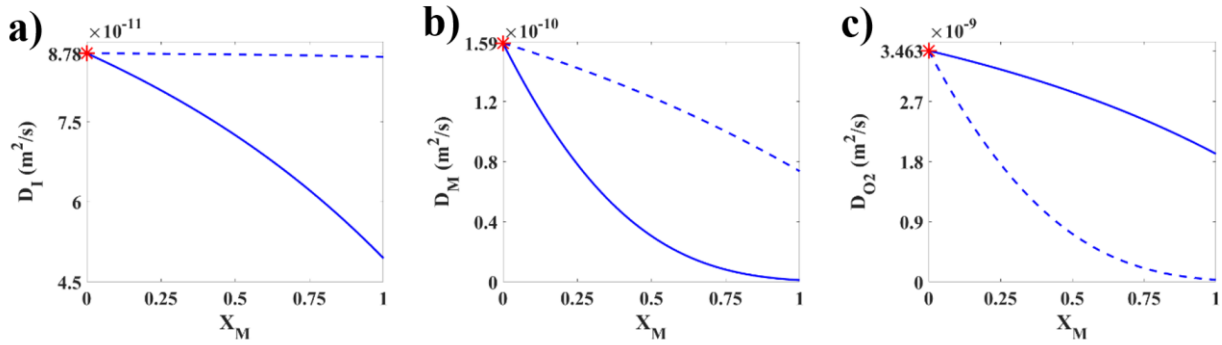


Fig. 2.3: Measured diffusivities * of a) initiator, b) monomer and c) oxygen along with predicted diffusivities as a function of monomer conversion. (----) predictions using initial parameter guesses for free-volume parameters A_I, A_M and A_{O_2} in Table 2.2, (—) predictions using estimated free-volume parameters obtained in the current study.

2.5 Parameter Estimation and Simulation Results

2.5.1 Parameter estimation

The proposed model requires 39 parameters to simulate the photopolymerization process. Fortunately, 30 of these parameters were previously estimated by Abdi et al. using their oxygen-free model (see Table A.7 in Appendix A) [15]. Three of the 9 new parameters are diffusivities

(D_{O_2-HDDA} , $D_{BAPO-HDDA}$ and $D_{HDDA-HDDA}$) which are measured directly in the current study (see Table 2.1). The remaining six parameters which require estimation are free-volume parameters and oxygen-related kinetic parameters whose initial guesses are provided in Table 2.2. Initial guesses for $k_{O_2,R}$, $\frac{k_{p,O_0}}{k_{p,R_0}} = \frac{k_{b,O_0}}{k_{b,R_0}}$ and $\frac{k_{t,O_0O_0}}{k_{t,RR_0}}$ are values obtained from Vo's parameter estimation study [16]. They are re-estimated in the current study to account for the improved model structure and information in the new data. Upper and lower parameter bounds in Table 2.2 are specified to ensure that all estimated parameters are physically realistic.

The least-squares objective function used for parameter estimation is:

$$J = \sum_{i=1}^{N_{X_V}} (X_{V_{meas},i} - X_{V,i})^2 \quad (2.6)$$

where $X_{V_{meas},i}$ is the i^{th} measured value of overall vinyl-group conversion, $X_{V,i}$ is the corresponding model prediction and $N_{X_V} = 1,655$ is the number of measured values used for parameter estimation (obtained from 32 experimental runs). Prior to conducting the parameter estimation, a formal estimability analysis was performed to confirm that all six parameters could be estimated uniquely using the available data [39]. The resulting parameter estimates are shown in the fifth column in Table 2.2.

Table 2.1: List of experimentally obtained parameters.

Parameter	Value	Unit
$D_{O_2}^0$	3.463×10^{-9}	$\frac{m^2}{s}$
H_S^{cp}	1.181×10^{-1}	$\frac{mol}{L Pa}$
D_{HDDA}^0	1.59×10^{-10}	$\frac{m^2}{s}$

D_{BAPO}^0	8.78×10^{-11}	$\frac{m^2}{s}$
--------------	------------------------	-----------------

Table 2.2: List of estimated parameters

Parameters	Lower bound	Upper bound	Initial Value	Estimate	Units
A_{O_2}	0	1	0.3	3.7628×10^{-2}	-
$k_{O_2,R}$	1×10^5	1×10^9	4.94×10^7	7.6828×10^6	L.mol ⁻¹ s ⁻¹
$\frac{k_{p,00}}{k_{p,R0}} = \frac{k_{b,00}}{k_{b,R0}}$	0	2×10^{-6}	3.53×10^{-10}	1.5405×10^{-6}	-
$\frac{k_{t,000}}{k_{t,R00}}$	0	5	1.5	5.6841×10^{-5}	-
A_{HDDA}	0	5×10^{-1}	4.9817×10^{-4}	3.1437×10^{-1}	-
A_{BAPO}	0	1×10^{-1}	0.049	3.6594×10^{-2}	-

2.5.2 Simulation results and model assessment

Fig. 2.4 compares the model predictions with the experimental results for the two runs that had the best fit to the data (in green) and the worst fit to the data (in red), respectively, according to their contributions to their least-squares objective function. The best-fit simulation results in green correspond to a relatively thick film ($\sim 17 \mu m$), a medium light intensity ($\sim 1180 W/m^2$) and a high BAPO level (4 wt%). The worst-fit simulation results in red are obtained for a run with similar film thickness ($\sim 20 \mu m$) and light intensity ($\sim 1200 W/m^2$), but with a low BAPO level (1 wt%). Plots showing the fit to the data for several additional runs used for parameter estimation are provided in Appendix A. In general, plots for runs with low BAPO (e.g. see Fig. A.2) reveal

that the model tends to underpredict the overall conversion when initial BAPO concentration is low. This result is not surprising because most of the kinetic parameters used in the simulations were estimated by Abdi et al., using a data set where all runs were conducted using a high BAPO concentration of 4 wt%. Abdi noted that there is considerable uncertainty associated with many of his model parameters and recommended future parameter estimation studies using experiments conducted over a wider operating range. For example, if additional experiments with low BAPO concentrations are used for parameter estimation, they may reveal that Abdi's estimated rate constant for some second-order termination reactions are too high and rate constants for some first-order backbiting reactions are too low. Adjusting these parameters may enable us to obtain an improved fit for the low BAPO run in Fig. 2.4, while maintaining a good fit for the high BAPO run. Simulation and experimental results in Fig. A.3, which compare the results for two runs with different film thicknesses, confirm that thicker films tend to result in higher conversions because they experience less oxygen penetration during the runs.

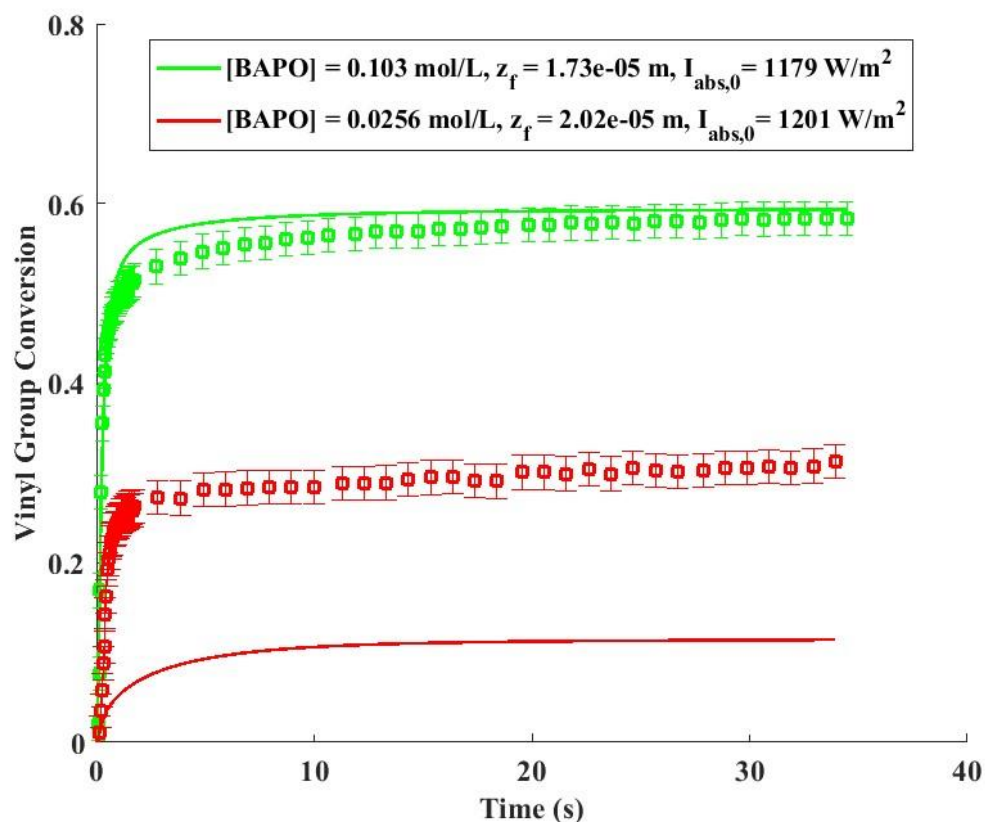


Fig. 2.4: Model predictions (curved lines) and the corresponding FTIR measured values for the experiments of those runs.

Fig. 2.5 shows the model's predictive ability using the three runs saved for validation. As expected, in Fig. 2.5a the model predicts correctly that increased light intensity increases the overall vinyl-group conversion. Fig. 2.5b shows the third validation run, which was conducted using a thicker film. Unfortunately, the model overpredicts the conversions in all three runs shown in Fig. 2.5.

In general, the proposed model performs better at fitting the objective function than predictions from Vo's ODE oxygen-inhibition model (i.e., the value of the objective function in Equation (2.6) is 49% lower). This is not surprising, since this model uses more data to get more accurate parameter estimates and uses PDEs to better account for oxygen and monomer diffusion.

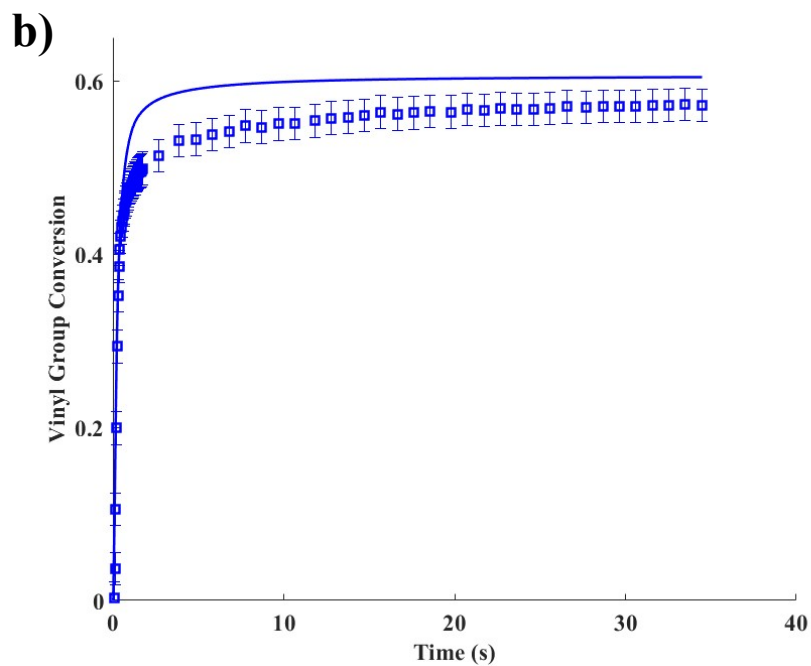
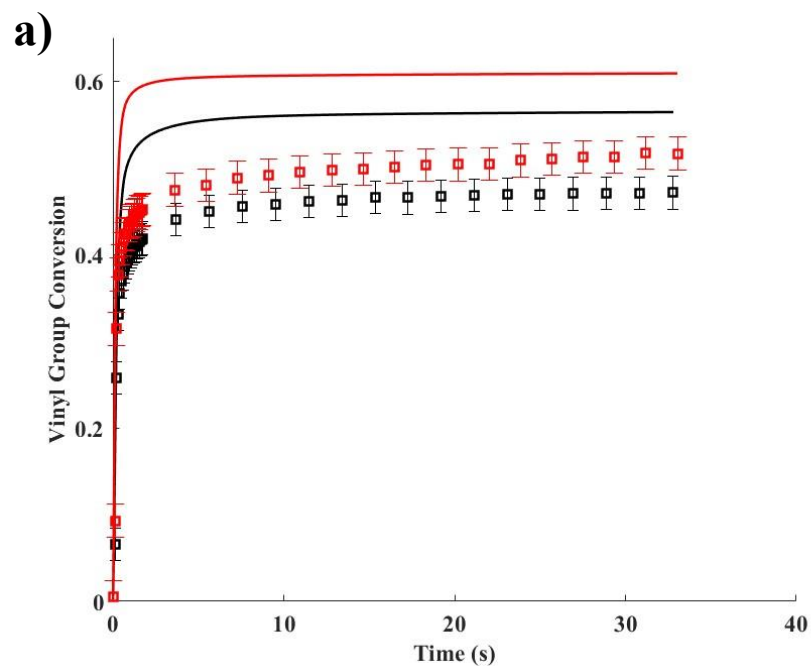


Fig. 2.5: Model predictions of a) two validation runs for experiments with thick film ($12\ \mu\text{m}$) and high BAPO level (4 wt%) using light intensities of — $2000\ \text{W}/\text{m}^2$ and — $3006\ \text{W}/\text{m}^2$, and an additional validation run b) — using a thicker film ($18\ \mu\text{m}$), high BAPO level (4 wt%) and low light intensity of $1198\ \text{W}/\text{m}^2$.

Fig. 2.6 shows predicted changes of oxygen concentrations with time at different depths in the film for a run conducted with a thick film ($\sim 18 \mu\text{m}$), high light intensity (5916 W/m^2) and a high BAPO level (4 wt%). Note that the concentration of oxygen is initially uniform throughout the entire film; however, as soon as polymerization starts, the oxygen concentration drops rapidly, causing new oxygen to start diffusing into the film from the air through the top surface. Notice that the oxygen concentration at the top surface stays constant at $2.5 \times 10^{-3} \text{ mol/L}$, which is in equilibrium with the air. At 10% of the film depth, the oxygen concentration drops to $\sim 1.3 \times 10^{-3} \text{ mol/L}$ nearly instantaneously due to fast reactions with initiator radicals, and then rises slowly as the initiator concentration falls and oxygen from the air has time to diffuse into the film. At the bottom of the film the oxygen concentration remains near zero for $\sim 0.8 \text{ s}$ because the thick film reduces the rate of oxygen diffusion. After 3 seconds when all the reactions cease, the oxygen concentration becomes uniform within the film. Fig. 2.7 shows the total vinyl-group concentration changing with time at different depths within the film. It confirms that at deeper levels within the film, the total vinyl-group concentration is lower than the concentration near the surface, because less oxygen inhibition occurs at the bottom of the film. Additional figures showing how initiator and monomer concentrations vary over the depth of the film are provided in Appendix A. Only small concentration gradients are predicted for the initiator, which are due to a decrease in light intensity with film depth. As a result, we recommend that initiator diffusion should be neglected in future modelling studies aimed at parameter estimation. Large time-varying concentration gradients are predicted for the monomer due to oxygen-induced changes in free-radical concentrations.

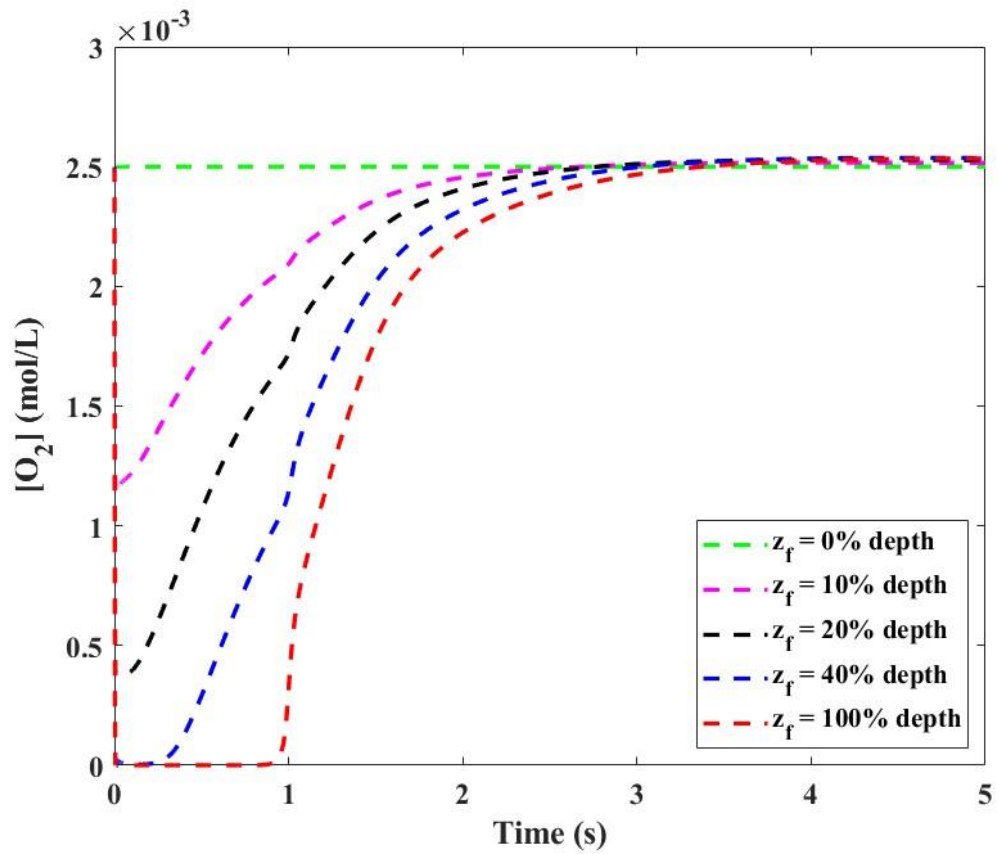


Fig. 2.6: Oxygen concentration levels with respect to time at different film depths

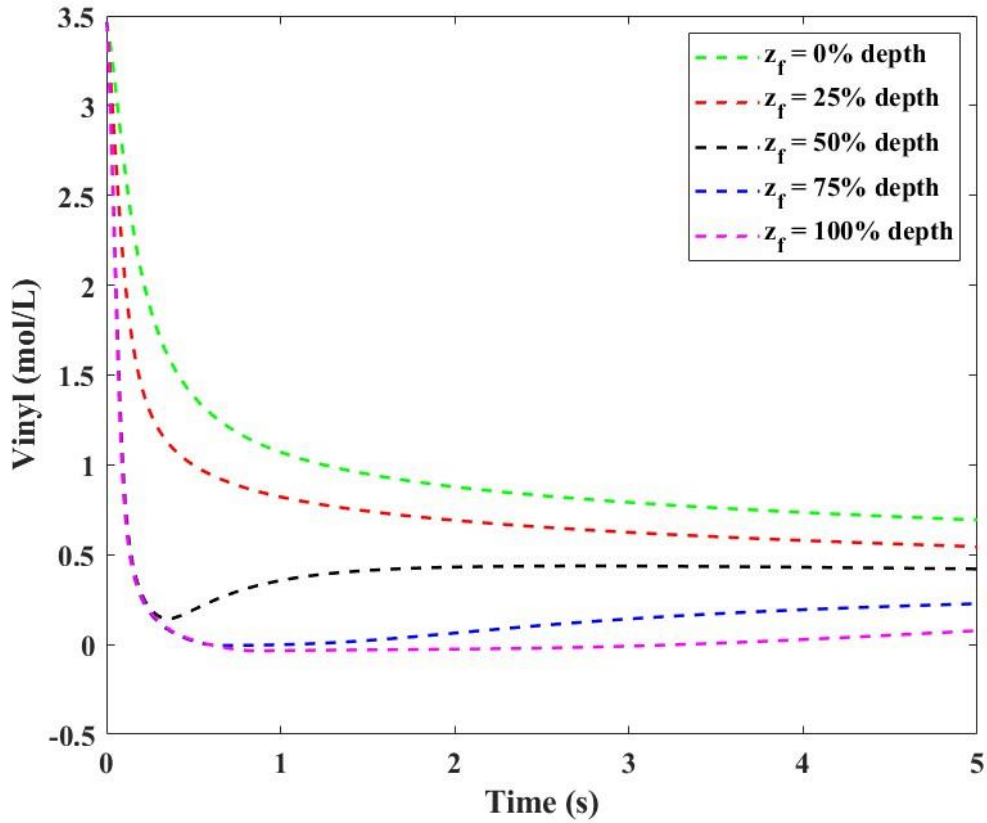


Fig. 2.7: Vinyl group concentration levels with respect to time at different film depths

2.6 Conclusion

A fundamental model was developed to account for oxygen diffusion and associated inhibition during the photopolymerization of HDDA with the bifunctional initiator BAPO. This study includes experiments to measure the diffusivities of oxygen, HDDA and BAPO in HDDA. Optical measurements were used to determine that $D_{O_2} = 3.48 \times 10^{-9} \frac{m^2}{s}$ in HDDA monomer. DOSY NMR was used to determine that $D_{HDDA} = 1.59 \times 10^{-10} \frac{m^2}{s}$ and $D_{BAPO} = 8.78 \times 10^{-11} \frac{m^2}{s}$. These measured values are then used in a mathematical model that predicts concentration gradients that arise in HDDA polymer films during photopolymerization.

PDE model equations are derived based on a comprehensive reaction mechanism. Real-time FTIR data for vinyl-group conversion in 35 runs are used to support parameter estimation and model validation. The resulting PDE model and parameter estimates are used to predict the behavior of HDDA photopolymerization using a variety of film thicknesses (8 – 17 μm), BAPO levels (1 – 4 wt%) and light intensities (200 – 6000 W/m^2). Unlike earlier models, the proposed model provides accurate predictions for runs with higher BAPO levels and light intensities.

In future, it will be important to re-estimate some of the kinetic parameters obtained by Abdi et al which were held constant during the current modelling study. We are hopeful that improved parameter estimates will lead to better predictions for experiments with low BAPO levels and light intensities. The current model assumes that the film has constant density during polymerization, which is not the case. As photopolymerization proceeds, film shrinkage of up to 12% can occur because HDDA polymer is denser than the monomer. An updated model that accounts for shrinkage is currently under development and will be used in future parameter estimation studies. The measured diffusivities and parameter estimates from the current study will be used as initial guesses for this ongoing research, which will produce a more accurate model that can be used reliably over a wider range of conditions of industrial interest. Model based design of experiments will be helpful for selecting future experimental settings that lead to enhanced information about important model parameters [40].

2.7 Author Contributions

I, Alaa El Halabi, developed the software, wrote the original draft of this paper, and played a major part in developing the methodology and investigating the results. Kaveh Abdi provided support in formal analysis, software development, and review and editing. Anh-Duong Dieu Vo provided

support also in formal analysis, software development and review and editing. Ardalan Ebrahimzadeh performed the experiment to obtain oxygen diffusivity. Jasper F. van den Hoek performed DOSY NMR experiments to obtain BAPO and HDDA diffusivities. Luuk van der Velden, Marjolein N. van der Linden, and Robin X. E. Willemse are Canon scientists responsible for data curation used in parameter estimation, supporting supervision, and some review and editing. Piet D. Iedema helped in conceptualization, funding acquisition, project administration, and supervision. Kimberley B. McAuley is my supervisor and was of great help in conceptualization, funding acquisition, project administration and was the lead in review and editing of this paper.

Chapter 3

Modeling of 1,6-hexanediol Diacrylate Photopolymerization with Spatial Gradients and Film Shrinkage*

Department of Chemical Engineering, Queen's University, Kingston, ON, Canada

3.1 Summary

A dynamic model is proposed to account for shrinkage and swelling during the photopolymerization of 1,6-hexanediol diacrylate (HDDA) with the bifunctional initiator bis-acylphosphine oxide (BAPO) in the presence of oxygen. The model is composed of 14 partial differential equations (PDEs) that are used to track changes in film thickness along with time- and spatially- varying concentrations of monomer, initiator, oxygen, pendant vinyl groups and seven types of radicals. Shrinkage has a noticeable influence on the model predictions. For a variety of simulated photopolymerization experiments, there is ~9% discrepancy between predicted overall vinyl-group conversions obtained from the current model with shrinkage and a previous model without. Prediction discrepancies become larger for simulated experiments involving thin films ($8 \mu\text{m}$) or low light intensities ($1200 \text{ W}/\text{m}^2$). In future, it will be important to re-estimate the kinetic parameters used in the shrinkage model to obtain accurate model predictions for use in process improvement studies.

* El Halabi, A., K. Abdi, A. D. D. Vo, P. Iedema, and K. B. McAuley (2024). " Modeling of 1,6-hexanediol Diacrylate Photopolymerization with Spatial Gradients and Film Shrinkage" *Macromolecular Reaction Engineering* special issue in honor of M. Nomura

3.2 Introduction

Free radical photopolymerization is used in many industrial applications including automobile coatings, protective films, printed materials, and dental fillings [26]. 1,6-Hexanediol Diacrylate (HDDA) is a divinyl monomer that undergoes photopolymerization in the presence of photoinitiators under ultraviolet (UV) light [15, 16, 18, 25, 41]. One complication that arises during HDDA photopolymerization is shrinkage, which occurs as the monomer is converted into denser polymer. Ji et al. measured the volumetric shrinkage of polyHDDA at different curing temperatures using reflective laser scanning and concluded that up to 17% shrinkage can occur for photopolymerizations conducted at 20 °C [42]. Torres-Knoop et al. performed molecular simulations of HDDA photopolymerization and predicted $14 \pm 2\%$ volumetric shrinkage [24].

Several kinetic models have been developed for HDDA photopolymerization which focus on the influence of light intensity, film thickness, initiator concentration, and oxygen contamination on vinyl group conversion [15, 16, 18, 25, 41]. Early models used a simplified reaction mechanism that assumes the same reactivity for monomeric vinyl groups and pendant vinyl groups along the polymer chains [18, 25, 43]. Shrinkage was not considered in these early models. Recently, more complicated kinetic models were developed to account for different reactivities for different types of vinyl groups and a wide variety of side reactions (i.e. backbiting, cyclization, and oxygen related reactions) [15, 16, 41]. These models account for five different types of polymeric free radicals and for the influence of free-volume effects on termination rate constants, as is common in many polymerization models [44]. These models also account for free-volume effects on the initiator efficiency and other types of rate constants, but they ignore the influence of shrinkage and swelling on polymerization kinetics. The most recent model from our research group uses partial differential equations (PDEs) to account for spatial variations in the rates of these reactions with time [41].

The objective of the current study is to extend this model to account for shrinkage and to explore whether shrinkage has an important influence on spatially-varying reaction rates in the polyHDDA film.

Most of the experimental research on volumetric shrinkage during photopolymerization of acrylates has focused on dental resin composites [45-48]. Linden and Jakubiak [49] provide an excellent review of these experimental results and the associated consequences including internal stresses and micro-cracks. A key application area for HDDA photopolymerization is high-speed printing where shrinkage can cause several issues including film swelling and wrinkling, varying mechanical properties, and decreased overall conversion [25, 42].

Until now, shrinkage has not been included in mathematical models for acrylate polymerization in films where spatial variations occur. However, shrinkage has been included in models for polymerization of methyl methacrylate (MMA) and a more complex divinyl acrylate monomer in well-mixed batch reactors [50-53]. As a result, these models account for the influence of shrinkage on reactant concentrations and the overall volume of the reaction mixture, which changes with time. Accounting for shrinkage in polyacrylate films with spatially-varying species' concentrations is a more complex issue because the extent of the shrinkage is different at different locations within the film. In addition, diffusion of unreacted monomer during the polymerization influences the density and the extent of the local shrinkage. These issues are considered in the current study where a PDE model is formulated and solved to predict changes in local species concentrations and the overall film thickness as photopolymerization proceeds. A novel mathematical transformation is developed and implemented so the resulting moving-boundary problem can be readily solved using the standard "pdepe" solver in MATLAB.

This paper is organized as follows. First, the reaction mechanism for photopolymerization of HDDA and the corresponding modeling assumptions are described. Second, a new dimensionless spatial coordinate w is introduced so that $w = 0$ always corresponds to the top surface of the film and $w = 1$ always corresponds to the bottom, even though the overall film thickness z_f (in meters) changes with time. Next, material-balance PDEs are derived in terms of the new coordinate w and the time t after the start of photopolymerization. The resulting model equations are solved numerically, and the simulation results are compared to simulations where shrinkage is ignored. Finally, recommendations are made regarding the need for kinetic parameters to be re-estimated so that accurate predictions will be obtained using the new model.

3.3 Reaction Mechanism and Modeling Assumptions

The reaction mechanism in the current model was first developed by Abdi et al. and was extended by Vo et al. to account for the influence of oxygen [15, 16]. A detailed list of initiation, propagation, crosslinking, cyclization, backbiting, termination and oxygen-related reactions is provided in Table B.1 in Appendix B. BAPO initiator decomposition (See Fig. 3.1a) is the first step in the reaction mechanism, wherein weak carbon-phosphorus bonds decompose under UV radiation to produce two types of radicals. One is a carbon-centered radical labeled I^\bullet and the other is a phosphorus-centered radical \tilde{I}^\bullet . Both I^\bullet and \tilde{I}^\bullet can initiate polymerization. Notice that \tilde{I}^\bullet contains an additional weak carbon-phosphorus bond that can decompose later during the polymerization as shown in Fig. 3.1b. The label I_p^\bullet is used to indicate the resulting phosphorus-centered polymeric radical. When free radicals react with HDDA (See Fig. 3.2a), the resulting radical end group R^\bullet has an associated vinyl group, arising from the second vinyl group on the HDDA monomer. The macroradical R^\bullet can propagate with HDDA monomer (See Fig. 3.2a) or can undergo a cyclization

reaction as shown in Fig. 3.2b where the vinyl group on R^{\bullet} is consumed, producing a cyclic radical C^{\bullet} . We assume that these propagation and cyclization reactions are sufficiently fast that consumption of the vinyl group on R^{\bullet} by other reactions (e.g., crosslinking) can be neglected. This assumption is listed as Assumption B.2.7 in Table B.2 in Appendix B, along with all other modeling assumptions. If propagation, instead of cyclization, consumes an R^{\bullet} group then its unreacted vinyl group becomes a pendant vinyl group V_p that can participate in a future crosslinking reaction (See Fig. 3.2c). As shown Fig. 3.2d, R^{\bullet} end groups can abstract a nearby hydrogen atom via a backbiting reaction to produce the tertiary radical T^{\bullet} . If oxygen is present, R^{\bullet} and other radical end groups can consume oxygen to produce peroxidic radicals denoted by O^{\bullet} (See Fig. 3.2e). These peroxidic radicals hinder polymerization because they propagate more slowly than R^{\bullet} , C^{\bullet} , B^{\bullet} and T^{\bullet} radicals. Furthermore, they readily terminate with other radicals (See Table S2), thereby reducing the overall concentration of propagating radicals and the rate of polymerization reactions. Additionally, all algebraic equations used in the model are provided in Table B.3 in Appendix B [5, 39, 54-57].

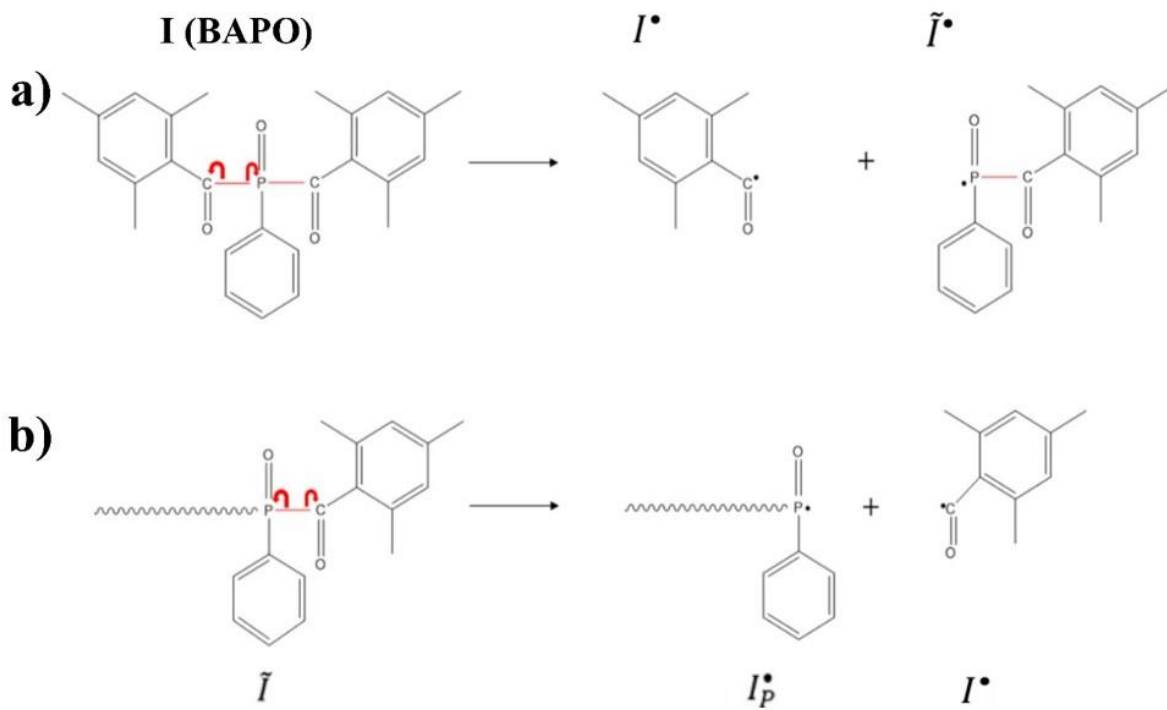


Fig. 3.1: Decomposition of a) initiator molecules and b) remaining carbon-phosphorous bonds in I^\sim . Adapted from [15].

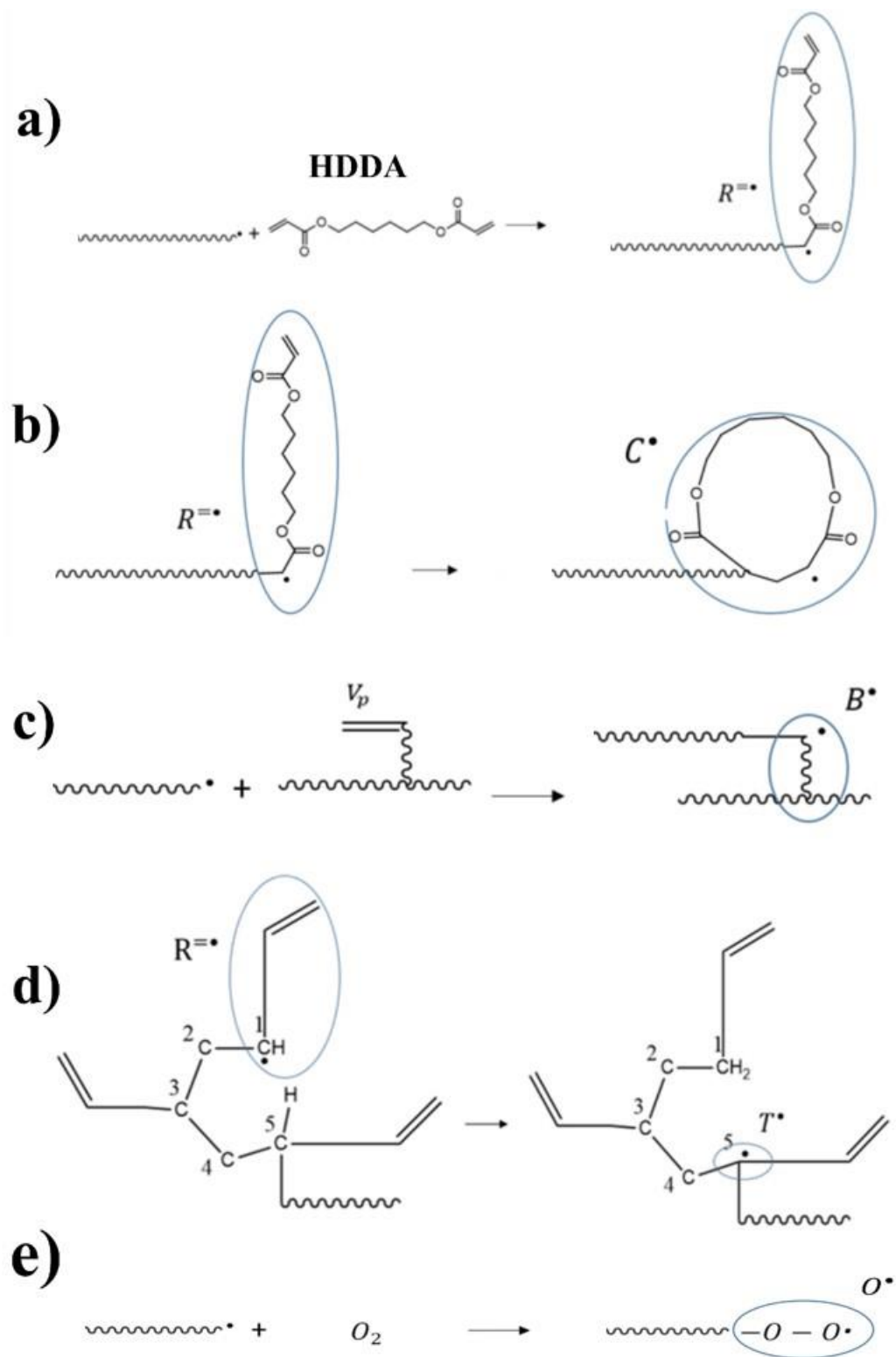


Fig. 3.2: Formation of different macroradicals: a) regular radical ends R^\bullet , b) cyclized radical ends C^\bullet , c) branch-point radical ends B^\bullet , d) tertiary radical ends T^\bullet and e) peroxidic radicals O^\bullet . Adapted from [16].

3.4 Model Development

When the HDDA film shrinks, the top surface of the film moves closer to the bottom surface. PDEs can be developed to describe this photopolymerization process, but an important complication arises. Either the top surface of the film or the bottom surface needs to be treated as a moving boundary, making the model equations difficult to solve. Numerical methods have been developed to solve systems of PDEs with moving boundaries, using advanced moving mesh and finite element strategies [58-60]. Unfortunately, these methods often require long computation times and can be difficult to implement and tune. In the current modeling study, we adopt a different approach (using calculus and transformations) so that the moving-boundary PDEs are transformed into a system of new PDEs using a dimensionless spatial coordinate w , which has fixed boundaries. This new coordinate w is defined so that $w = 0$ corresponds to the top surface of the film and $w = 1$ corresponds to the bottom surface of the film, even though the film is shrinking with time. A similar approach has been used to deal with moving-boundary PDE models that arise for other polymerization processes [61, 62]. For example, Yao et al. used transformations to model a solid-phase polymerization reactor that has a time-varying bed level due to mismatch between polymer inflow and outflow rates. They transformed their PDEs using a simple transformation $w = z/H$ where z (in meters) is the real position in the bed and H (in meters) is the time-varying bed height [62]. Unfortunately, the current HDDA modeling work requires a more complicated transformation, which will be described below.

3.4.1 Definition of the dimensionless spatial coordinate w

Consider a film layer with thickness z_f (in meters), which is time-varying because the film shrinks due to density changes during polymerization. Imagine dividing this film into 10 segments with

thicknesses Δz as shown in Fig. 3.3. Assume that no polymer molecules are able to diffuse across the boundaries between the segments, but HDDA monomer and oxygen molecules can readily diffuse because of their small size (See Assumption B.2.1 in Table B.2 in Appendix B). As photopolymerization proceeds, each segment will tend to shrink due to polymerization reactions. Also, some segments will tend to become thicker than others as monomer diffuses toward the bottom of the film due to concentration gradients. The reason for these gradients is that oxygen concentrations are high near the top surface (which is exposed to air). Oxygen inhibition reactions, shown in Table B.1, lead to lower polymerization rates (and higher monomer concentrations) near the top surface of the film. The dimensionless variable w is defined so that any polymer molecule that forms at an initial position w stays at the same position in the w coordinate, even though this polymer molecule could move up or down in the real spatial coordinate z due to film shrinkage and diffusion of small molecules. A complicated relationship exists between z and w because a polymer molecule that forms at time $t \cong 0$ at a position halfway between the top and the bottom of the film does not end up halfway between the top and bottom at the end of a photopolymerization experiment. Instead, it will end up relatively nearer to the top surface of the polymer film due to downward diffusion of monomer over the course of the experiment. This fact makes a simple transformation of the form $w = z/z_f$ inappropriate.

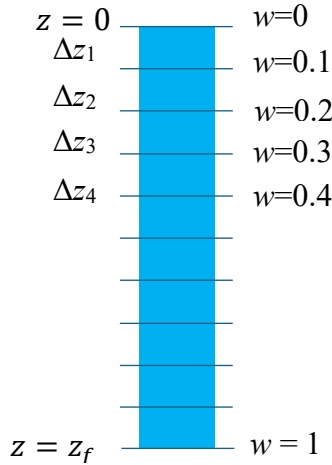


Fig. 3.3: Relationship between spatial coordinate z and transformed coordinate w at time 0.

3.4.2 Deriving the relationship between w and z

Consider the thin segment of film in Fig. 3.4, which has height Δz and scaled height Δw . The thickness of this segment (in meters) will change over time due to monomer diffusion and to polymerization. We assume that thickness changes due to diffusion of oxygen can be neglected, because oxygen is present only in low amounts (Assumption B.2.1 in Table B.2). Also assume that volume changes due to mixing of species can be neglected. A material balance on the i^{th} segment of thickness Δw during a period of time Δt (in seconds) gives:

$$\begin{aligned} \text{change in volume} &= \text{volume of monomer} - \text{volume of monomer} - \text{shrinkage within} \\ &\quad \text{diffusing in} \quad \text{diffusing out} \quad \text{the segment due to} \\ &\quad \quad \quad \quad \quad \quad \quad \quad \quad \quad \quad \quad \text{polymerization} \end{aligned} \quad (3.1)$$

The change in volume of the segment in m^3 is $\Delta(A\Delta z_i)$ where A (in m^2) is the surface area of the

film. The volume of monomer that diffuses in at the top of the segment is $-D_M \frac{\partial[M]}{\partial z} \Big|_{t,w} \frac{M_{HDDA}}{\rho_{HDDA}} A \Delta t$

where D_M is the diffusivity of the monomer in $m^2 s^{-1}$, $[M]$ is the concentration of monomer in $mol m^{-3}$, M_{HDDA} is the molar mass of monomer in $g mol^{-1}$ and ρ_{HDDA} (in $kg m^{-3}$) is the density of monomer. The volume of monomer that diffuses out at the bottom of the segment is

$-D_M \frac{\partial[M]}{\partial z} \Big|_{t,w+\Delta w} \frac{M_{HDDA}}{\rho_{HDDA}} A \Delta t$. The shrinkage within the segment due to polymerization reactions is $A \Delta z_i \Delta t M_{HDDA} \left(\frac{1}{\rho_{HDDA}} - \frac{1}{\rho_{pol}} \right) R_M$ where ρ_{pol} (in $kg\ m^{-3}$) is the density of the polymer and R_M is the rate of monomer consumption in $mol\ m^{-3}\ s^{-1}$:

$$R_M = \sum_X 2k_{p,X}[M][X] \quad (3.2)$$

where $k_{p,X}$ is the kinetic rate constant for monomer consumption via radicals of type X (where X = R^{\bullet} , B^{\bullet} , C^{\bullet} , T^{\bullet} , O^{\bullet} , I^{\bullet} , \tilde{I}^{\bullet} or I_p^{\bullet}). Substituting into equation (3.1) gives:

$$\begin{aligned} \Delta(A \Delta z_i) = & -D_M \frac{\partial[M]}{\partial z} \Big|_{t,w} \frac{M_{HDDA}}{\rho_{HDDA}} A \Delta t + D_M \frac{\partial[M]}{\partial z} \Big|_{t,w+\Delta w} \frac{M_{HDDA}}{\rho_{HDDA}} A \Delta t \\ & - A \Delta z_i \Delta t M_{HDDA} \left(\frac{1}{\rho_{HDDA}} - \frac{1}{\rho_{pol}} \right) R_M \end{aligned} \quad (3.3)$$

Our goal is to use equation (3.3) to determine values of z (in meters) corresponding to particular values of w . For example, when 10 discrete segments are considered, as shown in Fig. 3.3, $w = 0.4$ corresponds to the bottom of the 4th segment from the top surface. To determine the corresponding value of z and how it changes over time, we need to track the thickness changes in the top 4 segments and add them together. At the bottom of the 4th segment, the change in the spatial coordinate z during the period Δt is the total change in the thicknesses of the top 4 segments:

$$A \Delta \sum_{i=1}^4 (\Delta z_i) = D_M \frac{\partial[M]}{\partial z} \Big|_{t,w=0.4} \frac{M_{HDDA}}{\rho_{HDDA}} A \Delta t - A \Delta t M_{HDDA} \left(\frac{1}{\rho_{HDDA}} - \frac{1}{\rho_{pol}} \right) \sum_{i=1}^4 \Delta z_i R_M \quad (3.4)$$

Notice that the only diffusion term in equation (3.4) is due to monomer diffusing out of the bottom of the 4th segment, because there is no monomer diffusion into the top surface of the first segment and terms for rates of diffusion between segments cancel out.

Dividing both sides of equation (3.4) by $A\Delta t$ and taking the limit as $\Delta z \rightarrow 0$, while staying at $w = 0.4$, gives:

$$\frac{\Delta \int_{w=0}^{w=0.4} 1 dz}{\Delta t} = D_M \left. \frac{\partial [M]}{\partial z} \right|_{t,w=0.4} \frac{M_{HDDA}}{\rho_{HDDA}} - M_{HDDA} \left(\frac{1}{\rho_{HDDA}} - \frac{1}{\rho_{pol}} \right) \int_{w=0}^{w=0.4} R_M dz \quad (3.5)$$

After some simplification, use of the chain rule, and consideration of any arbitrary value of w rather than $w = 0.4$, equation (3.5) becomes the following PDE:

$$\left. \frac{\partial z}{\partial t} \right|_{w=0.4} = D_M \left. \frac{\partial [M]}{\partial w} \right|_t \left(\left. \frac{\partial z}{\partial w} \right|_t \right)^{-1} \frac{M_{HDDA}}{\rho_{HDDA}} - M_{HDDA} \left(\frac{1}{\rho_{HDDA}} - \frac{1}{\rho_{pol}} \right) Q \quad (3.6)$$

where $Q = \int_{z=0}^{z(w=0.4)} R_M dz$

A detailed derivation of equation (3.6), showing all the steps is provided in section B3 in Appendix B. In summary, this PDE describes dynamic changes in the real spatial position z of polymer molecules that formed at the start of the polymerization at any relative position w . Notice that the first term on the right-hand side of equation (3.6) is concerned with monomer diffusion and the second term is concerned with density changes due to polymerization reactions. All other PDEs in the model are derived using material balances on individual species or polymeric end groups. As an example, the balance for unreacted HDDA monomer is provided in the next section. A complete list of the PDEs and associated initial and boundary conditions is provided in Table B.4 in Appendix B.

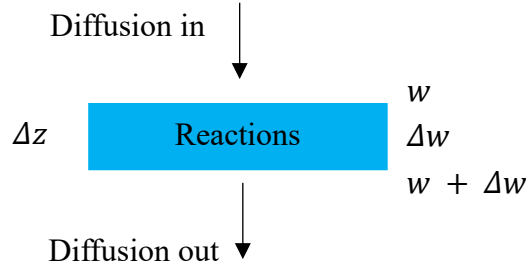


Fig. 3.4: Phenomena leading to shrinkage and swelling of a thin segment of the film

3.4.3 Material balance PDE for HDDA monomer

A material balance (in *mol*) on HDDA monomer in an arbitrary segment of initial thickness Δz with relative thickness Δw (see Fig. 3.4) during a short period of time Δt is:

$$\begin{array}{l} \text{accumulation} \\ \text{of monomer} \end{array} = \begin{array}{l} \text{monomer} \\ \text{diffusing in} \end{array} - \begin{array}{l} \text{monomer} \\ \text{diffusing out} \end{array} - \begin{array}{l} \text{monomer consumed} \\ \text{by reaction} \end{array} \quad (3.7)$$

Accumulation of monomer in the segment is $\Delta([M]A\Delta z)$ *mol* where $[M]$ is the local HDDA monomer concentration in mol m^{-3} . The amount of monomer that diffuses in at the top of the

segment is $-D_M \frac{\partial[M]}{\partial z} \Big|_{t,w} A\Delta t$ *mol* where D_M is the diffusivity of the monomer in $\text{m}^2 \text{s}^{-1}$. The

amount of monomer that diffuses out at the bottom of the segment is $-D_M \frac{\partial[M]}{\partial z} \Big|_{t,w+\Delta w} A\Delta t$ *mol*.

The amount of monomer that gets consumed due to polymerization reactions is $A\Delta z\Delta t R_M$ *mol*.

Substituting into equation (3.7) gives:

$$\Delta([M]A\Delta z) \Big|_w = -D_M \frac{\partial[M]}{\partial z} \Big|_{t,w} A\Delta t + D_M \frac{\partial[M]}{\partial z} \Big|_{t,w+\Delta w} A\Delta t - A\Delta z\Delta t R_M \quad (3.8)$$

After dividing by A , Δt and Δw , use of the chain rule and some algebra results in the PDE:

$$\begin{aligned}
\left. \frac{\partial [M]}{\partial t} \right|_w &= \left. \frac{\partial^2 [M]}{\partial w^2} \right|_t D_M \left(\left. \frac{\partial z}{\partial w} \right|_t \right)^{-2} + \left(\left. \frac{\partial [M]}{\partial w} \right|_t \right)^2 \frac{A_M (v_{f0} - v_{f1})}{[M]_0 (v_f)^2} D_M \left(\left. \frac{\partial z}{\partial w} \right|_t \right)^{-2} - R_M \\
- [M] &\left(\frac{M_{HDDA}}{\rho_{HDDA}} \left. \frac{\partial^2 [M]}{\partial w^2} \right|_t D_M \left(\left. \frac{\partial z}{\partial w} \right|_t \right)^{-2} + \frac{M_{HDDA}}{\rho_{HDDA}} \left(\left. \frac{\partial [M]}{\partial w} \right|_t \right)^2 \frac{A_M (v_{f0} - v_{f1})}{[M]_0 (v_f)^2} D_M \left(\left. \frac{\partial z}{\partial w} \right|_t \right)^{-2} - \right. \\
&M_{HDDA} R_M \left(\frac{1}{\rho_{HDDA}} - \frac{1}{\rho_{pol}} \right)
\end{aligned} \tag{3.9}$$

A detailed derivation of equation (3.9) and other PDEs in Table B.4 is provided in the Appendix B. In summary, the PDE in equation (3.9) describes dynamic changes in local monomer concentration $[M]$ with respect to t and the transformed position w . Notice that the first and second terms on the right-hand side of equation (3.9) are concerned with monomer diffusion, the third term is concerned with the rate of monomer consumption due to reactions, and the last term (which extends over two lines) is concerned with film shrinkage. Table B.4 reveals that the other model PDEs share a similar structure to equation (3.9), consisting of a reaction rate term and a shrinkage term, with only the oxygen and monomer PDEs including diffusion terms. Initial and boundary conditions for these PDEs are provided in Table B.4.

3.5 Simulation Results and Model Assessment

Fig. 3.5 shows the predicted position z as a function of time corresponding to four different values of w , during photopolymerization in a relatively thick film ($18 \mu m$) with high UV light intensity ($6000 W/m^2$) and a high BAPO level ($4 wt\%$). The four positions considered are $w = 0$ (the top surface of the film), $w = 0.2$ (corresponding to non-diffusing species that start 20% of the way between the top and bottom of the film), $w = 0.5$ and $w = 1$ (the bottom of the film). As shown in Fig. 5, the predicted overall film thickness shrinks from $18 \mu m$ to $15.93 \mu m$ ($\sim 12\%$ shrinkage)

within the first second of photopolymerization. The film does not shrink the full possible amount of 17 %, because the final predicted overall conversion of vinyl groups is 70 % rather than 100 %. The plot for $w = 0.5$ (in black) is interesting because it reveals that any non-diffusing material that starts off halfway down in the film ends up at $z = 7.77 \mu\text{m}$ which is closer to the top surface of the film than the bottom. This result makes sense because monomer molecules tend to diffuse from the top portion of the film (where polymerization rates are low) toward the bottom portion of the film (where polymerization rates are higher). As a result, a greater mass of polymer is formed below $w = 0.5$ than above.

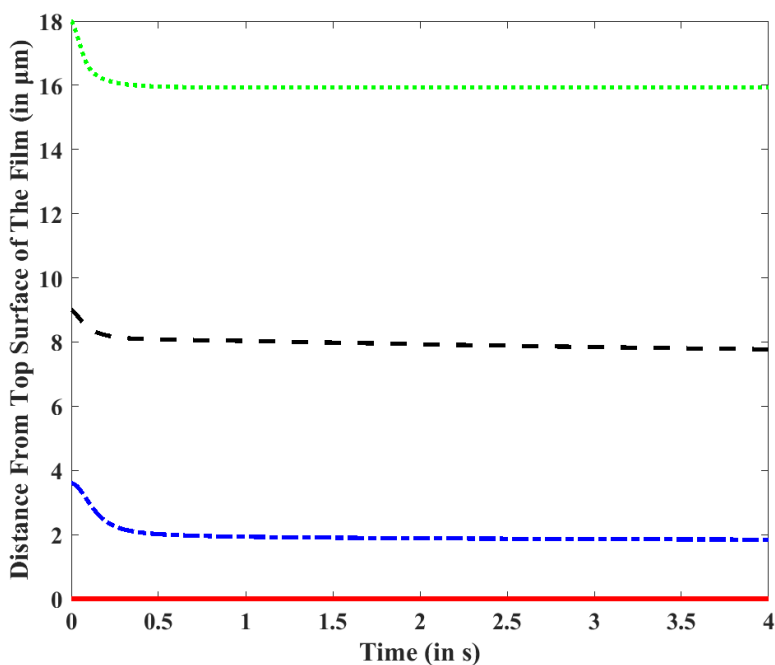


Fig. 3.5: Position z vs time for (—) the top surface of the film where $w = 0$, (---) $w = 0.2$, (---) $w = 0.5$, and (---) the bottom surface of the film $w = 1$. This simulation was conducted for a thick film ($18 \mu\text{m}$), using high light intensity (6000 W/m^2) and a high BAPO level (4 wt%).

Fig. 3.6 shows the predicted position z for a run with low BAPO (1 wt%). In simulations like this one, where initiator levels are low, the overall amount of film shrinkage is less than in Fig. 3.5, because low initiator leads to lower monomer conversion. The curve for $w = 0.5$ in Fig. 6 reveals

that non-diffusing species move quite significantly within the film due to high rates of diffusion for unreacted monomer, which persists after $t = 2$ s.

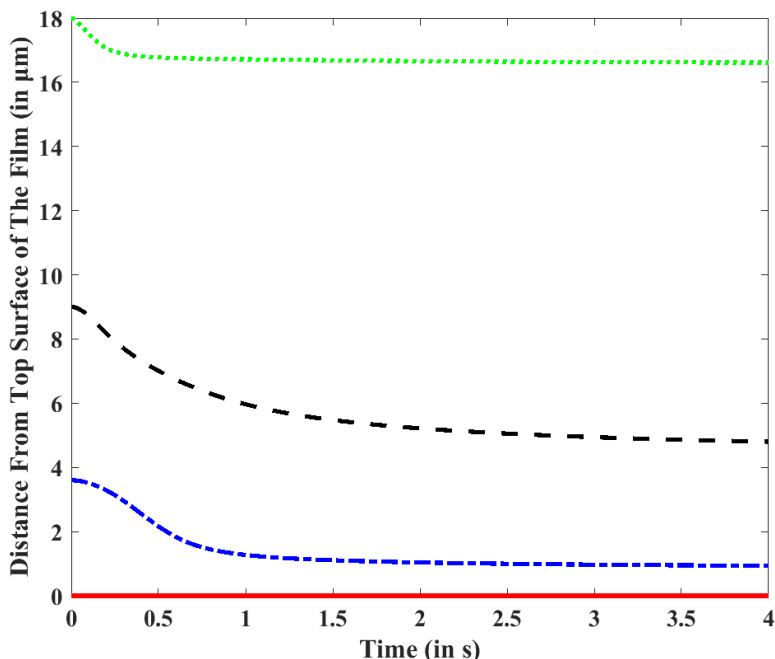


Fig. 3.6: Position z vs time for (—) the top surface of the film where $w = 0$, (---) $w = 0.2$, (---) $w = 0.5$, and (---) the bottom surface of the film $w = 1$. This simulation was conducted for a thick film ($18 \mu\text{m}$), using high light intensity (6000 W/m^2) and a low BAPO level ($1 \text{ wt}\%$).

Fig. 3.7 shows the predicted oxygen concentrations within the film at different times for the same run as in Fig. 3.5. The oxygen concentration at the top surface of the film remains constant at $2.5 \times 10^{-3} \text{ mol/L}$, because the top surface is in equilibrium with air (Assumption B.2.27 in Table B.2). At $w = 0.2$, the oxygen concentration drops almost instantaneously to $\sim 0.4 \times 10^{-3} \text{ mol/L}$ due to fast initiator decomposition and subsequent free-radical reactions that consume oxygen to form peroxidic radicals. After the initial decrease, the predicted oxygen concentration gradually increases as initiator levels decline and oxygen from the air has time to diffuse within the film. At the bottom surface of the film, the predicted oxygen concentration drops quickly and remains near zero for ~ 0.8 s due to the large film thickness, which provides a greater resistance for oxygen

diffusion. After 3 seconds, when all the reactions cease due to depletion of the initiator and consumption of the resulting free radicals, $[O_2]$ returns to equilibrium throughout the film. Fig. 3.8 shows changes in the unreacted monomer concentration during the same simulated run. At large values of w (deeper within the film), $[M]$ is lower compared to the corresponding concentration at the top surface, because high $[O_2]$ near the surface inhibits polymerization. Notice that, at $w = 0.5$, monomer concentration initially decreases due to polymerization reactions and then subsequently increases as new monomer diffuses downward from the top region of the film. Monomer diffusion is also evident in the top layers of the film, where the concentration does not reach steady state immediately after reactions cease at around 4 seconds. Instead, $[M]$ near the top continues to decrease gradually as the monomer slowly diffuses downward. When a longer simulation time is used (not shown), the local monomer concentrations continue to move toward a uniform equilibrium concentration.

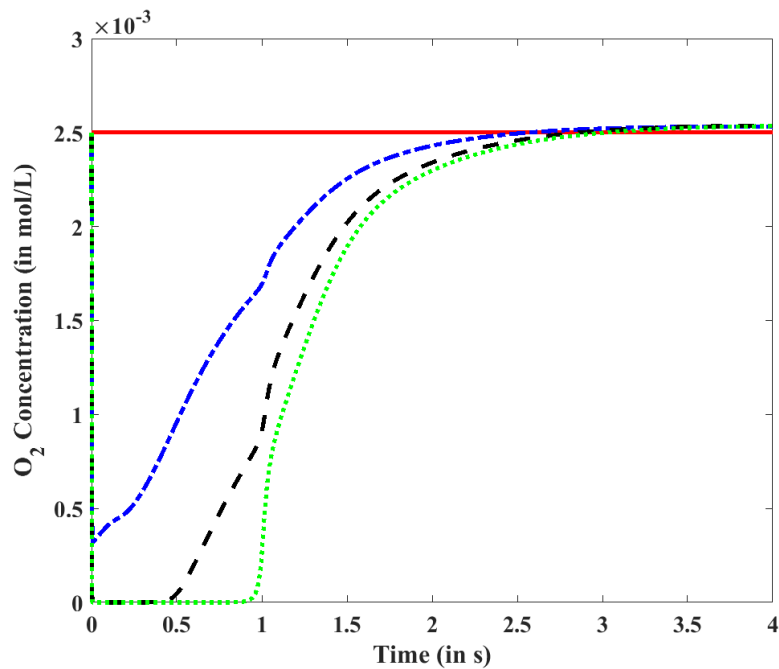


Fig. 3.7: Oxygen concentration vs time for (—) the top surface of the film where $w = 0$, (---) $w = 0.2$, (---) $w = 0.5$, and (···) the bottom surface of the film $w = 1$. This simulation was

conducted for a thick film ($18 \mu\text{m}$), using high light intensity (6000 W/m^2) and a high BAPO level (4 wt%).

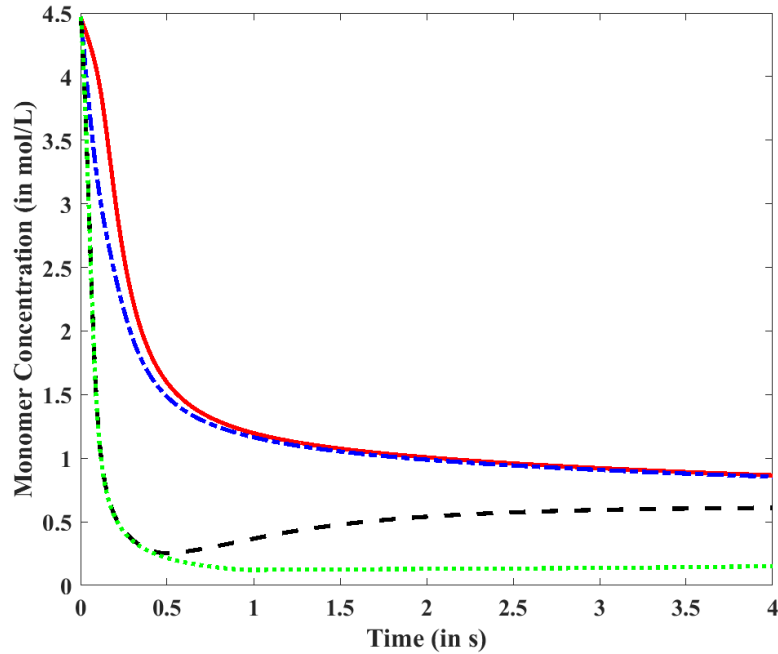


Fig. 3.8: Monomer concentration vs time for (—) the top surface of the film where $w = 0$, (---) $w = 0.2$, (---) $w = 0.5$, and (---) the bottom surface of the film $w = 1$. This simulation was conducted for a thick film ($18 \mu\text{m}$), using high light intensity (6000 W/m^2) and a high BAPO level (4 wt%).

Figures 3.9 to 3.11 are used to investigate whether shrinkage has an important influence on predicted concentrations and conversion within polyHDDA films. Fig. 3.9 compares predictions from the current model with predictions from an earlier model where shrinkage is neglected [17] for two runs with different film thicknesses. As expected, a higher overall vinyl-group conversion is predicted for the run with larger thickness because the thicker film experiences less oxygen contamination. Notice that there is a substantial discrepancy between the model predictions with shrinkage and without shrinkage for both film thicknesses. These results suggest that it may be important to account for film shrinkage when models are used to design and optimize photopolymerization ink recipes and printing processes. Notice that the discrepancy is larger for

the thinner film where oxygen diffuses more easily, and oxygen inhibition has a larger influence on reaction rates within the film.

Fig. 3.10 investigates the influence of light intensity on overall vinyl-group conversion in a thick film with and without shrinkage. The discrepancy between the model with shrinkage and that without shrinkage is greater for the run with lower light intensity where there is more unreacted monomer that can diffuse. Fig. 3.11 investigates the influence of initiator level on overall vinyl-group conversion in the same thick film, with and without shrinkage. The two runs in Fig. 3.11 have similar discrepancies between the two models. Note that the kinetic parameters used in the simulations in figures 3.9 to 3.11 were estimated using models where shrinkage was ignored. In future, it will be important to re-estimate the model parameters while accounting for shrinkage so that accurate predictions can be obtained.

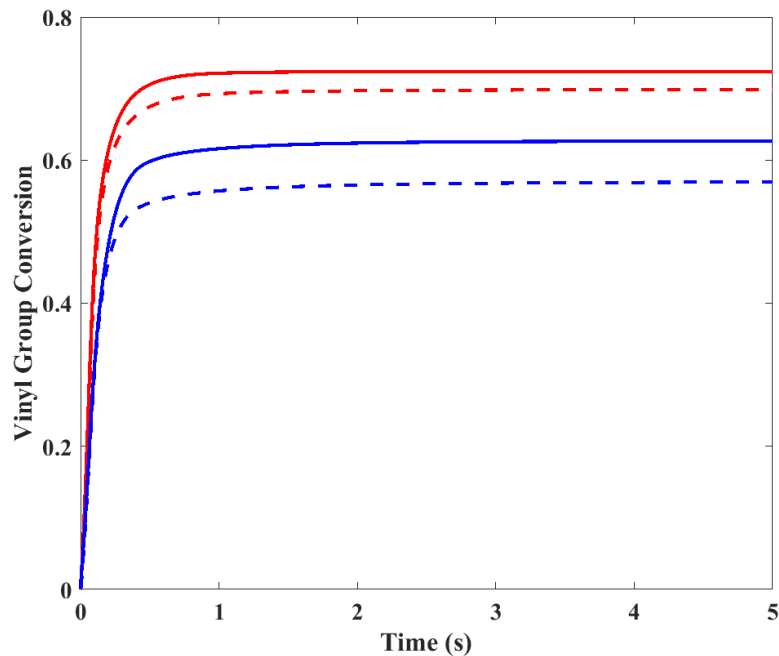


Fig. 3.9: Plot of shrinkage run (—) and no shrinkage run (---) with high thickness (18 μm) vs shrinkage run (—) and no shrinkage run (---) with low thickness (8 μm)

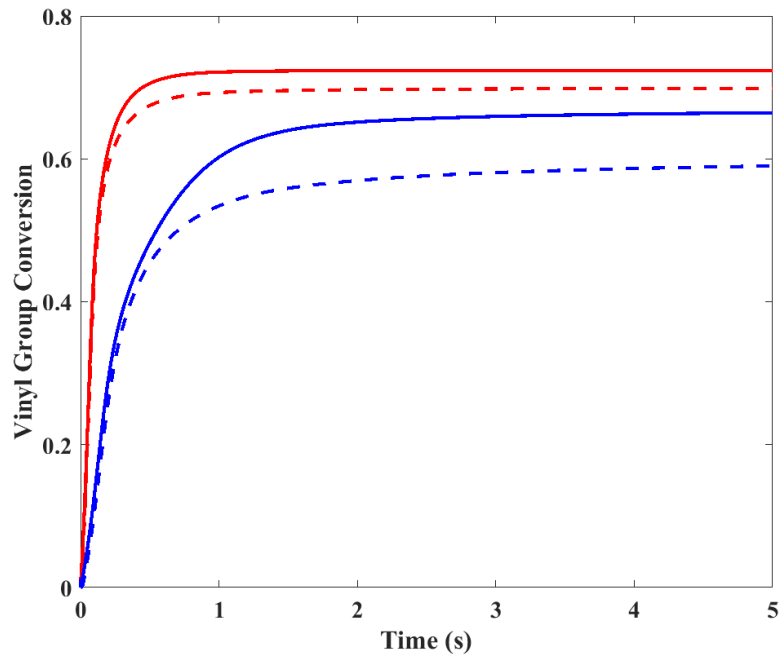


Fig. 3.10: Plot of shrinkage run (—) and no shrinkage run (---) with high light intensity (6000 W/m^2) vs shrinkage run (—) and no shrinkage run (---) with low light intensity (1200 W/m^2)

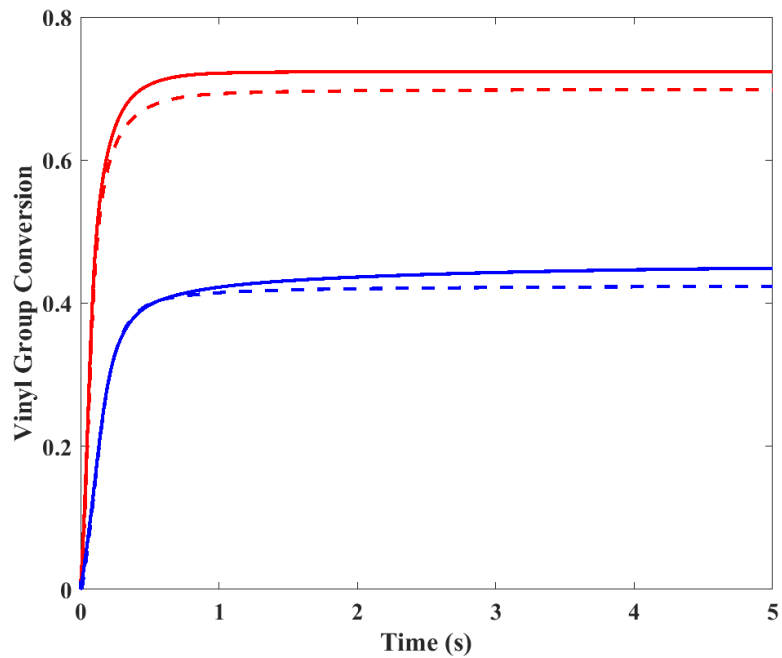


Fig. 3.11: Plot of shrinkage run (—) and no shrinkage run (---) with a high BAPO level (4 wt%) vs shrinkage run (—) and no shrinkage run (---) with a low BAPO level (1 wt%)

3.6 Conclusions

A fundamental model was developed to account for film shrinkage during the photopolymerization of HDDA with the bifunctional initiator BAPO in the presence of oxygen. This shrinkage arises because the polyHDDA is denser than the monomer. Partial differential equations were derived that account for a comprehensive reaction mechanism involving cyclization, crosslinking, backbiting, and oxygen inhibition. Local shrinkage and swelling within the film are accounted for using diffusion and reaction terms. The model relies on a dimensionless spatial coordinate w so that the moving-boundary PDE problem (in the original spatial coordinate z) becomes a fixed-boundary problem that can be solved using the traditional MATLAB “pdepe” solver. The resulting model tracks the concentrations of oxygen, HDDA monomer, BAPO initiator, free-radical end groups and pendant vinyl groups as a function of position and time.

Model predictions reveal that shrinkage has an important influence on predictions of overall vinyl-group conversion in the film. When conversion predictions are compared to those from a model that neglects shrinkage, discrepancies can reach up to 10%. Prediction discrepancies become larger for simulated experiments involving thin films ($8\ \mu\text{m}$) compared to thicker films ($18\ \mu\text{m}$). As well, discrepancies are larger for simulations with lower light intensities ($1200\ \text{W}/\text{m}^2$) compared to higher light intensities ($6000\ \text{W}/\text{m}^2$). In future, it will be important to re-estimate the kinetic parameters used in the model because these estimates were obtained from previous studies where shrinkage was ignored. We anticipate that the shrinkage model with updated parameters will lead to more reliable model predictions for use in process improvement studies.

3.7 Acknowledgements

We thank Luuk van der Velden, Robin Willemse and Marjolein van der Linden from Canon Production Printing for helpful technical advice. Financial support from MITACS is gratefully acknowledged by Anh-Duong Dieu Vo, Kaveh Abdi, and Kimberley B. McAuley. Financial support from the Natural Sciences and Engineering Research Council of Canada (NSERC) is also acknowledged by Kimberley B. McAuley. This project has received funding from the ECSEL Joint Undertaking (JU) under grant agreement No 876362. The JU receives support from the European Union's Horizon 2020 research and innovation programme and Austria, Belgium, Czech Republic, Finland, Germany, Italy, Latvia, Netherlands, Poland, and Switzerland.

3.8 Author Contributions

I, Alaa El Halabi, developed the software, wrote the original draft of this paper, and played a major part in conceptualizing shrinkage, developing the methodology and investigating the results. Kaveh Abdi provided support in formal analysis, software development, and review and editing. Anh-Duong Dieu Vo provided support also in formal analysis, conceptualization, software development and review and editing. Piet D. Iedema helped in conceptualization, project administration, and supervision. Kimberley B. McAuley is my supervisor and was of great help in conceptualization, funding acquisition, project administration and was the lead in review and editing of this paper.

Chapter 4

Summary, Conclusions and Recommendations

In Chapter 2, a PDE model for the photopolymerization of HDDA, which accounts for spatial variations and diffusive effects is proposed. This model was developed to predict the overall vinyl group conversion and to track different species concentrations throughout the film. Additionally, our collaborators at Canon Production Printing conducted experiments to measure the diffusivities of oxygen, HDDA monomer, and initiator in pure HDDA monomer. They also provided us with FTIR experimental data for photopolymerization experiments using a range of film thicknesses ($8 - 17 \mu m$), light intensities ($200 - 6000 W/m^2$), and initial BAPO concentrations ($1 - 4 wt\%$) to aid parameter estimation. These data were used to estimate six model parameters, three of which are oxygen-related kinetic parameters for the rates of propagation, crosslinking and termination of peroxidic radicals. The remaining three parameters are free volume parameters to account for the influence of monomer conversion on the diffusion coefficients of HDDA monomer, oxygen and initiator as polymerization proceeds. The resulting model provides accurate predictions for runs with different film thicknesses and light intensities, but underpredicts the overall vinyl group conversion for runs with a low BAPO level (i.e., $1 wt\%$). This is not surprising, because 30 out of the total 39 parameter values in the model were obtained from a previous modeling and parameter estimation study by Abdi et al. [15] that relied only on runs with high BAPO ($4 wt\%$). Based on the results from Chapter 2, I recommend that additional parameter estimation should be conducted in the future. Also, I recommend that BAPO diffusion can be ignored in future models, because accounting for the small amount of initiator diffusion that

occurred has negligible influence on model predictions. I also recommended that shrinkage should be considered in future models, which is the topic of Chapter 3.

In Chapter 3, a PDE model for the photopolymerization of HDDA that accounts for film shrinkage and spatial variations is proposed. The change in film thickness depends on the shrinkage caused by density changes when less-dense monomer is converted to denser polymer. A further complication is that monomer diffusion within the film due to concentration gradients causes motion within the film. Accounting for shrinkage (and diffusion) causes the resulting PDE model to become a moving boundary problem. Solving moving boundary problems can be computationally expensive and often requires complex numerical methods. Instead, I propose a coordinate transformation from the original spatial coordinate z (in meters) to a dimensionless spatial coordinate w that goes from 0 at the upper film surface to 1 at bottom boundary of the film. The proposed PDE model with the dimensionless spatial coordinate w is a fixed boundary problem that can be solved using MATLAB's standard PDE solver "pdepe". Implementing the new PDEs in MATLAB's "pdepe" requires some algebraic rearrangement and additional state variables, which are discussed thoroughly in section B4 in Appendix B. The resulting model can predict the overall vinyl-group conversion and individual species concentrations at different positions within the film. Comparisons of predicted vinyl-group conversions using models with and without shrinkage reveal that there is a noticeable influence of ~9 % when shrinkage is included. I have the following overall recommendations for the thesis:

- i.* Parameter estimation should be done again using the shrinkage model since previous parameter estimation was performed using a model where shrinkage was ignored;
- ii.* HDDA Monomer density is well known, but poly-HDDA (with high vinyl-group conversion) should be measured precisely so that accurate model predictions can be

obtained. Additional photopolymerization data, collected over a wide range of operating conditions, should also be obtained for use in future parameter estimation studies;

- iii.* If data are available for photopolymerization using additional monomers and photoinitiators, then the model equations should be extended to account for them. Estimation of the resulting new kinetic and diffusion parameters will be required so that accurate predictions can be obtained.

References

- [1] K. Anseth, S. Newman, and C. Bowman, "Polymeric dental composites: properties and reaction behavior of multimethacrylate dental restorations," in *Biopolymers II*, 1995: Springer, pp. 177-217.
- [2] K. A. Berchtold, J. Nie, J. W. Stansbury, B. Hacıoğlu, E. R. Beckel, and C. N. Bowman, "Novel monovinyl methacrylic monomers containing secondary functionality for ultrarapid polymerization: steady-state evaluation," *Macromolecules*, vol. 37, no. 9, pp. 3165-3179, 2004.
- [3] P. M. Johnson, T. B. Reynolds, J. W. Stansbury, and C. N. Bowman, "High throughput kinetic analysis of photopolymer conversion using composition and exposure time gradients," *Polymer*, vol. 46, no. 10, pp. 3300-3306, 2005.
- [4] J. B. Hutchison *et al.*, "Robust polymer microfluidic device fabrication via contact liquid photolithographic polymerization (CLiPP)," *Lab on a Chip*, vol. 4, no. 6, pp. 658-662, 2004.
- [5] M. D. Goodner and C. N. Bowman, "Development of a comprehensive free radical photopolymerization model incorporating heat and mass transfer effects in thick films," *Chemical Engineering Science*, vol. 57, no. 5, pp. 887-900, 2002.
- [6] L. G. Lovell, K. A. Berchtold, J. E. Elliott, H. Lu, and C. N. Bowman, "Understanding the kinetics and network formation of dimethacrylate dental resins," *Polymers for Advanced Technologies*, vol. 12, no. 6, pp. 335-345, 2001.
- [7] H. Lu, J. A. Carioscia, J. W. Stansbury, and C. N. Bowman, "Investigations of step-growth thiol-ene polymerizations for novel dental restoratives," *Dental Materials*, vol. 21, no. 12, pp. 1129-1136, 2005.
- [8] R. J. Zwiers and G. C. Dortant, "Aspherical lenses produced by a fast high-precision replication process using UV-curable coatings," *Applied optics*, vol. 24, no. 24, pp. 4483-4488, 1985.
- [9] T. T. McMahon and K. Zadnik, "Twenty-five years of contact lenses: the impact on the cornea and ophthalmic practice," *Cornea*, vol. 19, no. 5, pp. 730-740, 2000.
- [10] H. Ma, R. H. Davis, and C. N. Bowman, "A novel sequential photoinduced living graft polymerization," *Macromolecules*, vol. 33, no. 2, pp. 331-335, 2000.

- [11] V. S. Khire, T. Y. Lee, and C. N. Bowman, "Surface modification using thiol– acrylate conjugate addition reactions," *Macromolecules*, vol. 40, no. 16, pp. 5669-5677, 2007.
- [12] K. S. Anseth, A. T. Metters, S. J. Bryant, P. J. Martens, J. H. Elisseeff, and C. N. Bowman, "In situ forming degradable networks and their application in tissue engineering and drug delivery," *Journal of controlled release*, vol. 78, no. 1-3, pp. 199-209, 2002.
- [13] E. Anadioti, B. Kane, and E. Soulas, "Current and emerging applications of 3D printing in restorative dentistry," *Current oral Health reports*, vol. 5, pp. 133-139, 2018.
- [14] J. Young, S. Fox, and K. Anseth, "A novel device for producing three-dimensional objects," 1999.
- [15] K. Abdi *et al.*, "Mathematical modeling and parameter estimation for 1, 6-Hexanediol diacrylate photopolymerization with bifunctional initiator," *Chemical Engineering Science*, vol. 262, p. 118011, 2022.
- [16] A. D. D. Vo *et al.*, "Mathematical modelling for 1, 6-hexanediol diacrylate photopolymerization in presence of oxygen," *The Canadian Journal of Chemical Engineering*, vol. 101, no. 9, pp. 4807-4818, 2023.
- [17] A. El Halabi *et al.*, "Accounting for spatial variations during photopolymerization of 1, 6-hexane-diol diacrylate in the presence of oxygen," *AIChE Journal*, p. e18490, 2023.
- [18] P. Iedema, V. Schamböck, H. Boonen, J. Koskamp, S. Schellekens, and R. Willemse, "Photocuring of di-acrylate," *Chemical Engineering Science*, vol. 176, pp. 491-502, 2018.
- [19] F. C. TSE and O. C. Sandall, "Diffusion coefficients for oxygen and carbon dioxide in water at 25 C by unsteady state desorption from a quiescent liquid," *Chemical Engineering Communications*, vol. 3, no. 3, pp. 147-153, 1979.
- [20] G. Maria, "A review of algorithms and trends in kinetic model identification for chemical and biochemical systems," *Chemical and Biochemical Engineering Quarterly*, vol. 18, no. 3, pp. 195-222, 2004.
- [21] T. G. Dobre and J. G. S. Marcano, *Chemical engineering: Modeling, simulation and similitude*. John Wiley & Sons, 2007.
- [22] P. Érdi and J. Tóth, *Mathematical models of chemical reactions: theory and applications of deterministic and stochastic models*. Manchester University Press, 1989.
- [23] S. Asprey and S. Macchietto, "Statistical tools for optimal dynamic model building," *Computers & Chemical Engineering*, vol. 24, no. 2-7, pp. 1261-1267, 2000.

- [24] A. Torres-Knoop, I. Kryven, V. Schamboeck, and P. D. Iedema, "Modeling the free-radical polymerization of hexanediol diacrylate (HDDA): a molecular dynamics and graph theory approach," *Soft matter*, vol. 14, no. 17, pp. 3404-3414, 2018.
- [25] P. Iedema, V. Schamböck, H. Boonen, M. van der Linden, and R. Willemse, "Photocuring of di-acrylate in presence of oxygen," *Chemical Engineering Science*, vol. 207, pp. 130-144, 2019.
- [26] C. N. Bowman and C. J. Kloxin, "Toward an enhanced understanding and implementation of photopolymerization reactions," *AIChE Journal*, vol. 54, no. 11, pp. 2775-2795, 2008.
- [27] W. K. Neo and M. B. Chan-Park, "Application of a new model and measurement technique for dynamic shrinkage and conversion of multi-acrylates photopolymerized at different UV intensities," *Polymer*, vol. 48, no. 11, pp. 3337-3348, 2007.
- [28] J. E. Elliott, J. W. Anseth, and C. N. Bowman, "Kinetic modeling of the effect of solvent concentration on primary cyclization during polymerization of multifunctional monomers," *Chemical Engineering Science*, vol. 56, no. 10, pp. 3173-3184, 2001.
- [29] S. Li, C. Bian, Z. X. Liu, Y. N. Zhou, and Z. H. Luo, "Identifying the essential roles of light and sonication in dual-stimuli regulated bulk atom transfer radical polymerization by multiscale simulation," *AIChE Journal*, vol. 69, no. 10, p. e18155, 2023.
- [30] J. Jin, J. K. Guo, Y. N. Zhou, and Z. H. Luo, "Kinetic features of iron-based electrochemically mediated ATRP revealed by Monte Carlo simulation," *AIChE Journal*, vol. 67, no. 2, p. e17098, 2021.
- [31] E. Andrzejewska, "Photopolymerization kinetics of multifunctional monomers," *Progress in polymer science*, vol. 26, no. 4, pp. 605-665, 2001.
- [32] K. Taki, Y. Watanabe, T. Tanabe, H. Ito, and M. Ohshima, "Oxygen concentration and conversion distributions in a layer-by-layer UV-cured film used as a simplified model of a 3D UV inkjet printing system," *Chemical Engineering Science*, vol. 158, pp. 569-579, 2017.
- [33] C. Decker and A. D. Jenkins, "Kinetic approach of oxygen inhibition in ultraviolet-and laser-induced polymerizations," *Macromolecules*, vol. 18, no. 6, pp. 1241-1244, 1985.
- [34] A. K. O'Brien and C. N. Bowman, "Modeling the effect of oxygen on photopolymerization kinetics," *Macromolecular Theory and Simulations*, vol. 15, no. 2, pp. 176-182, 2006.

- [35] E. Andrzejewska, M. B. Bogacki, M. Andrzejewski, and M. Janaszczyk, "Termination mechanism during the photo-induced radical cross-linking polymerization in the presence and absence of oxygen," *Physical Chemistry Chemical Physics*, vol. 5, no. 12, pp. 2635-2642, 2003.
- [36] Z. Zhao, X. Mu, J. Wu, H. J. Qi, and D. Fang, "Effects of oxygen on interfacial strength of incremental forming of materials by photopolymerization," *Extreme Mechanics Letters*, vol. 9, pp. 108-118, 2016.
- [37] D. M. Grant and R. K. Harris, "Encyclopedia of Nuclear Magnetic Resonance, Advances in NMR," *Spectroscopy*, vol. 9, 1996.
- [38] V. Besse, M. A. Derbanne, T.-N. Pham, W. D. Cook, and L. Le Pluart, "Photopolymerization study and adhesive properties of self-etch adhesives containing bis (acyl) phosphine oxide initiator," *Dental Materials*, vol. 32, no. 4, pp. 561-569, 2016.
- [39] K. A. McLean and K. B. McAuley, "Mathematical modelling of chemical processes—obtaining the best model predictions and parameter estimates using identifiability and estimability procedures," *The Canadian Journal of Chemical Engineering*, vol. 90, no. 2, pp. 351-366, 2012.
- [40] A. D. D. Vo, A. Shahmohammadi, and K. B. McAuley, "Model-based design of experiments for polyether production from bio-based 1, 3-propanediol," *AIChE Journal*, vol. 67, no. 11, p. e17394, 2021.
- [41] A. El Halabi *et al.*, "Accounting for Spatial Variations during Photopolymerization of 1, 6-hexane-diol Diacrylate in the Presence of Oxygen," *Authorea Preprints*, 2023.
- [42] L. Ji, W. Chang, M. Cui, and J. Nie, "Photopolymerization kinetics and volume shrinkage of 1, 6-hexanediol diacrylate at different temperature," *Journal of Photochemistry and Photobiology A: Chemistry*, vol. 252, pp. 216-221, 2013.
- [43] P. M. Johnson, J. W. Stansbury, and C. N. Bowman, "Kinetic modeling of a comonomer photopolymerization system using high-throughput conversion data," *Macromolecules*, vol. 41, no. 1, pp. 230-237, 2008.
- [44] X. Liu, F. Mizutani, and M. Nomura, "Study on the Rate of Seeded Emulsion Copolymerization of Styrene and Acrylonitrile Using Polystyrene Latex Particles as Seed," *Industrial & Engineering Chemistry Research*, vol. 53, no. 2, pp. 664-671, 2014.

- [45] I. E. Ruyter and I. J. Sjoevik, "Composition of dental resin and composite materials," *Acta Odontologica Scandinavica*, vol. 39, no. 3, pp. 133-146, 1981.
- [46] J. Stansbury and W. Bailey, "Evaluation of spiro orthocarbonate monomers capable of polymerization with expansion as ingredients in dental composite materials," in *Progress in biomedical polymers*: Springer, 1990, pp. 133-139.
- [47] D. Tilbrook, R. Clarke, N. Howle, and M. Braden, "Photocurable epoxy-polyol matrices for use in dental composites I," *Biomaterials*, vol. 21, no. 17, pp. 1743-1753, 2000.
- [48] Q. Wan, S. R. Schricker, and B. M. Culbertson, "Methacryloyl derivitized hyperbranched polyester. 2. Photo-polymerization and properties for dental resin systems," 2000.
- [49] L.-A. Linden and J. Jakubiak, "Contraction (shrinkage) in polymerization. Part II: dental resin composites," 2001.
- [50] S. Balke and A. Hamielec, "Bulk polymerization of methyl methacrylate," *Journal of applied Polymer science*, vol. 17, no. 3, pp. 905-949, 1973.
- [51] B. M. Louie, G. M. Carratt, and D. S. Soong, "Modeling the free radical solution and bulk polymerization of methyl methacrylate," *Journal of applied polymer science*, vol. 30, no. 10, pp. 3985-4012, 1985.
- [52] J. W. Stansbury, "Dimethacrylate network formation and polymer property evolution as determined by the selection of monomers and curing conditions," *Dental Materials*, vol. 28, no. 1, pp. 13-22, 2012.
- [53] D. Victoria-Valenzuela, J. Herrera-Ordonez, and G. Luna-Barcenas, "Toward a General Methodology for Modeling Diffusive-Controlled Reactions in Free Radical Polymerization," *Macromolecular Theory and Simulations*, vol. 25, no. 1, pp. 28-44, 2016.
- [54] M. D. Goodner, H. R. Lee, and C. N. Bowman, "Method for determining the kinetic parameters in diffusion-controlled free-radical homopolymerizations," *Industrial & engineering chemistry research*, vol. 36, no. 4, pp. 1247-1252, 1997.
- [55] M. Wenand and A. V. McCormick, "A kinetic model for radical trapping in photopolymerization of multifunctional monomers," *Macromolecules*, vol. 33, no. 25, pp. 9247-9254, 2000.
- [56] K. S. Anseth and C. N. Bowman, "Reaction diffusion enhanced termination in polymerizations of multifunctional monomers," *Polymer reaction engineering*, vol. 1, no. 4, pp. 499-520, 1993.

- [57] R. A. Hutchinson, "Modeling of free-radical polymerization kinetics with crosslinking for methyl methacrylate/ethylene glycol dimethacrylate," *Polymer reaction engineering*, vol. 1, no. 4, pp. 521-577, 1993.
- [58] W. Huang and R. D. Russell, "Moving mesh strategy based on a gradient flow equation for two-dimensional problems," *SIAM Journal on Scientific Computing*, vol. 20, no. 3, pp. 998-1015, 1998.
- [59] J. Shen and X. Yang, "An efficient moving mesh spectral method for the phase-field model of two-phase flows," *Journal of computational physics*, vol. 228, no. 8, pp. 2978-2992, 2009.
- [60] E. J. Holm and H. P. Langtangen, "A unified finite element model for the injection molding process," *Computer Methods in Applied Mechanics and Engineering*, vol. 178, no. 3-4, pp. 413-429, 1999.
- [61] G. D. Verros, D. S. Achilias, and G. I. Giannoukos, "Development of a comprehensive mathematical model for free radical suspension polymerization of methyl methacrylate," *Polymer Engineering & Science*, vol. 51, no. 4, pp. 670-678, 2011.
- [62] K. Z. Yao and K. B. McAuley, "Simulation of continuous solid-phase polymerization of nylon 6, 6 (II): processes with moving bed level and changing particle properties," *Chemical engineering science*, vol. 56, no. 18, pp. 5327-5342, 2001.
- [63] H. John, I. Lienhard, and V. Lienhard, "A heat transfer textbook," *Phlogiston Press, Cambridge*, 2008.
- [64] H. A. Boonen, J. A. Koskamp, W. Theiss, P. D. Iedema, and R. X. Willemse, "Simultaneous real-time analysis of bulk and bottom cure of ultraviolet-curable inks using fourier transform infrared spectroscopy," *Applied Spectroscopy*, vol. 71, no. 12, pp. 2699-2706, 2017.

Appendix A

Supplementary Information - Chapter 2

A1 Custom-built Oxygen Measurement Enclosure

The custom-built oxygen measurement enclosure is described in the schematic below. This setup starts by purging all oxygen from the system by a nitrogen gas flow. Right after, atmospheric oxygen is let back into the system where it is allowed to diffuse through the sample container. At the bottom of the container, the optical sensor detects oxygen concentrations, and with that information, a plot of oxygen diffusion with time can be plotted. The boundary conditions used to calculate the oxygen diffusion coefficient can also be found below.

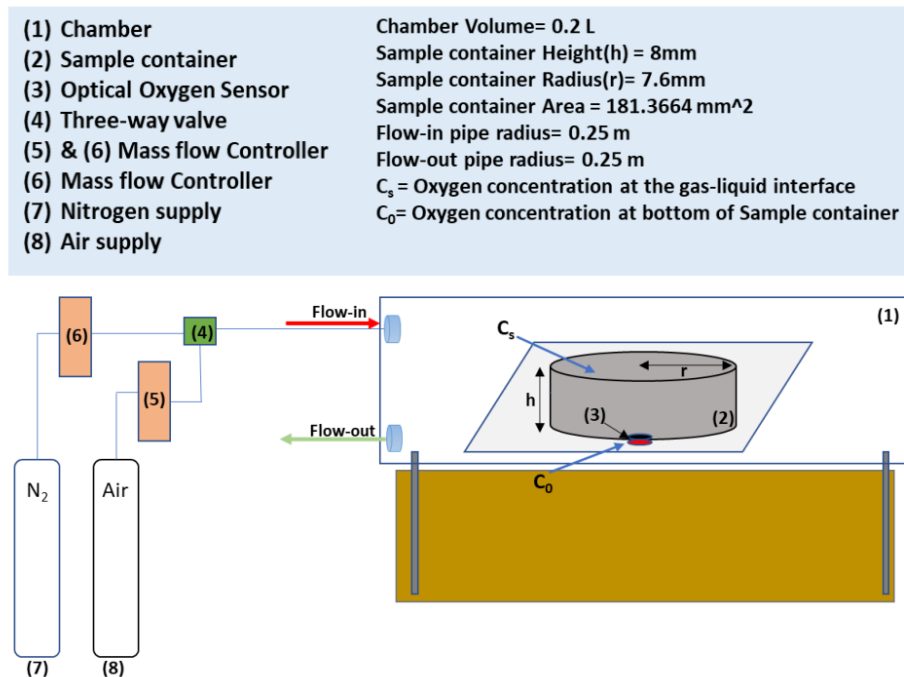


Fig. A.1: Oxygen Sensor Schematic

Table A.1: Initial and boundary conditions for solving Fick's second law [63].

Initial Condition	Boundary Conditions
At $t = 0$ $[O_2] = 0$	At $z = 0$ (i.e., at top film surface) $[O_2] = H_s^{cp} P_{O_2}$ Where $P_{O_2} = 2.128 \times 10^4 Pa$ At $z = z_f$ (i.e., at the film bottom) $\frac{\partial [O_2]}{\partial z} = 0$

A2 DOSY NMR

Fig. A.2 shows the DOSY NMR results of BAPO (1% by weight) and HDDA in a HDDA monomer medium. Six NMR peaks for BAPO and six NMR peaks for HDDA obtained at 25°C were used for determining the diffusion coefficients. The individual diffusion coefficients for each peak were calculated and then their average was reported as the final measured diffusivity.

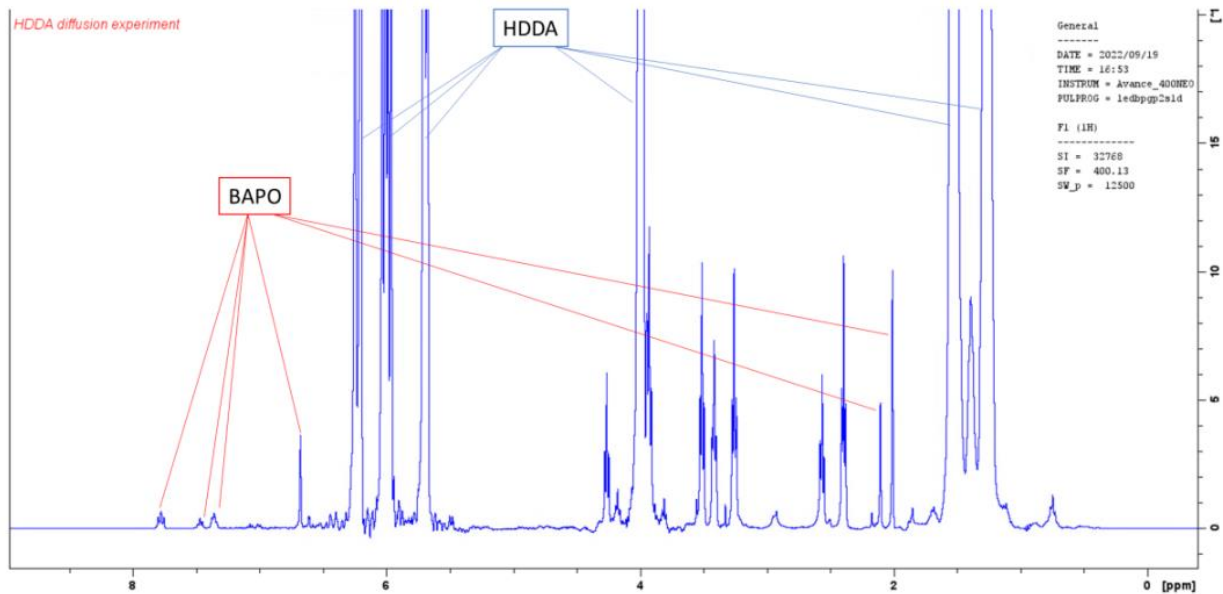


Fig. A.2: 1D-dosy at 10% gradient strength with 1% BAPO in HDDA.

A3 Film Thickness Measurements

Film thickness is calculated from the interference pattern from near-infrared (NIR) reflectance measurements. The sinusoid of the interference pattern in the obtained spectra is fitted from the following equation:

$$y = A\sin(\omega x + \varphi) + B \quad (\text{A.1})$$

where A is amplitude, ω is angular frequency, φ is phase shift and B is offset. After the angular frequency is obtained, the thickness of the film is calculated using:

$$h = \frac{\omega}{4\pi\sqrt{(n_1)^2 - (n_2)^2\sin^2\theta}} \quad (\text{A.2})$$

where n_1 is the refractive index of the HDDA film (estimated to be 1.55), n_2 is the refractive index of the surrounding air ($n_2 = 1.00$), θ is the angle of the incidence light. The NIR spectra were recorded with the NIR Quest 256-2.5 spectrometer (Ocean Optics) with a 600 μm VIS/NIR reflection probe and halogen light source HL-2000-FHSA (Ocean Optics). Fig. S3 shows a typical example of the interference pattern in the NIR spectrum of a smooth HDDA layer and a schematic of how the incident light is used to calculate the thickness of the film.

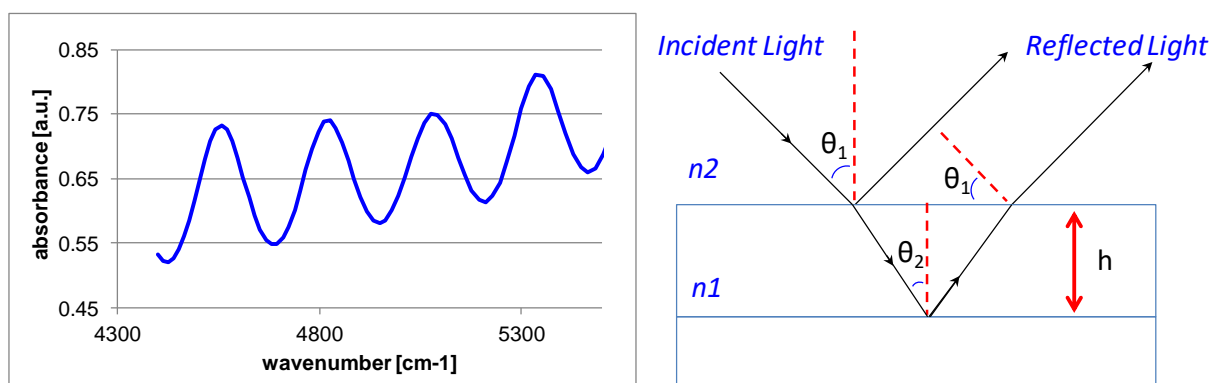


Fig. A.3: Calculation of the layer thickness using NIR spectra. the clear interference pattern in the NIR spectrum is shown on the left; A schematic presentation of the interference pattern and the angles is shown on the right.

A4 Data Collection

The Fourier Transform Infrared equipment used for the measurements, detailed in Boonen et. Al [64], employs a Bruker Vertex 80 FT-IR spectrometer to simultaneously record real-time IR spectra in ATR and transmission at a frequency of 10 spectra per second. The IR beam is divided into two parts, one for transmission measurement and the other for ATR measurement. A HDDA layer with the desired thickness is placed on the temperature-controlled (25°C) single reflection Germanium ATR unit. This layer is then exposed to 405 nm UV light from a LED lamp (Phoseon Technology FireFly FF20050x20A, C405). Then the transmission data provides information about the average bulk cure. The spectra are normalized by the C=O bond at 1720 cm^{-1} to account for changes in density and refractive index during the curing process. Further details are provided elsewhere [15, 25, 64].

A5 Reaction scheme

Fig. A.4 presents the reactions involving free-radical end groups that arise in this model. Note that the ester ligands (containing vinyl groups) that are attached to carbons 1, 3 and 5 in Fig. A.4d are shown in a simplified fashion as “_____//”.

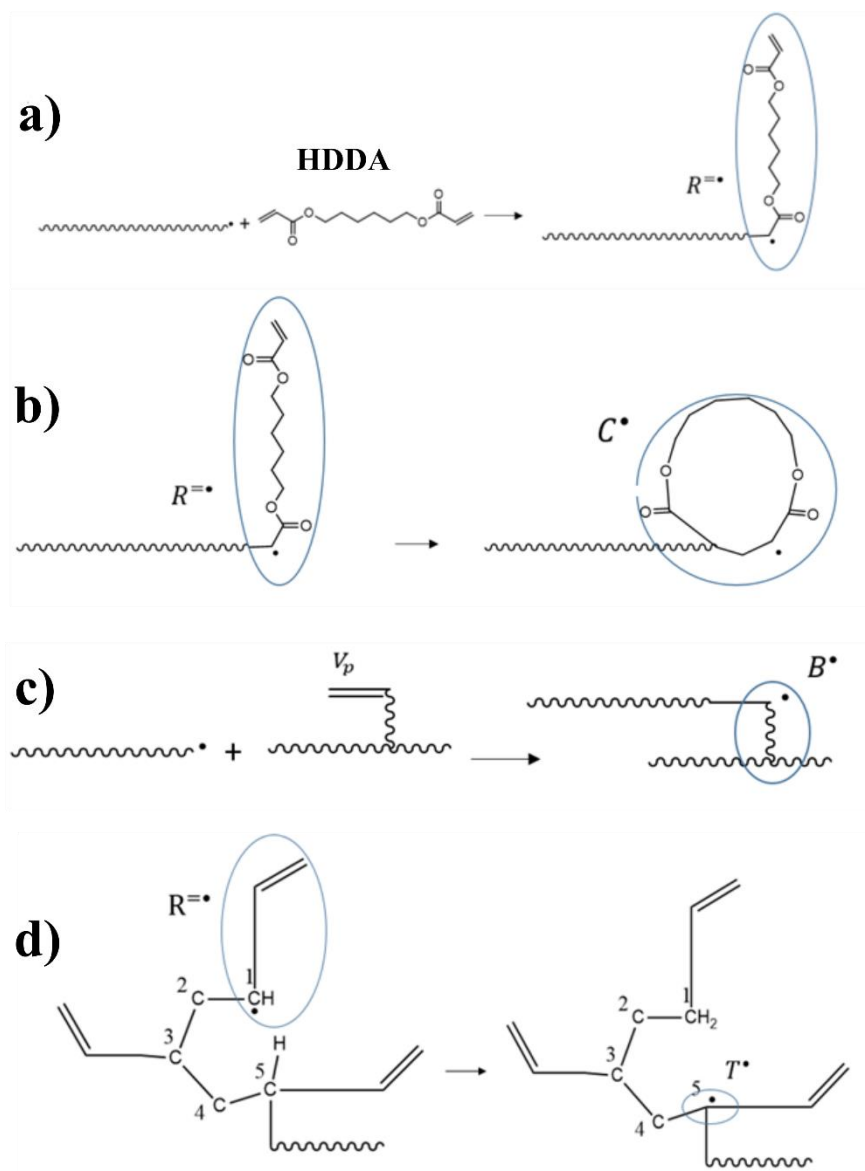


Fig. A.4: Formation of different macroradicals: a) regular radical ends R^\bullet , b) cyclized radical ends C^\bullet , c) crosslinking radical ends B^\bullet , d) tertiary radical ends T^\bullet [15, 16]

A6 List of reactions, assumptions, PDEs and their initial and boundary conditions.

Table A.2 provides the list of all the assumptions made to attain the proposed model. The list of all the reactions involved in the proposed model for the photopolymerization of HDDA in the presence of oxygen is provided in Table A.3. Table A.4 provides a list of Algebraic equations for different model parameters.

Table A.5 presents a list of the 13 PDEs used in the model. Equations 5.1 to 5.10 are dynamic material balances on the initiator I , unreacted initiator fragments \tilde{I} , monomer M , pendant vinyl groups V_p , dissolved oxygen, and free radicals of types R^{\bullet} , C^{\bullet} , B^{\bullet} , T^{\bullet} and O^{\bullet} , respectively. Notice that the balances on monomer, initiator and oxygen contain diffusion terms, but balances on the polymeric species (i.e., \tilde{I} , V_p , R^{\bullet} , C^{\bullet} , B^{\bullet} , T^{\bullet} and O^{\bullet}) do not (see assumption 1 in Table A.2). Details concerning the derivations of Equations 5.1 and 5.8 are provided in section A7 below. The other PDEs in Table A.5 are derived in a similar fashion.

Table A.6 provides the initial and boundary conditions for the material balance PDEs in Table A.5. Equations (5.3 - 5.5) are PDEs that were replaced by algebraic equations using the steady state hypothesis, hence there is no need to define their initial and boundary conditions. As shown in the boundary conditions of Equation (6.1), no diffusion occurs through the bottom surface of the film (at $z = z_f$). The diffusion boundary condition of the oxygen at the top surface of the film, required for Equation (6.8) is derived from Henry's law, where the Henry's law constant is determined experimentally in section titled "Measurement of the diffusion coefficient of oxygen in HDDA" in the paper.

Table A.2: Model Assumptions [15, 16]

-
- 1 The monomer/polymer is a single-phase film with constant density (i.e., shrinkage due to polymerization is negligible). Oxygen, monomer and initiator are able to diffuse within the film, but polymeric molecules cannot, due to their large size.
 - 2 Temperature is constant at 25 °C.
 - 3 The initiator moieties remaining after initiator decomposition have the same absorbance properties as the initiator.
 - 4 Radicals of type \tilde{I}^\bullet are consumed by initiation reactions and termination reactions before their weak carbon-phosphorous bond has an opportunity to break. This assumption is valid because the rate of consumption of the free radical on \tilde{I}^\bullet is typically 10^9 times faster than the rate of dissociation of the weak carbon-phosphorous bond.
 - 5 In this terminal model, reaction rates depend only on the types of end groups on polymer chains. Penultimate effects are neglected.
 - 6 The effect of stabilizer is neglected.
 - 7 End groups of type R^\bullet contain a vinyl group and a free radical. It is assumed that the short-lived free radical is consumed much more rapidly than the corresponding vinyl group. When the radical on R^\bullet is consumed by propagation, crosslinking, backbiting and termination reactions, the corresponding vinyl group on R^\bullet becomes a pendant vinyl group that can participate in subsequent reactions. This assumption is valid because the rate of consumption of a pendant vinyl group is $\sim 10^5$ times slower than the rate of consumption of the corresponding radical.
-

-
- 8 Chain-transfer to monomer and chain-transfer to polymer are neglected.
- 9 Carbon-centered and phosphorous-centered initiator radicals have similar relative propensities when reacting with pendant vinyl groups compared with monomeric vinyl groups (i.e., $\frac{k_{in,IVP0}}{k_{in,IM0}} = \frac{k_{in,\tilde{I}VP0}}{k_{in,\tilde{I}M0}}$).
- 10 All phosphorous-centered radicals have the same kinetically-controlled reactivity, independent of whether they are generated by initiator decomposition or decomposition of initiator moieties \tilde{I} attached to polymer molecules (i.e., $k_{in,\tilde{I}M0} = k_{in,IpM0}$ and $k_{in,\tilde{I}VP0} = k_{in,IpVP0}$).
- 11 The kinetically dependent rate coefficient for self-termination reactions involving two phosphorous-centered radicals \tilde{I}^\bullet and I_p^\bullet are the same (i.e., $k_{t_{in,\tilde{I}I0}} = k_{t_{in,IpI0}}$).
- 12 Self-termination reactions for initiator radicals (i.e., I^\bullet , \tilde{I}^\bullet , and I_p^\bullet) are ignored so that the stationary state hypothesis can be readily applied to compute the concentrations of these short-lived radicals. Cross-termination reactions between I^\bullet and \tilde{I}^\bullet and between I^\bullet and I_p^\bullet are ignored in the balance on I^\bullet .
- 13 All macroradicals have the same relative propensities for crosslinking and propagation reactions (i.e., $\frac{k_{b,R0}}{k_{p,R0}} = \frac{k_{b,B0}}{k_{p,B0}} = \frac{k_{b,C0}}{k_{p,C0}} = \frac{k_{b,T0}}{k_{p,T0}} = \frac{k_{b,O0}}{k_{p,O0}}$).
- 14 Cyclization reactions may occur between a radical end R^\bullet and its vinyl group, but not with other vinyl groups on the polymer.
-

-
- 15 The only radical ends that participate in backbiting reactions are R^{\bullet} , C^{\bullet} , and O^{\bullet} . Backbiting generates tertiary radicals T^{\bullet} .
- 16 Termination reactions involving two secondary macroradicals are termination-by-combination reactions.
- 17 Termination reactions involving tertiary radical T^{\bullet} and other radicals are termination-by-disproportionation reactions.
- 18 Rate constants for cross-termination of radicals are obtained using the geometric mean of the corresponding self-termination rate constants.
- 19 The reactivity of terminal vinyl groups (which result from termination by disproportionation) is the same as the reactivity of pendant vinyl groups.
- Initiation reactions involving small initiator fragments I^{\bullet} and \tilde{I}^{\bullet} are kinetically-controlled rather than diffusionally-controlled. Diffusion-control is considered for initiation involving polymeric initiator fragments I_p^{\bullet} . Reactions between all radicals and oxygen, which is a small molecule, are kinetically-controlled rather than diffusionally-controlled. Backbiting and cyclization are also kinetically-controlled. Crosslinking and termination reactions are diffusionally-controlled because they involve two large molecules. Propagation is also diffusionally-controlled because the parameter estimation study by Abdi et al. showed that accounting for diffusional effects for propagation rate constants resulted in a noticeable improvement in model fit to the data [2].
- 20
- 21 Reaction diffusion, which influences termination rates, occurs predominantly by consumption of monomer vinyl groups rather than pendant vinyl groups.
-

22 The free volume fraction of the film v_f is assumed to change linearly with monomer conversion X_M .

23 To reduce the number of free-volume parameters in the model, reactions are divided into three classes: *i*) propagation reactions involving a small monomer molecule and a free-radical on a large molecule, *ii*) crosslinking reactions involving two large molecules, and *iii*) termination reactions involving two large molecules. Each class has its own free-volume parameters, and free-volume parameters are assumed to be the same for all reactions within a class. Further, the initiator efficiencies f and \tilde{f} are assumed to have the same free-volume parameters.

24 All radicals have the same relative propensities for oxygen incorporation compared to their corresponding propensities for propagation or initiation with monomer.

$$\left(\text{i.e., } \frac{k_{O_2,R0}}{k_{p,R0}} = \frac{k_{O_2,B0}}{k_{p,B0}} = \frac{k_{O_2,C0}}{k_{p,C0}} = \frac{k_{O_2,T0}}{k_{p,T0}} = \frac{k_{O_2,I0}}{k_{in,IM0}} = \frac{k_{O_2,I0}}{k_{in,IM0}} = \frac{k_{O_2,IP0}}{k_{in,IPM0}}\right).$$

25 Peroxidic radicals have the same relative propensities for backbiting and propagation reactions compared to the corresponding backbiting and propagation reactions of R^{\bullet} (i.e.,

$$\frac{k_{bb,O0}}{k_{p,O0}} = \frac{k_{bb,R0}}{k_{p,R0}})$$

26 Peroxy groups within polymer molecules, which are created by propagation of peroxy radicals, do not decompose to produce radicals over the duration of the experiments. Also, hydroperoxide end groups, which result from backbiting reactions of peroxidic radicals, do not decompose to produce radicals during the experiments.

Table A.3: List of reactions of the photopolymerization of HDDA in the presence of oxygen

Reaction Description	Reaction	
Decomposition	$I \xrightarrow{2k_d} fI^\bullet + f\tilde{I}^\bullet$	(R1)
	$\tilde{I} \xrightarrow{k_{\tilde{d}}} \tilde{f}I^\bullet + \tilde{f}I_P^\bullet$	(R2)
Initiation	$I^\bullet + M \xrightarrow{2k_{in,IM}} R^{\bullet}$	(R3)
	$\tilde{I}^\bullet + M \xrightarrow{2k_{in,IM}} R^{\bullet} + \tilde{I}$	(R4)
	$I_P^\bullet + M \xrightarrow{2k_{in,IPM}} R^{\bullet}$	(R5)
	$I^\bullet + V_P \xrightarrow{k_{in,IVP}} B^\bullet$	(R6)
	$\tilde{I}^\bullet + V_P \xrightarrow{k_{in,\tilde{I}VP}} B^\bullet + \tilde{I}$	(R7)
	$I_P^\bullet + V_P \xrightarrow{k_{in,IPVP}} B^\bullet$	(R8)
Propagation	$R^{\bullet} + M \xrightarrow{2k_{p,R}} R^{\bullet} + V_P$	(R9)
	$C^\bullet + M \xrightarrow{2k_{p,C}} R^{\bullet}$	(R10)
	$B^\bullet + M \xrightarrow{2k_{p,B}} R^{\bullet}$	(R11)
Branching and Crosslinking	$T^\bullet + M \xrightarrow{2k_{p,T}} R^{\bullet}$	(R12)
	$R^{\bullet} + V_P \xrightarrow{k_{b,R}} B^\bullet + V_P$	(R13)
	$C^\bullet + V_P \xrightarrow{k_{b,C}} B^\bullet$	(R14)
	$B^\bullet + V_P \xrightarrow{k_{b,B}} B^\bullet$	(R15)
	$T^\bullet + V_P \xrightarrow{k_{b,T}} B^\bullet$	(R16)

Cyclization	$R^{\bullet} \xrightarrow{k_C} C^{\bullet}$	(R17)
Backbiting	$R^{\bullet} \xrightarrow{k_{bb}} T^{\bullet} + V_P$	(R18)
	$C^{\bullet} \xrightarrow{k_{bb}} T^{\bullet}$	(R19)
Termination	$I^{\bullet} + C^{\bullet} \xrightarrow{k_{t,IC}} D$	(R20)
	$I^{\bullet} + B^{\bullet} \xrightarrow{k_{t,IB}} D$	(R21)
	$I^{\bullet} + T^{\bullet} \xrightarrow{k_{t,IT}} D$	(R22)
	$\tilde{I}^{\bullet} + C^{\bullet} \xrightarrow{k_{t,\tilde{I}C}} D + \tilde{I}$	(R23)
	$\tilde{I}^{\bullet} + B^{\bullet} \xrightarrow{k_{t,\tilde{I}B}} D + \tilde{I}$	(R24)
	$\tilde{I}^{\bullet} + T^{\bullet} \xrightarrow{k_{t,\tilde{I}T}} D + \tilde{I}$	(R25)
	$I_p^{\bullet} + C^{\bullet} \xrightarrow{k_{t,I_pC}} D$	(R26)
	$I_p^{\bullet} + B^{\bullet} \xrightarrow{k_{t,I_pB}} D$	(R27)
	$I_p^{\bullet} + T^{\bullet} \xrightarrow{k_{t,I_pT}} D$	(R28)
	$R^{\bullet} + R^{\bullet} \xrightarrow{k_{t,RR}} D + 2V_P$	(R29)
	$C^{\bullet} + C^{\bullet} \xrightarrow{k_{t,CC}} D$	(R30)
	$B^{\bullet} + B^{\bullet} \xrightarrow{k_{t,BB}} D$	(R31)
	$T^{\bullet} + T^{\bullet} \xrightarrow{k_{t,TT}} 2D + V_P$	(R32)
	$R^{\bullet} + C^{\bullet} \xrightarrow{k_{t,RC}} D + V_P$	(R33)
$R^{\bullet} + B^{\bullet} \xrightarrow{k_{t,RB}} D + V_P$	(R34)	

	$R^{\bullet} + T^{\bullet} \xrightarrow{k_{t,RT}} 2D + 2V_P$	(R35)
	$C^{\bullet} + B^{\bullet} \xrightarrow{k_{t,CB}} D$	(R36)
	$C^{\bullet} + T^{\bullet} \xrightarrow{k_{t,CT}} 2D + V_P$	(R37)
	$B^{\bullet} + T^{\bullet} \xrightarrow{k_{t,BT}} 2D + V_P$	(R38)
Oxygen Incorporation	$I^{\bullet} + O_2 \xrightarrow{k_{O_2,I}} O^{\bullet}$	(R39)
	$\tilde{I}^{\bullet} + O_2 \xrightarrow{k_{O_2,\tilde{I}}} O^{\bullet} + \tilde{I}$	(R40)
	$I_P^{\bullet} + O_2 \xrightarrow{k_{O_2,I_P}} O^{\bullet}$	(R41)
	$R^{\bullet} + O_2 \xrightarrow{k_{O_2,R}} O^{\bullet} + V_P$	(R42)
	$B^{\bullet} + O_2 \xrightarrow{k_{O_2,B}} O^{\bullet}$	(R43)
	$C^{\bullet} + O_2 \xrightarrow{k_{O_2,C}} O^{\bullet}$	(R44)
	$T^{\bullet} + O_2 \xrightarrow{k_{O_2,T}} O^{\bullet}$	(R45)
Propagation of peroxidic radicals (slow)	$O^{\bullet} + M \xrightarrow{2k_{p,O}} R^{\bullet}$	(R46)
	$O^{\bullet} + V_P \xrightarrow{k_{b,O}} B^{\bullet}$	(R47)
Backbiting of peroxidic radicals	$O^{\bullet} \xrightarrow{k_{bb,O}} T^{\bullet}$	(R48)
Termination of peroxidic radicals	$O^{\bullet} + O^{\bullet} \xrightarrow{k_{t,OO}} D + O_2$	(R49)
	$O^{\bullet} + I^{\bullet} \xrightarrow{k_{t,IO}} D$	(R50)
	$O^{\bullet} + \tilde{I}^{\bullet} \xrightarrow{k_{t,I\tilde{O}}} D + \tilde{I}$	(R51)
	$O^{\bullet} + I_P^{\bullet} \xrightarrow{k_{t,I_P O}} D$	(R52)

	$O^\bullet + R^\bullet \xrightarrow{k_{t,RO}} D + V_p$	(R53)
	$O^\bullet + B^\bullet \xrightarrow{k_{t,BO}} D$	(R54)
	$O^\bullet + C^\bullet \xrightarrow{k_{t,CO}} D$	(R55)
	$O^\bullet + T^\bullet \xrightarrow{k_{t,TO}} D$	(R56)

Table A.4: List of Algebraic Equations

4.1	$I_l = I_{l,0} e^{-\varepsilon[I]_0 z}$	[5]
4.2	$k_d = \frac{\varepsilon \phi \lambda I_l}{N_A h c}$	[5]
4.3	$v_f = v_{f,0} + (v_{f,1} - v_{f,0}) X_M$	[54]
4.4	$f = \frac{1}{\left[1 - \left(1 - \frac{1}{f_0} \right) e^{A_f \left(\frac{1}{v_f} - \frac{1}{v_{f,0}} \right)} \right]}$	[55]
4.5	$k_{in,j} = \frac{k_{in,j_0}}{\left[1 + e^{A_{in,j} \left(\frac{1}{v_f} - \frac{1}{v_{fc,in,j}} \right)} \right]}$	[56]
4.6	$k_{p,j} = \frac{k_{p,j_0}}{\left[1 + e^{A_p \left(\frac{1}{v_f} - \frac{1}{v_{fc,p,j}} \right)} \right]}$	[56]
4.7	$k_{b,j} = \frac{k_{b,j_0}}{\left[1 + e^{A_b \left(\frac{1}{v_f} - \frac{1}{v_{fc,b}} \right)} \right]}$	[56]
4.8	$k_c = \frac{k_{c_0}}{\left[1 + e^{A_c \left(\frac{1}{v_f} - \frac{1}{v_{fc,c}} \right)} \right]}$	[56]

$$4.9 \quad k_{bb,j} = \frac{k_{bb,j_0}}{\left[1 + e^{A_{bb}\left(\frac{1}{v_f} - \frac{1}{v_{fc,bb}}\right)}\right]} \quad [56]$$

$$4.10 \quad k_{t_{in,jj}} = \frac{k_{t_{in,jj_0}}}{\left[1 + e^{A_{t,in,jj}\left(\frac{1}{v_f} - \frac{1}{v_{fc,t,jj}}\right)}\right]} \quad [56]$$

$$4.11 \quad k_{t,ij} = \sqrt{k_{t,ii} k_{t,jj}} \quad [57]$$

$$4.12 \quad k_{t,RR} = k_{t,RR_0} \left[1 + \frac{1}{e^{-A_{t,jj}\left(\frac{1}{v_f} - \frac{1}{v_{fc,t,jj}}\right)} + \frac{R_{rd}k_{p,RM}[M]}{k_{t,RR_0}}}\right]^{-1} \quad [39]$$

$$4.13 \quad D_X = D_{X_{HDDA}} \exp\left[-A_X\left(\frac{1}{v_f} - \frac{1}{v_{f_0}}\right)\right] \quad [16]$$

Table A.5: Material balances for chemical species and end-groups developed by Vo et al. [16]. These equations are solved along with Equations 2, 3 and 4 using PDEPE solver in MATLAB.

$$5.1 \quad \frac{\partial[\tilde{I}]}{\partial t} = -k_{\tilde{d}}[\tilde{I}] + 2k_{in,\tilde{I}M}[\tilde{I}^{\bullet}][M] + k_{in,\tilde{I}V_p}[\tilde{I}^{\bullet}][V_p] + k_{t,\tilde{I}R}[\tilde{I}^{\bullet}][R^{\bullet}] + k_{t,\tilde{I}B}[\tilde{I}^{\bullet}][B^{\bullet}] +$$

$$k_{t,\tilde{I}C}[\tilde{I}^{\bullet}][C^{\bullet}] + k_{t,\tilde{I}T}[\tilde{I}^{\bullet}][T^{\bullet}] + k_{t,\tilde{I}O}[\tilde{I}^{\bullet}][O^{\bullet}] + k_{t,\tilde{I}I}[\tilde{I}^{\bullet}][I^{\bullet}] + k_{t,\tilde{I}\tilde{I}}[\tilde{I}^{\bullet}][\tilde{I}^{\bullet}] +$$

$$k_{t,\tilde{I}I_p}[\tilde{I}^{\bullet}][I_p^{\bullet}] + k_{O_2,\tilde{I}}[\tilde{I}^{\bullet}][O_2]$$

$$5.2 \quad \frac{\partial[I^{\bullet}]}{\partial t} = 2fk_d[I] + \tilde{f}k_{\tilde{d}}[\tilde{I}] - 2k_{in,IM}[M] - k_{in,IV_p}[V_p] - k_{t,IR}[R^{\bullet}] - k_{t,IB}[B^{\bullet}] -$$

$$k_{t,IC}[C^{\bullet}] - k_{t,IT}[T^{\bullet}] - k_{t,IO}[O^{\bullet}] - k_{O_2,I}[O_2]$$

which becomes, after applying SSH:

$$[I^\bullet] = \frac{2fk_d[I] + \tilde{f}k_{\tilde{d}}[\tilde{I}]}{\left(\begin{array}{l} + 2k_{in,IM}[M] + k_{in,IV_P}[V_P] \\ + k_{t,IR}[R^{\bullet}] + k_{t,IB}[B^\bullet] + k_{t,IC}[C^\bullet] + k_{t,IT}[T^\bullet] \\ + k_{t,IO}[O^\bullet] + k_{O_2,I}[O_2] \end{array} \right)}$$

$$5.3 \quad \frac{\partial [I^\bullet]}{\partial t} = 2fk_d[I] - 2k_{in,IM}[M] - k_{in,IV_P}[V_P] - k_{t,IR}[R^{\bullet}] - k_{t,IB}[B^\bullet] - k_{t,IC}[C^\bullet] - \\ k_{t,IT}[T^\bullet] - k_{t,II}[I^\bullet] - k_{t,IO}[O^\bullet] - k_{O_2,I}[O_2]$$

which becomes, after applying SSH:

$$[\tilde{I}^\bullet] = \frac{2fk_d[I]}{\left(\begin{array}{l} + 2k_{in,IM}[M] + k_{in,IV_P}[V_P] \\ + k_{t,\tilde{I}R}[R^{\bullet}] + k_{t,\tilde{I}B}[B^\bullet] + k_{t,\tilde{I}C}[C^\bullet] + k_{t,\tilde{I}T}[T^\bullet] + k_{t,\tilde{I}I}[I^\bullet] \\ + k_{t,\tilde{I}O}[O^\bullet] + k_{O_2,\tilde{I}}[O_2] \end{array} \right)}$$

$$5.4 \quad \frac{\partial [I_P^\bullet]}{\partial t} = \tilde{f}k_{\tilde{d}}[\tilde{I}] - 2k_{in,I_P M}[M] - k_{in,I_P V_P}[V_P] - k_{t,I_P R}[R^{\bullet}] - k_{t,I_P B}[B^\bullet] - k_{t,I_P C}[C^\bullet] - \\ k_{t,I_P T}[T^\bullet] - k_{t,I_P I}[I^\bullet] - k_{t,\tilde{I}I_P}[\tilde{I}^\bullet] - k_{t,I_P O}[O^\bullet] - k_{O_2,I_P}[O_2]$$

which becomes, after applying SSH:

$$[I_P^\bullet] = \frac{\tilde{f}k_{\tilde{d}}[\tilde{I}]}{\left(\begin{array}{l} + 2k_{in,I_P M}[M] + k_{in,I_P V_P}[V_P] \\ + k_{t,I_P R}[R^{\bullet}] + k_{t,I_P B}[B^\bullet] + k_{t,I_P C}[C^\bullet] + k_{t,I_P T}[T^\bullet] + k_{t,I_P I}[I^\bullet] + k_{t,\tilde{I}I_P}[\tilde{I}^\bullet] \\ + k_{t,I_P O}[O^\bullet] + k_{O_2,I_P}[O_2] \end{array} \right)}$$

$$5.5 \quad \frac{\partial [V_P]}{\partial t} = 2k_{p,R}[R^{\bullet}][M] + k_{bb,R}[R^{\bullet}] + k_{t,RR}[R^{\bullet}][R^{\bullet}] + k_{t,RB}[R^{\bullet}][B^\bullet] + \\ k_{t,RC}[R^{\bullet}][C^\bullet] + 2k_{t,RT}[R^{\bullet}][T^\bullet] + k_{t,RO}[R^{\bullet}][O^\bullet] + k_{t,IR}[I^\bullet][R^{\bullet}] + \\ k_{t,\tilde{I}R}[\tilde{I}^\bullet][R^{\bullet}] + k_{t,I_P R}[I_P^\bullet][R^{\bullet}] + k_{t,BT}[B^\bullet][T^\bullet] + k_{t,CT}[C^\bullet][T^\bullet] + \\ k_{t,TT}[T^\bullet][T^\bullet] + k_{t,TO}[O^\bullet][T^\bullet] + k_{t,IT}[I^\bullet][T^\bullet] + k_{t,\tilde{I}T}[\tilde{I}^\bullet][T^\bullet] +$$

$$k_{t,IPT}[I_P^\bullet][T^\bullet] - k_{in,IV_P}[I^\bullet][V_P] - k_{in,\tilde{I}V_P}[\tilde{I}^\bullet][V_P] - k_{in,I_PV_P}[I_P^\bullet][V_P] -$$

$$k_{b,B}[B^\bullet][V_P] - k_{b,C}[C^\bullet][V_P] - k_{b,T}[T^\bullet][V_P] - k_{b,O}[O^\bullet][V_P] + k_{O_2,R}[R^{\bullet\bullet}][O_2]$$

$$5.6 \quad \frac{\partial[R^{\bullet\bullet}]}{\partial t} = 2k_{in,IM}[I^\bullet][M] + 2k_{in,\tilde{I}M}[\tilde{I}^\bullet][M] + 2k_{in,I_PM}[I_P^\bullet][M] + 2k_{p,B}[B^\bullet][M] +$$

$$2k_{p,C}[C^\bullet][M] + 2k_{p,T}[T^\bullet][M] + 2k_{p,O}[O^\bullet][M] - k_{b,R}[R^{\bullet\bullet}][V_P] -$$

$$k_C[R^{\bullet\bullet}] - k_{bb,R}[R^{\bullet\bullet}] - k_{t,RR}[R^{\bullet\bullet}][R^{\bullet\bullet}] - k_{t,RB}[R^{\bullet\bullet}][B^\bullet] - k_{t,RC}[R^{\bullet\bullet}][C^\bullet] -$$

$$k_{t,RT}[R^{\bullet\bullet}][T^\bullet] - k_{t,RO}[R^{\bullet\bullet}][O^\bullet] - k_{t,IR}[I^\bullet][R^{\bullet\bullet}] - k_{t,\tilde{I}R}[\tilde{I}^\bullet][R^{\bullet\bullet}] -$$

$$k_{t,I_PR}[I_P^\bullet][R^{\bullet\bullet}] - k_{O_2,R}[R^{\bullet\bullet}][O_2]$$

$$5.7 \quad \frac{\partial[B^\bullet]}{\partial t} = k_{in,IV_P}[I^\bullet][V_P] + k_{in,\tilde{I}V_P}[\tilde{I}^\bullet][V_P] + k_{in,I_PV_P}[I_P^\bullet][V_P] + k_{b,R}[R^{\bullet\bullet}][V_P] +$$

$$k_{b,C}[C^\bullet][V_P] + k_{b,T}[T^\bullet][V_P] + k_{b,O}[O^\bullet][V_P] -$$

$$2k_{p,B}[B^\bullet][M] - k_{t,RB}[R^{\bullet\bullet}][B^\bullet] - k_{t,BB}[B^\bullet][B^\bullet] - k_{t,BC}[B^\bullet][C^\bullet] -$$

$$k_{t,BT}[B^\bullet][T^\bullet] - k_{t,BO}[B^\bullet][O^\bullet] - k_{t,IB}[I^\bullet][B^\bullet] - k_{t,\tilde{I}B}[\tilde{I}^\bullet][B^\bullet] -$$

$$k_{t,I_PB}[I_P^\bullet][B^\bullet] - k_{O_2,B}[B^\bullet][O_2]$$

$$5.8 \quad \frac{\partial[C^\bullet]}{\partial t} = k_C[R^{\bullet\bullet}] - 2k_{p,C}[C^\bullet][M] - k_{b,C}[C^\bullet][V_P] - k_{bb,R}[C^\bullet] - k_{t,RC}[R^{\bullet\bullet}][C^\bullet] -$$

$$k_{t,BC}[B^\bullet][C^\bullet] - k_{t,CC}[C^\bullet][C^\bullet] - k_{t,CT}[C^\bullet][T^\bullet] - k_{t,CO}[C^\bullet][O^\bullet] -$$

$$k_{t,IC}[I^\bullet][C^\bullet] - k_{t,\tilde{I}C}[\tilde{I}^\bullet][C^\bullet] - k_{t,I_PC}[I_P^\bullet][C^\bullet] - k_{O_2,C}[C^\bullet][O_2]$$

$$5.9 \quad \frac{\partial[T^\bullet]}{\partial t} = k_{bb,R}[R^{\bullet\bullet}] + k_{bb,R}[C^\bullet] + k_{bb,O}[O^\bullet] - 2k_{p,T}[T^\bullet][M] - k_{b,T}[T^\bullet][V_P] -$$

$$k_{t,RT}[R^{\bullet\bullet}][T^\bullet] - k_{t,BT}[B^\bullet][T^\bullet] - k_{t,CT}[C^\bullet][T^\bullet] - k_{t,TT}[T^\bullet][T^\bullet] -$$

$$k_{t,TO}[T^\bullet][O^\bullet] - k_{t,IT}[I^\bullet][T^\bullet] - k_{t,\tilde{I}T}[\tilde{I}^\bullet][T^\bullet] - k_{t,I_PT}[I_P^\bullet][T^\bullet] - k_{O_2,T}[T^\bullet][O_2]$$

$$\begin{aligned}
5.10 \quad \frac{\partial [O^\bullet]}{\partial t} = & + k_{O_2,I}[I^\bullet][O_2] + k_{O_2,\tilde{I}}[\tilde{I}^\bullet][O_2] + k_{O_2,I_P}[I_P^\bullet][O_2] + k_{O_2,R}[R^{\bullet\bullet}][O_2] + \\
& k_{O_2,B}[B^\bullet][O_2] + k_{O_2,C}[C^\bullet][O_2] + k_{O_2,T}[T^\bullet][O_2] - 2 k_{p,O} [O^\bullet][M] - \\
& k_{b,O} [O^\bullet][V_p] - k_{bb,O}[O^\bullet] - k_{t,IO}[I^\bullet][O^\bullet] - k_{t,\tilde{I}O}[\tilde{I}^\bullet][O^\bullet] - k_{t,I_PCO}[I_P^\bullet][O^\bullet] - \\
& k_{t,RO}[R^{\bullet\bullet}][O^\bullet] - k_{t,BO}[B^\bullet][O^\bullet] - k_{t,CO}[C^\bullet][O^\bullet] - k_{t,TO}[T^\bullet][O^\bullet] - \\
& k_{t,OO}[O^\bullet][O^\bullet]
\end{aligned}$$

Table A.6: list of initial and boundary conditions for the equations in Table A.5 and the PDEs in Equations 2, 3 and 4.

6.1	<p style="text-align: center;">Initiator fragment</p> <p style="text-align: center;">For $t = 0$ and $0 \leq z \leq z_f$:</p> <p style="text-align: center;">$[\tilde{I}] = 0$</p>
6.5	<p style="text-align: center;">Pendant vinyl group</p> <p style="text-align: center;">for $t = 0$ and $0 \leq z \leq z_f$:</p> <p style="text-align: center;">$[V_p] = 0$</p>
6.6	<p style="text-align: center;">Regular radical</p> <p style="text-align: center;">for $t = 0$ and $0 \leq z \leq z_f$:</p> <p style="text-align: center;">$[R^{\bullet\bullet}] = 0$</p>
6.7	<p style="text-align: center;">Crosslinking radical</p> <p style="text-align: center;">for $t = 0$ and $0 \leq z \leq z_f$:</p> <p style="text-align: center;">$[B^\bullet] = 0$</p>
6.8	<p style="text-align: center;">Cyclic radical</p> <p style="text-align: center;">for $t = 0$ and $0 \leq z \leq z_f$:</p> <p style="text-align: center;">$[C^\bullet] = 0$</p>

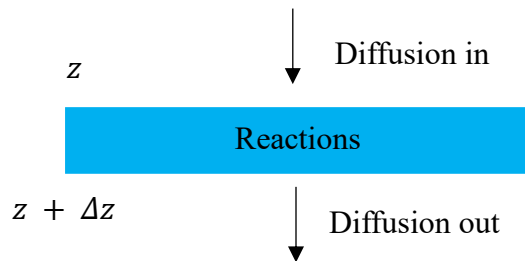
6.9	<p style="text-align: center;">Tertiary radical</p> <p style="text-align: center;">for $t = 0$ and $0 \leq z \leq z_f$:</p> $[T^*] = 0$
6.10	<p style="text-align: center;">Peroxic radical</p> <p style="text-align: center;">for $t = 0$ and $0 \leq z \leq z_f$:</p> $[O^*] = 0$
6.11	<p style="text-align: center;">Initiator</p> <p style="text-align: center;">For $t = 0$ and $0 \leq z \leq z_f$:</p> $[I] = [I]_0$ <p style="text-align: center;">for $t > 0$ and $z = 0$:</p> $\left. \frac{\partial [I]}{\partial z} \right _{z=0} = 0$ <p style="text-align: center;">for $t > 0$ and $z = z_f$:</p> $\left. \frac{\partial [I]}{\partial z} \right _{z=z_f} = 0$
6.12	<p style="text-align: center;">Monomer</p> <p style="text-align: center;">for $t = 0$ and $0 \leq z \leq z_f$:</p> $[M] = [M]_0 = 4.75 \left(\frac{mol}{L} \right)$ <p style="text-align: center;">for $t > 0$ and $z = 0$:</p> $\left. \frac{\partial [M]}{\partial z} \right _{z=0} = 0$ <p style="text-align: center;">for $t = 0$ and $z = z_f$:</p> $\left. \frac{\partial [M]}{\partial z} \right _{z=z_f} = 0$
6.13	<p style="text-align: center;">Oxygen</p> <p style="text-align: center;">for $t = 0$ and $0 \leq z \leq z_f$:</p> $[O_2] = H_s^{cp} P_{O_2}$ <p style="text-align: center;">for $t > 0$ and $z = 0$:</p>

	$[O_2] = H_s^{cp} P_{O_2}$ <p>for $t = 0$ and $z = z_f$:</p> $\left. \frac{\partial [O_2]}{\partial z} \right _{z=z_f} = 0$
--	---

A7 Derivation of two PDEs

A7.1 Deriving PDE for initiator shown in Equation (2.2) in Chapter 2

Consider a short period of time Δt (s) in a film layer with thickness Δz (m). This film has cross sectional area A (m²):



accumulation of I (mol) = diffusion in – diffusion out – consumption by reactions

Substituting for the various terms gives:

$$\Delta[I]A\Delta z = D_I \left. \frac{\partial [I]}{\partial z} \right|_z A\Delta t - D_I \left. \frac{\partial [I]}{\partial z} \right|_{z+\Delta z} A\Delta t + (-2k_d[I]A\Delta z\Delta t) \quad (\text{A.3})$$

Dividing both sides of Equation (A.3) by $A\Delta z$ and Δt gives:

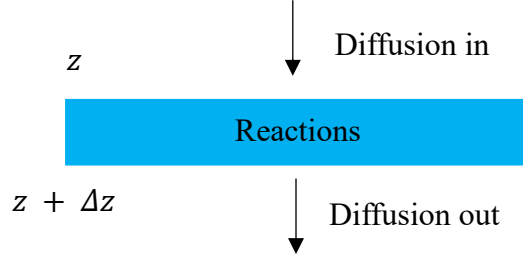
$$\frac{\Delta[I]}{\Delta t} = D_I \left. \frac{\partial [I]}{\partial z} \right|_z \frac{1}{\Delta z} - D_I \left. \frac{\partial [I]}{\partial z} \right|_{z+\Delta z} \frac{1}{\Delta z} + (-2k_d[I]) \quad (\text{A.4})$$

As $\Delta t \rightarrow 0$ and $\Delta z \rightarrow 0$, Equation (A.4) becomes:

$$\frac{\partial[I]}{\partial t} = D_I \frac{\partial^2[I]}{\partial z^2} \Big|_t - 2k_d[I] \quad (2.2)$$

A7.2 Deriving PDE for oxygen shown in Equation (2.4) in Chapter 2

Consider a short period of time Δt (s) in a film layer with thickness Δz (m). This film has cross sectional area A (m^2):



*accumulation of O_2 (mol) = diffusion in – diffusion out – consumption by reactions
+ regeneration by reactions*

Substituting for the various terms gives:

$$\begin{aligned} \Delta[O_2]A\Delta z = & D_{O_2} \frac{\partial[O_2]}{\partial z} \Big|_z A\Delta t - D_{O_2} \frac{\partial[O_2]}{\partial z} \Big|_{z+\Delta z} A\Delta t \\ & + \left(-k_{O_2,R}[O_2][R^{\bullet}]A\Delta z\Delta t - k_{O_2,B}[O_2][B^{\bullet}]A\Delta z\Delta t \right. \\ & - k_{O_2,C}[O_2][C^{\bullet}]A\Delta z\Delta t - k_{O_2,T}[O_2][T^{\bullet}]A\Delta z\Delta t - k_{O_2,I}[O_2][I^{\bullet}]A\Delta z\Delta t \\ & - k_{O_2,\tilde{I}}[O_2][\tilde{I}^{\bullet}]A\Delta z\Delta t - k_{O_2,I_P}[O_2][I_P^{\bullet}]A\Delta z\Delta t \\ & \left. + \frac{1}{2}k_{t,OO}[O^{\bullet}][O^{\bullet}]A\Delta z\Delta t \right) \end{aligned} \quad (A.5)$$

Dividing both sides of equation (S3) by $A\Delta z$ and Δt gives:

$$\begin{aligned} \frac{\Delta[O_2]}{\Delta t} = & D_{O_2} \frac{\partial[O_2]}{\partial z} \Big|_z \frac{1}{\Delta z} - D_{O_2} \frac{\partial[O_2]}{\partial z} \Big|_{z+\Delta z} \frac{1}{\Delta z} \\ & + \left(-k_{O_2,R}[O_2][R^{\bullet}] - k_{O_2,B}[O_2][B^{\bullet}] - k_{O_2,C}[O_2][C^{\bullet}] - k_{O_2,T}[O_2][T^{\bullet}] \right. \\ & \left. - k_{O_2,I}[O_2][I^{\bullet}] - k_{O_2,\tilde{I}}[O_2][\tilde{I}^{\bullet}] - k_{O_2,I_P}[O_2][I_P^{\bullet}] + \frac{1}{2}k_{t,OO}[O^{\bullet}][O^{\bullet}] \right) \end{aligned} \quad (A.6)$$

As $\Delta t \rightarrow 0$ and $\Delta z \rightarrow 0$, equation (S4) becomes:

$$\begin{aligned} \frac{\partial [O_2]}{\partial t} = D_{O_2} \frac{\partial^2 [O_2]}{\partial z^2} \Big|_t &- k_{O_2,R}[O_2][R^{\bullet}] - k_{O_2,B}[O_2][B^{\bullet}] - k_{O_2,C}[O_2][C^{\bullet}] \\ &- k_{O_2,T}[O_2][T^{\bullet}] - k_{O_2,I}[O_2][I^{\bullet}] - k_{O_2,I}[O_2][\tilde{I}^{\bullet}] - k_{O_2,I_P}[O_2][I_P^{\bullet}] \\ &+ \frac{1}{2} k_{t,OO}[O^{\bullet}][O^{\bullet}] \end{aligned} \quad (2.4)$$

A8 Diffusivities of monomer and initiator

Figures A.5 and A.6 show predictions of how the initiator and monomer concentrations, respectively, change with time and location for an experiment with a relatively thick film and high light intensity. In these figures simulations are also shown with initiator and monomer diffusion turned off, revealing that initiator diffusion is of little importance but monomer diffusion is important.

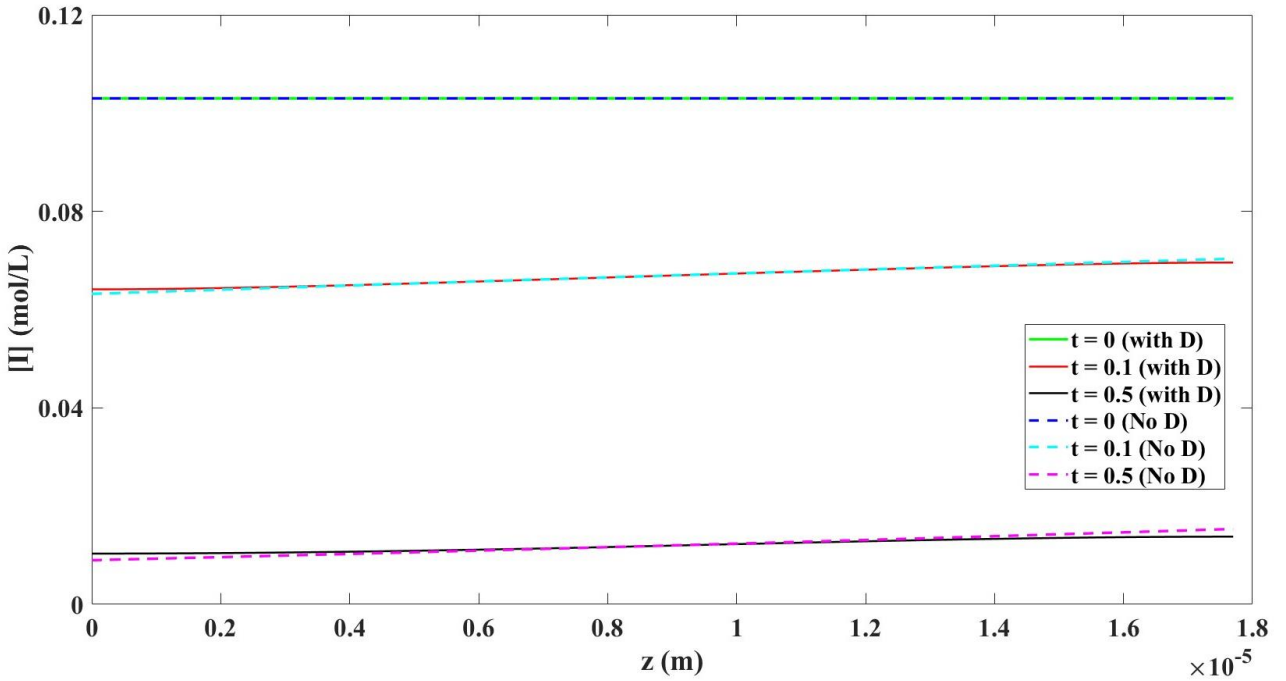


Fig. A.5. Initiator concentration vs depth at different times, with diffusivity both turned off (Dashed lines) and on (Solid lines)

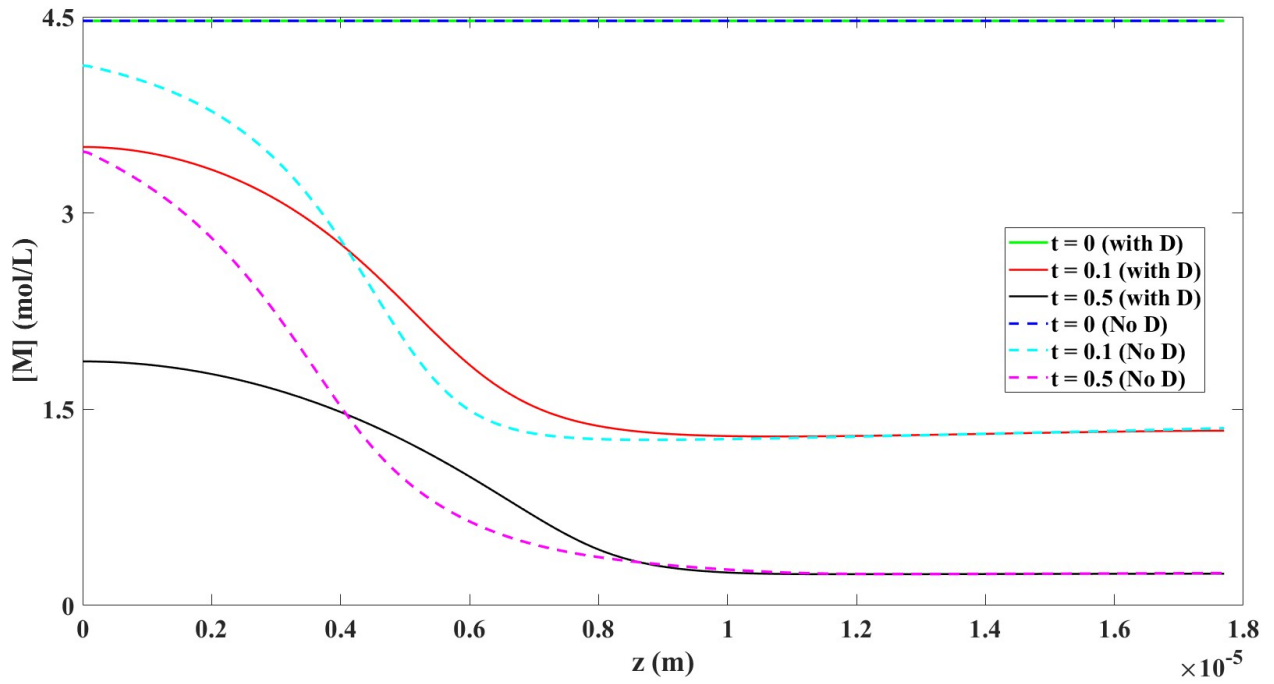


Fig. A.6. Monomer concentration vs depth at different times, with diffusivity both turned off (Dashed lines) and on (Solid lines)

A9 Parameter estimates from Abdi's model

A table presenting a full list of the parameter estimates obtained by Abdi et al can be found below [15]. Those parameters are used as fixed parameter values to 30 out of the 39 parameters of the current model.

Table A.7: List of parameters and their estimates obtained from Abdi's model [15]

Parameter	Estimate	Units	Parameter	Estimate	Units
$v_{f,0}$	6.366×10^{-2}	-	$\frac{k_{b,R0}}{k_{p,R0}}$	10.000×10^{-1}	-
$\frac{v_{f,1}}{v_{f,0}}$	4.999×10^{-1}	-	$\frac{k_{c0}}{k_{p,R0}}$	3.347	-
f_0	9.959×10^{-1}	-	$\frac{k_{bb0}}{k_{p,R0}}$	1.001×10^{-3}	-

A_f	5.000×10^{-1}	-	$\frac{k_{p,B0}}{k_{p,R0}} = \frac{k_{b,B0}}{k_{b,R0}}$	4.834×10^{-2}	-
$\frac{\bar{f}}{f}$	1.200	-	$\frac{k_{p,C0}}{k_{p,R0}} = \frac{k_{b,C0}}{k_{b,R0}}$	5.008×10^{-1}	-
ϕ	8.995×10^{-1}	-	$\frac{k_{p,T0}}{k_{p,R0}} = \frac{k_{b,T0}}{k_{b,R0}}$	5.027×10^{-4}	-
$\frac{k_{\bar{d}}}{k_d}$	5.724×10^{-1}	-	$k_{t_{in,II0}}$	6.983×10^8	$\text{L mol}^{-1} \text{s}^{-1}$
$k_{in,IM0}$	1.005×10^6	$\text{L mol}^{-1} \text{s}^{-1}$	$\frac{k_{t_{in,II0}}}{k_{t_{in,III0}}}$	1.149	-
$\frac{k_{in,IM0}}{k_{in,IM0}}$	5.027×10^{-3}	-	R_{rd}	7.308	L mol^{-1}
$\frac{k_{in,IVp0}}{k_{in,IM0}} = \frac{k_{in,IVp0}}{k_{in,IM0}} =$	9.996×10^{-1}	-	$A_{t,RR}$	10.000×10^{-1}	-
$\frac{k_{in,IVp0}}{k_{in,IPM0}}$					
$A_{b,R}$	5.911×10^{-1}	-	$v_{fc,tRR}$	8.553×10^{-2}	-
$\frac{A_{p,R}}{A_{b,R}}$	9.451×10^{-1}	-	$k_{t,RR0}$	1.695×10^8	$\text{L mol}^{-1} \text{s}^{-1}$
$\frac{v_{fc,bR}}{v_{fc,tRR}}$	5.292×10^{-1}	-	$\frac{k_{t,BB0}}{k_{t,RR0}}$	1.001×10^{-2}	-
$\frac{v_{fc,pR}}{v_{fc,bR}}$	8.713×10^{-1}	-	$\frac{k_{t,CC0}}{k_{t,RR0}}$	1.500	-
$k_{p,R0}$	1.001×10^4	$\text{L mol}^{-1} \text{s}^{-1}$	$\frac{k_{t,TT0}}{k_{t,RR0}}$	8.795×10^{-2}	-

A10 Parameter Estimation Notes

In Chapter 2, parameter estimation involved minimizing a least-squares objective function based on vinyl group conversion data. Given the complexity of the model equations, we encountered

challenges with local minima during estimation. To address this, we conducted parameter estimation ten times, each with different initial parameter values by applying 5 – 10% perturbations to the starting conditions. The set of parameter estimates that yielded the lowest objective function value J was selected for this chapter.

Please note that confidence intervals for the parameters are not included, as the model requires further refinement; the assumption of a "perfect model" is not valid, and re-estimation will be necessary.

A11 Additional Simulation Results and Plots

A plot shows the simulation results for runs with low BAPO levels is presented in Fig. A.7. Also, another plot that shows the simulation results for two runs with different film thicknesses is shown below in Fig. A.8. This plot confirms that in thicker films, the overall vinyl-group conversion is higher.

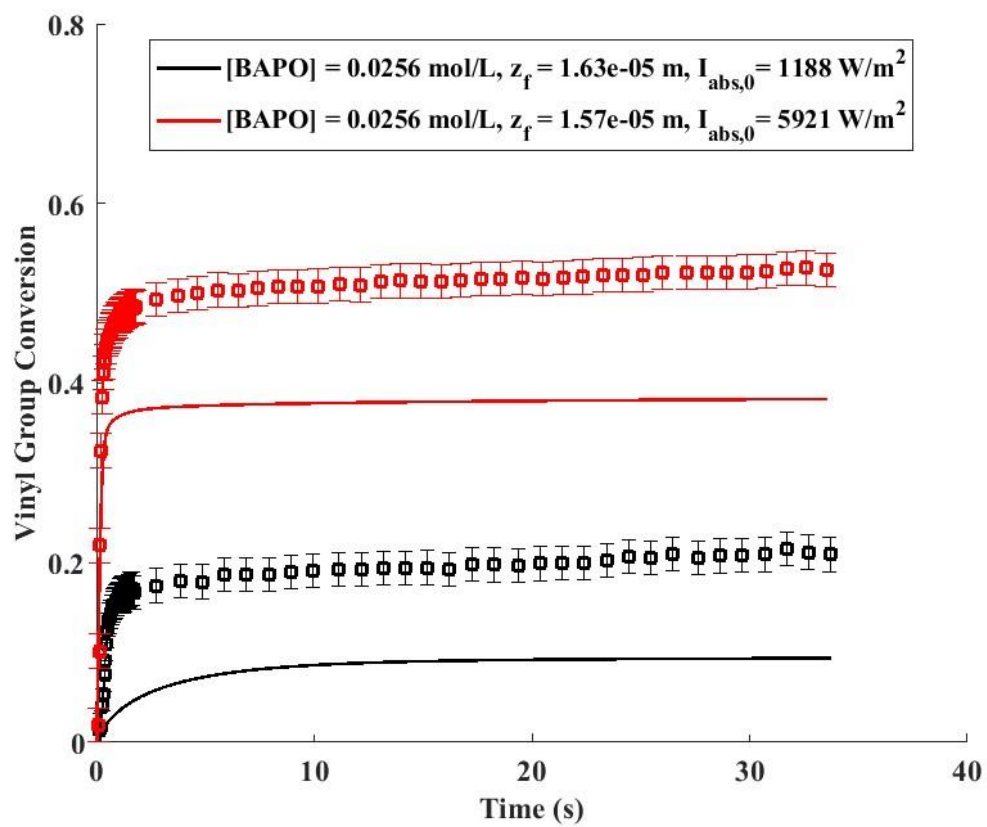


Fig. A.7. Low BAPO (1 wt%) level plots

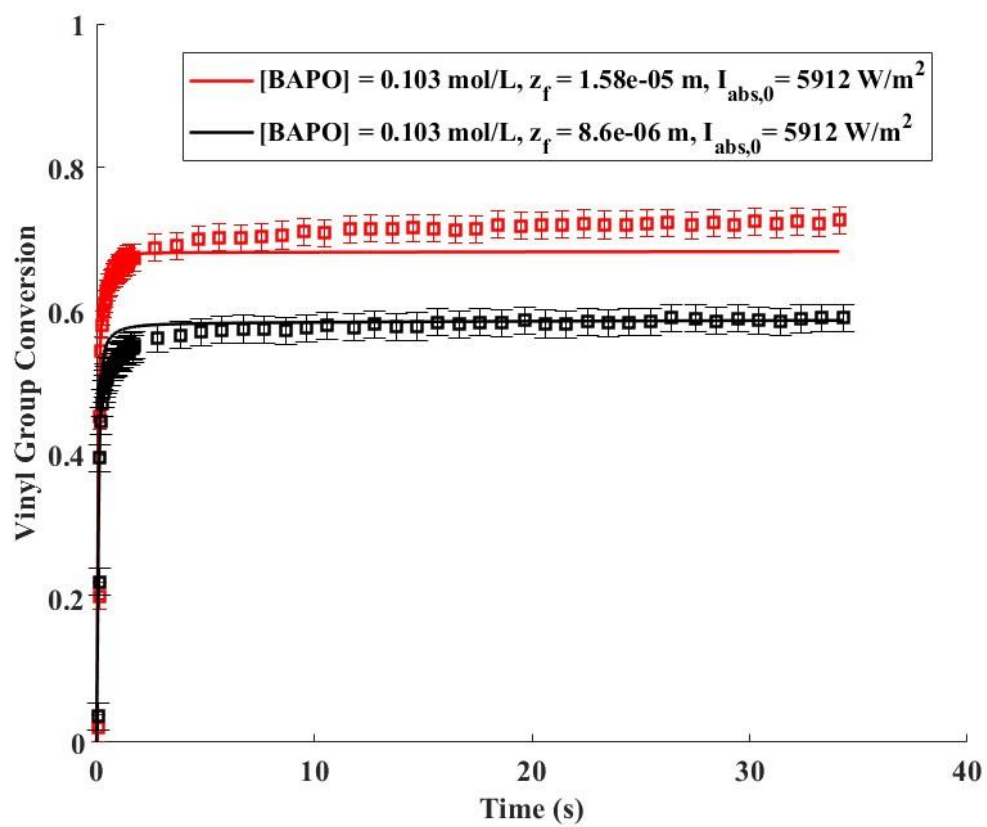


Fig. A.8. Thickness plots

Appendix B

Supplementary Information - Chapter 3

B1 List of Reactions and Assumptions

Table B.1 provides a full list of the reactions considered in the model. Table B.2 provides a detailed list of model assumptions. Assumptions B.2.2 through B.2.26 are identical to those made in a previous HDDA modeling paper [17] (Chapter 2) that accounts for spatial variations. Assumptions B.2.1 has been modified to account for film shrinkage during the photopolymerization of HDDA. Additionally, assumption B.2.27 was added regarding oxygen concentration at the surface of the film.

Table B.1: List of reactions of the photopolymerization of HDDA [17]

Reaction Description	Reaction	
Decomposition	$I \xrightarrow{2k_d} fI^\bullet + f\tilde{I}^\bullet$	(R1)
	$\tilde{I} \xrightarrow{k_{\tilde{d}}} \tilde{f}I^\bullet + \tilde{f}I_P^\bullet$	(R2)
Initiation	$I^\bullet + M \xrightarrow{2k_{in,IM}} R^{\bullet}$	(R3)
	$\tilde{I}^\bullet + M \xrightarrow{2k_{in,\tilde{I}M}} R^{\bullet} + \tilde{I}$	(R4)
	$I_P^\bullet + M \xrightarrow{2k_{in,I_P M}} R^{\bullet}$	(R5)
	$I^\bullet + V_P \xrightarrow{k_{in,IV_P}} B^\bullet$	(R6)
	$\tilde{I}^\bullet + V_P \xrightarrow{k_{in,\tilde{I}V_P}} B^\bullet + \tilde{I}$	(R7)
	$I_P^\bullet + V_P \xrightarrow{k_{in,I_P V_P}} B^\bullet$	(R8)
Propagation	$R^{\bullet} + M \xrightarrow{2k_{p,R}} R^{\bullet} + V_P$	(R9)
	$C^\bullet + M \xrightarrow{2k_{p,C}} R^{\bullet}$	(R10)
	$B^\bullet + M \xrightarrow{2k_{p,B}} R^{\bullet}$	(R11)
Crosslinking	$T^\bullet + M \xrightarrow{2k_{p,T}} R^{\bullet}$	(R12)
	$R^{\bullet} + V_P \xrightarrow{k_{b,R}} B^\bullet + V_P$	(R13)

	$C^\bullet + V_P \xrightarrow{k_{b,C}} B^\bullet$	(R14)
	$B^\bullet + V_P \xrightarrow{k_{b,B}} B^\bullet$	(R15)
	$T^\bullet + V_P \xrightarrow{k_{b,T}} B^\bullet$	(R16)
Cyclization	$R^\bullet \xrightarrow{k_C} C^\bullet$	(R17)
Backbiting	$R^\bullet \xrightarrow{k_{bb}} T^\bullet + V_P$	(R18)
	$C^\bullet \xrightarrow{k_{bb}} T^\bullet$	(R19)
Termination	$I^\bullet + C^\bullet \xrightarrow{k_{t,IC}} D$	(R20)
	$I^\bullet + B^\bullet \xrightarrow{k_{t,IB}} D$	(R21)
	$I^\bullet + T^\bullet \xrightarrow{k_{t,IT}} D$	(R22)
	$\tilde{I}^\bullet + C^\bullet \xrightarrow{k_{t,\tilde{I}C}} D + \tilde{I}$	(R23)
	$\tilde{I}^\bullet + B^\bullet \xrightarrow{k_{t,\tilde{I}B}} D + \tilde{I}$	(R24)
	$\tilde{I}^\bullet + T^\bullet \xrightarrow{k_{t,\tilde{I}T}} D + \tilde{I}$	(R25)
	$I_P^\bullet + C^\bullet \xrightarrow{k_{t,I_P C}} D$	(R26)
	$I_P^\bullet + B^\bullet \xrightarrow{k_{t,I_P B}} D$	(R27)
	$I_P^\bullet + T^\bullet \xrightarrow{k_{t,I_P T}} D$	(R28)
	$R^\bullet + R^\bullet \xrightarrow{k_{t,RR}} D + 2V_P$	(R29)
	$C^\bullet + C^\bullet \xrightarrow{k_{t,CC}} D$	(R30)
	$B^\bullet + B^\bullet \xrightarrow{k_{t,BB}} D$	(R31)
	$T^\bullet + T^\bullet \xrightarrow{k_{t,TT}} 2D + V_P$	(R32)
	$R^\bullet + C^\bullet \xrightarrow{k_{t,RC}} D + V_P$	(R33)
	$R^\bullet + B^\bullet \xrightarrow{k_{t,RB}} D + V_P$	(R34)
	$R^\bullet + T^\bullet \xrightarrow{k_{t,RT}} 2D + 2V_P$	(R35)
	$C^\bullet + B^\bullet \xrightarrow{k_{t,CB}} D$	(R36)
	$C^\bullet + T^\bullet \xrightarrow{k_{t,CT}} 2D + V_P$	(R37)
	$B^\bullet + T^\bullet \xrightarrow{k_{t,BT}} 2D + V_P$	(R38)
	Oxygen Incorporation	$I^\bullet + O_2 \xrightarrow{k_{O_2,I}} O^\bullet$
$\tilde{I}^\bullet + O_2 \xrightarrow{k_{O_2,\tilde{I}}} O^\bullet + \tilde{I}$		(R40)
$I_P^\bullet + O_2 \xrightarrow{k_{O_2,I_P}} O^\bullet$		(R41)

	$R^{\bullet} + O_2 \xrightarrow{k_{O_2,R}} O^{\bullet} + V_P$	(R42)
	$B^{\bullet} + O_2 \xrightarrow{k_{O_2,B}} O^{\bullet}$	(R43)
	$C^{\bullet} + O_2 \xrightarrow{k_{O_2,C}} O^{\bullet}$	(R44)
	$T^{\bullet} + O_2 \xrightarrow{k_{O_2,T}} O^{\bullet}$	(R45)
Propagation of peroxidic radicals (slow)	$O^{\bullet} + M \xrightarrow{2k_{p,O}} R^{\bullet}$	(R46)
	$O^{\bullet} + V_P \xrightarrow{k_{b,O}} B^{\bullet}$	(R47)
Backbiting of peroxidic radicals	$O^{\bullet} \xrightarrow{k_{bb,O}} T^{\bullet}$	(R48)
Termination of peroxidic radicals	$O^{\bullet} + O^{\bullet} \xrightarrow{k_{t,OO}} D + O_2$	(R49)
	$O^{\bullet} + I^{\bullet} \xrightarrow{k_{t,IO}} D$	(R50)
	$O^{\bullet} + \tilde{I}^{\bullet} \xrightarrow{k_{t,\tilde{I}O}} D + \tilde{I}$	(R51)
	$O^{\bullet} + I_P^{\bullet} \xrightarrow{k_{t,IP^{\bullet}O}} D$	(R52)
	$O^{\bullet} + R^{\bullet} \xrightarrow{k_{t,RO}} D + V_P$	(R53)
	$O^{\bullet} + B^{\bullet} \xrightarrow{k_{t,BO}} D$	(R54)
	$O^{\bullet} + C^{\bullet} \xrightarrow{k_{t,CO}} D$	(R55)
	$O^{\bullet} + T^{\bullet} \xrightarrow{k_{t,TO}} D$	(R56)

Table B.2: Model Assumptions [15-17]

-
- B.2.1** The monomer and polymer are present in a single phase. Oxygen and monomer are able to diffuse within the film, but polymeric molecules cannot, due to their large size. Diffusion of initiator is ignored because it is present in low concentrations and because initiator concentration gradients are small [17]. Although oxygen diffusion has an important influence on reactant concentrations, it does not have a direct influence on film thickness because only a small amount of oxygen is present. Volume changes due to mixing of species are neglected.
- B.2.2** Temperature is constant at 25 °C.
- B.2.3** The initiator moieties remaining after initiator decomposition have the same absorbance properties as the initiator.
- B.2.4** Radicals of type \tilde{I}^{\bullet} are consumed by initiation reactions and termination reactions before their weak carbon-phosphorous bond has an opportunity to break. This assumption is
-

valid because the rate of consumption of the free radical on \tilde{I}^\bullet is typically 10^9 times faster than the rate of dissociation of the weak carbon-phosphorous bond.

- B.2.5** In this terminal model, reaction rates depend only on the types of end groups on polymer chains. Penultimate effects are neglected.
- B.2.6** The effect of stabilizer is neglected.
- B.2.7** End groups of type R^{\bullet} contain a vinyl group and a free radical. It is assumed that the short-lived free radical is consumed much more rapidly than the corresponding vinyl group. When the radical on R^{\bullet} is consumed by propagation, crosslinking, backbiting and termination reactions, the corresponding vinyl group on R^{\bullet} becomes a pendant vinyl group that can participate in subsequent reactions. This assumption is valid because the rate of consumption of a pendant vinyl group is $\sim 10^5$ times slower than the rate of consumption of the corresponding radical.
- B.2.8** Chain-transfer to monomer and chain-transfer to polymer are neglected.
- B.2.9** Carbon-centered and phosphorous-centered initiator radicals have similar relative propensities when reacting with pendant vinyl groups compared with monomeric vinyl groups (i.e., $\frac{k_{in,IVP0}}{k_{in,IM0}} = \frac{k_{in,IVP0}}{k_{in,\tilde{I}M0}}$).
- B.2.10** All phosphorous-centered radicals have the same kinetically-controlled reactivity, independent of whether they are generated by initiator decomposition or decomposition of initiator moieties \tilde{I} attached to polymer molecules (i.e., $k_{in,\tilde{I}M0} = k_{in,I_P M0}$ and $k_{in,\tilde{I}V_P0} = k_{in,I_P V_P0}$).
- B.2.11** The kinetically dependent rate coefficient for self-termination reactions involving two phosphorous-centered radicals \tilde{I}^\bullet and I_P^\bullet are the same (i.e., $k_{t_{in},\tilde{I}\tilde{I}0} = k_{t_{in},I_P I_P0}$).
- B.2.12** Self-termination reactions for initiator radicals (i.e., I^\bullet , \tilde{I}^\bullet , and I_P^\bullet) are ignored so that the stationary state hypothesis can be readily applied to compute the concentrations of these short-lived radicals. Cross-termination reactions between I^\bullet and \tilde{I}^\bullet and between I^\bullet and I_P^\bullet are ignored in the balance on I^\bullet .
- B.2.13** All macroradicals have the same relative propensities for crosslinking and propagation reactions (i.e., $\frac{k_{b,R0}}{k_{p,R0}} = \frac{k_{b,B0}}{k_{p,B0}} = \frac{k_{b,C0}}{k_{p,C0}} = \frac{k_{b,T0}}{k_{p,T0}} = \frac{k_{b,O0}}{k_{p,O0}}$).
- B.2.14** Cyclization reactions may occur between a radical end R^{\bullet} and its vinyl group, but not with other vinyl groups on the polymer.
- B.2.15** The only radical ends that participate in backbiting reactions are R^{\bullet} , C^\bullet , and O^\bullet . Backbiting generates tertiary radicals T^\bullet .
-

-
- B.2.16** Termination reactions involving two secondary macroradicals are termination-by-combination reactions.
- B.2.17** Termination reactions involving tertiary radical T^\bullet and other radicals are termination-by-disproportionation reactions.
- B.2.18** Rate constants for cross-termination of radicals are obtained using the geometric mean of the corresponding self-termination rate constants.
- B.2.19** The reactivity of terminal vinyl groups (which result from termination by disproportionation) is the same as the reactivity of pendant vinyl groups.

B.2.20 Initiation reactions involving small initiator fragments I^\bullet and \tilde{I}^\bullet are kinetically-controlled rather than diffusionally-controlled. Diffusion-control is considered for initiation involving polymeric initiator fragments I_p^\bullet . Reactions between all radicals and oxygen, which is a small molecule, are kinetically-controlled rather than diffusionally-controlled. Backbiting and cyclization are also kinetically-controlled. Crosslinking and termination reactions are diffusionally-controlled because they involve two large molecules. Propagation is also diffusionally-controlled because the parameter estimation study by Abdi et al. showed that accounting for diffusional effects for propagation rate constants resulted in a noticeable improvement in model fit to the data.

- B.2.21** Reaction diffusion, which influences termination rates, occurs predominantly by consumption of monomer vinyl groups rather than pendant vinyl groups.
- B.2.22** The free volume fraction of the film v_f is assumed to change linearly with monomer conversion X_M .
- B.2.23** To reduce the number of free-volume parameters in the model, reactions are divided into three classes: *i*) propagation reactions involving a small monomer molecule and a free-radical on a large molecule, *ii*) crosslinking reactions involving two large molecules, and *iii*) termination reactions involving two large molecules. Each class has its own free-volume parameters, and free-volume parameters are assumed to be the same for all reactions within a class. Further, the initiator efficiencies f and \tilde{f} are assumed to have the same free-volume parameters.
- B.2.24** All radicals have the same relative propensities for oxygen incorporation compared to their corresponding propensities for propagation or initiation with monomer.

$$\left(\text{i.e., } \frac{k_{O_2,R0}}{k_{p,R0}} = \frac{k_{O_2,B0}}{k_{p,B0}} = \frac{k_{O_2,C0}}{k_{p,C0}} = \frac{k_{O_2,T0}}{k_{p,T0}} = \frac{k_{O_2,I0}}{k_{in,IM0}} = \frac{k_{O_2,\tilde{I}0}}{k_{in,\tilde{I}M0}} = \frac{k_{O_2,IP0}}{k_{in,IPM0}}\right).$$

B.2.25 Peroxidic radicals have the same relative propensities for backbiting and propagation reactions compared to the corresponding backbiting and propagation reactions of R^{\bullet} (i.e., $\frac{k_{bb,O0}}{k_{p,O0}} = \frac{k_{bb,R0}}{k_{p,R0}}$)

Peroxy groups within polymer molecules, which are created by propagation of peroxy

B.2.26 radicals, do not decompose to produce radicals over the duration of the experiments. Also, hydroperoxide end groups, which result from backbiting reactions of peroxidic radicals, do not decompose to produce radicals during the experiments.

B.2.27 The top surface of the film always has an oxygen concentration $[O_2]^*$ which is the concentration in equilibrium with air.

B2 List of Algebraic Equations and PDEs

Table B.3 provides a list of Algebraic equations used for different model parameters.

Table B.4 presents a list of the 14 PDEs and their initial and boundary conditions used in the model.

Notice that the balances on monomer and oxygen contain diffusion terms, but balances on the polymeric species (i.e., \tilde{I} , V_p , R^{\bullet} , C^{\bullet} , B^{\bullet} , T^{\bullet} and O^{\bullet}) do not (see assumption B.2.1 in Table B.2).

Details concerning the derivations of some of these PDEs are provided in the Supplementary Information below. The other PDEs in Table B.4 are derived in a similar fashion. Equations (5.3 - 5.5) in Table B.4 are PDEs that were replaced by algebraic equations using the steady state hypothesis, hence there is no need to define their initial and boundary conditions.

Table B.3: List of algebraic equations [15-17]

B.3.1	$I_l = I_{l,0} e^{-\varepsilon[I]_0 z}$	[5]
B.3.2	$k_d = \frac{\varepsilon \phi \lambda I_l}{N_A h c}$	[5]

$$\mathbf{B.3.3} \quad v_f = v_{f,0} + (v_{f,1} - v_{f,0})X_M \quad [54]$$

$$\mathbf{B.3.4} \quad f = 1 / \left[1 - \left(1 - \frac{1}{f_0}\right) e^{A_f \left(\frac{1}{v_f} - \frac{1}{v_{f,0}}\right)} \right] \quad [55]$$

$$\mathbf{B.3.5} \quad k_{in,j} = k_{in,j_0} / \left[1 + e^{A_{in,j} \left(\frac{1}{v_f} - \frac{1}{v_{fc,in,j}}\right)} \right] \quad [56]$$

$$\mathbf{B.3.6} \quad k_{p,j} = k_{p,j_0} / \left[1 + e^{A_p \left(\frac{1}{v_f} - \frac{1}{v_{fc,p,j}}\right)} \right] \quad [56]$$

$$\mathbf{B.3.7} \quad k_{b,j} = k_{b,j_0} / \left[1 + e^{A_b \left(\frac{1}{v_f} - \frac{1}{v_{fc,b}}\right)} \right] \quad [56]$$

$$\mathbf{B.3.8} \quad k_c = k_{c_0} / \left[1 + e^{A_c \left(\frac{1}{v_f} - \frac{1}{v_{fc,c}}\right)} \right] \quad [56]$$

$$\mathbf{B.3.9} \quad k_{bb,j} = k_{bb,j_0} / \left[1 + e^{A_{bb} \left(\frac{1}{v_f} - \frac{1}{v_{fc,bb}}\right)} \right] \quad [56]$$

$$\mathbf{B.3.10} \quad k_{t,in,jj} = k_{t,in,jj_0} / \left[1 + e^{A_{t,in,jj} \left(\frac{1}{v_f} - \frac{1}{v_{fc,t,jj}}\right)} \right] \quad [56]$$

$$\mathbf{B.3.11} \quad k_{t,ij} = \sqrt{k_{t,ii} k_{t,jj}} \quad [57]$$

$$\mathbf{B.3.12} \quad k_{t,RR} = k_{t,RR_0} \left[1 + \frac{1}{e^{-A_{t,jj} \left(\frac{1}{v_f} - \frac{1}{v_{fc,t,jj}}\right)} + \frac{R_{rd} k_{p,RR} [M]}{k_{t,RR_0}}} \right]^{-1} \quad [39]$$

$$\mathbf{B.3.13} \quad D_X = D_{X_HDDA} \exp \left[-A_X \left(\frac{1}{v_f} - \frac{1}{v_{f_0}} \right) \right] \quad [17]$$

Table B.4: List of model PDEs along with their initial and boundary conditions

1) Initiator	
<p>For $t = 0$ and $0 \leq w \leq 1$:</p> <p>$[I] = [I]_0$</p>	$\frac{\partial [I]}{\partial t} \Big _w = R_I - [I] \left(\frac{M_{HDDA}}{\rho_{HDDA}} D_M \left(\frac{\partial z}{\partial w} \Big _t \right)^{-2} \frac{\partial^2 [M]}{\partial w^2} \Big _t \right.$ $+ \frac{M_{HDDA}}{\rho_{HDDA}} \left(\frac{\partial z}{\partial w} \Big _t \right)^{-2} \left(\frac{\partial [M]}{\partial w} \Big _t \right)^2 \frac{A_M (v_{f0} - v_{f1})}{[M]_0 v_f^2} D_M$ $\left. - M_{HDDA} \left(\frac{1}{\rho_{HDDA}} - \frac{1}{\rho_{pol}} \right) R_M \right)$ <p>where:</p> $R_I = -2k_d [I]$
2) Initiator fragment	
<p>For $t = 0$ and $0 \leq w \leq 1$:</p> <p>$[\tilde{I}] = 0$</p>	$\frac{\partial [\tilde{I}]}{\partial t} \Big _w = R_{\tilde{I}} - [\tilde{I}] \left(\frac{M_{HDDA}}{\rho_{HDDA}} D_M \left(\frac{\partial z}{\partial w} \Big _t \right)^{-2} \frac{\partial^2 [M]}{\partial w^2} \Big _t \right.$ $+ \frac{M_{HDDA}}{\rho_{HDDA}} \left(\frac{\partial z}{\partial w} \Big _t \right)^{-2} \left(\frac{\partial [M]}{\partial w} \Big _t \right)^2 \frac{A_M (v_{f0} - v_{f1})}{[M]_0 v_f^2} D_M$ $\left. - M_{HDDA} \left(\frac{1}{\rho_{HDDA}} - \frac{1}{\rho_{pol}} \right) R_M \right)$ <p>where:</p> $R_{\tilde{I}} = -k_{\tilde{d}} [\tilde{I}] + 2k_{in, \tilde{I}M} [\tilde{I}^*] [M] + k_{in, \tilde{I}V_p} [\tilde{I}^*] [V_p] + k_{t, \tilde{I}R} [\tilde{I}^*] [R^{\bullet}] + k_{t, \tilde{I}B} [\tilde{I}^*] [B^*]$ $+ k_{t, \tilde{I}C} [\tilde{I}^*] [C^*] + k_{t, \tilde{I}T} [\tilde{I}^*] [T^*] + k_{t, \tilde{I}O} [\tilde{I}^*] [O^*] + k_{t, \tilde{I}I} [\tilde{I}^*] [I^*] + k_{t, \tilde{I}\tilde{I}} [\tilde{I}^*] [\tilde{I}^*]$ $+ k_{t, \tilde{I}I_p} [\tilde{I}^*] [I_p^*] + k_{O_2, \tilde{I}} [\tilde{I}^*] [O_2]$

3) Initiator radical

$$\frac{\partial [I^*]}{\partial t} = 2fk_d[I] + \tilde{f}k_{\tilde{d}}[\tilde{I}] - 2k_{in,IM}[M] - k_{in,IV_P}[V_P] - k_{t,IR}[R^{\bullet}] - k_{t,IB}[B^*] - k_{t,IC}[C^*] - k_{t,IT}[T^*] - k_{t,IO}[O^*] - k_{O_2,I}[O_2]$$

which becomes, after applying SSH:

$$[I^*] = \frac{2fk_d[I] + \tilde{f}k_{\tilde{d}}[\tilde{I}]}{\left(\begin{array}{l} + 2k_{in,IM}[M] + k_{in,IV_P}[V_P] \\ + k_{t,IR}[R^{\bullet}] + k_{t,IB}[B^*] + k_{t,IC}[C^*] + k_{t,IT}[T^*] \\ + k_{t,IO}[O^*] + k_{O_2,I}[O_2] \end{array} \right)}$$

4) Initiator fragment radical

$$\frac{\partial [\tilde{I}^*]}{\partial t} = 2fk_d[I] - 2k_{in,\tilde{I}M}[M] - k_{in,\tilde{I}V_P}[V_P] - k_{t,\tilde{I}R}[R^{\bullet}] - k_{t,\tilde{I}B}[B^*] - k_{t,\tilde{I}C}[C^*] - k_{t,\tilde{I}T}[T^*] - k_{t,\tilde{I}I}[I^*] - k_{t,\tilde{I}O}[O^*] - k_{O_2,\tilde{I}}[O_2]$$

which becomes, after applying SSH:

$$[\tilde{I}^*] = \frac{2fk_d[I]}{\left(\begin{array}{l} + 2k_{in,\tilde{I}M}[M] + k_{in,\tilde{I}V_P}[V_P] \\ + k_{t,\tilde{I}R}[R^{\bullet}] + k_{t,\tilde{I}B}[B^*] + k_{t,\tilde{I}C}[C^*] + k_{t,\tilde{I}T}[T^*] + k_{t,\tilde{I}I}[I^*] \\ + k_{t,\tilde{I}O}[O^*] + k_{O_2,\tilde{I}}[O_2] \end{array} \right)}$$

5) Phosphorus centered initiator radical

$$\frac{\partial [I_P^*]}{\partial t} = \tilde{f}k_{\tilde{d}}[\tilde{I}] - 2k_{in,I_P M}[M] - k_{in,I_P V_P}[V_P] - k_{t,I_P R}[R^{\bullet}] - k_{t,I_P B}[B^*] - k_{t,I_P C}[C^*] - k_{t,I_P T}[T^*] - k_{t,I_P I}[I^*] - k_{t,I_P O}[O^*] - k_{O_2,I_P}[O_2]$$

which becomes, after applying SSH:

$$[I_P^*] = \frac{\tilde{f}k_{\tilde{d}}[\tilde{I}]}{\left(\begin{array}{l} + 2k_{in,I_{PM}}[M] + k_{in,I_{PV_P}}[V_P] \\ + k_{t,I_{PR}}[R^{\bullet}] + k_{t,I_{PB}}[B^{\bullet}] + k_{t,I_{PC}}[C^{\bullet}] + k_{t,I_{PT}}[T^{\bullet}] + k_{t,I_P}[I^{\bullet}] + k_{t,\tilde{I}_P}[\tilde{I}^{\bullet}] \\ + k_{t,I_{PO}}[O^{\bullet}] + k_{O_2,I_P}[O_2] \end{array} \right)}$$

6) Monomer

For $t = 0$ and $0 \leq w \leq 1$:

$$\left. \frac{\partial[M]}{\partial t} \right|_w = D_M \left(\left. \frac{\partial z}{\partial w} \right|_t \right)^{-2} \left. \frac{\partial^2[M]}{\partial w^2} \right|_t + \left(\left. \frac{\partial[M]}{\partial w} \right|_t \right)^2 \left(\left. \frac{\partial z}{\partial w} \right|_t \right)^{-2} D_M \frac{A_M(v_{f0} - v_{f1})}{[M]_0(v_f)^2} - R_M$$

$$[M] = [M]_0$$

$$= 4.75 \left(\frac{mol}{L} \right)$$

$$- [M] \left(\frac{M_{HDDA}}{\rho_{HDDA}} D_M \left(\left. \frac{\partial z}{\partial w} \right|_t \right)^{-2} \left. \frac{\partial^2[M]}{\partial w^2} \right|_t \right)$$

$$+ \frac{M_{HDDA}}{\rho_{HDDA}} \left(\left. \frac{\partial z}{\partial w} \right|_t \right)^{-2} \left(\left. \frac{\partial[M]}{\partial w} \right|_t \right)^2 \frac{A_M(v_{f0} - v_{f1})}{[M]_0 v_f^2} D_M$$

For $t > 0$ and $w = 0$:

$$- M_{HDDA} \left(\frac{1}{\rho_{HDDA}} - \frac{1}{\rho_{pol}} \right) R_M$$

$$\left. \frac{d[M]}{dw} \right|_{w=0} = 0$$

Where:

$$R_M = 2k_{in,IM} [I^{\bullet}][M] + 2k_{in,\tilde{I}M} [\tilde{I}^{\bullet}][M] + 2k_{in,I_{PM}} [I_P^{\bullet}][M] + 2k_{p,R} [R^{\bullet}][M]$$

For $t > 0$ and $w = 1$:

$$+ 2k_{p,B} [B^{\bullet}][M] + 2k_{p,C} [C^{\bullet}][M] + 2k_{p,T} [T^{\bullet}][M] + 2k_{p,O} [O^{\bullet}][M]$$

$$\left. \frac{d[M]}{dw} \right|_{w=1} = 0$$

7) Pendant vinyl group

<p>For $t = 0$ and $0 \leq w \leq 1$:</p> <p>$[V_P] = 0$</p>	$\frac{\partial [V_P]}{\partial t} \Big _w = R_{V_P}$ $- [V_P] \left(\frac{M_{HDDA}}{\rho_{HDDA}} D_M \left(\frac{\partial z}{\partial w} \Big _t \right)^{-2} \frac{\partial^2 [M]}{\partial w^2} \Big _t \right.$ $+ \frac{M_{HDDA}}{\rho_{HDDA}} \left(\frac{\partial z}{\partial w} \Big _t \right)^{-2} \left(\frac{\partial [M]}{\partial w} \Big _t \right)^2 \frac{A_M (v_{f0} - v_{f1})}{[M]_0 v_f^2} D_M$ $\left. - M_{HDDA} \left(\frac{1}{\rho_{HDDA}} - \frac{1}{\rho_{pol}} \right) R_M \right)$ <p>where:</p> $R_{V_P} = + 2k_{p,R} [R^{\bullet\bullet}][M] + k_{bb,R} [R^{\bullet\bullet}] + k_{t,RR} [R^{\bullet\bullet}][R^{\bullet\bullet}] + k_{t,RB} [R^{\bullet\bullet}][B^{\bullet}] + k_{t,RC} [R^{\bullet\bullet}][C^{\bullet}]$ $+ 2k_{t,RT} [R^{\bullet\bullet}][T^{\bullet}] + k_{t,RO} [R^{\bullet\bullet}][O^{\bullet}] + k_{t,IR} [I^{\bullet}][R^{\bullet\bullet}] + k_{t,\tilde{I}R} [\tilde{I}^{\bullet}][R^{\bullet\bullet}]$ $+ k_{t,IPR} [I_P^{\bullet}][R^{\bullet\bullet}] + k_{t,BT} [B^{\bullet}][T^{\bullet}] + k_{t,CT} [C^{\bullet}][T^{\bullet}] + k_{t,TT} [T^{\bullet}][T^{\bullet}]$ $+ k_{t,TO} [O^{\bullet}][T^{\bullet}] + k_{t,IT} [I^{\bullet}][T^{\bullet}] + k_{t,\tilde{I}T} [\tilde{I}^{\bullet}][T^{\bullet}] + k_{t,IP,T} [I_P^{\bullet}][T^{\bullet}]$ $- k_{in,IV_P} [I^{\bullet}][V_P] - k_{in,\tilde{I}V_P} [\tilde{I}^{\bullet}][V_P] - k_{in,IPV_P} [I_P^{\bullet}][V_P] - k_{b,B} [B^{\bullet}][V_P]$ $- k_{b,C} [C^{\bullet}][V_P] - k_{b,T} [T^{\bullet}][V_P] - k_{b,O} [O^{\bullet}][V_P] + k_{O_2,R} [R^{\bullet\bullet}][O_2]$
---	---

8) Oxygen

<p>For $t = 0$ and $0 \leq w \leq 1$:</p> <p>$[O_2] = [O_2]^*$</p> <p>$= 2.5 \times 10^{-3} \left(\frac{mol}{L}\right)$</p> <p>For $t > 0$ and $w = 0$:</p> <p>$[O_2] = [O_2]^*$</p> <p>$= 2.5 \times 10^{-3} \left(\frac{mol}{L}\right)$</p> <p>For $t > 0$ and $w = 1$:</p> <p>$\frac{d[O_2]}{dw} \Big _{w=1} = 0$</p>	$\frac{\partial [O_2]}{\partial t} \Big _w = D_{O_2} \left(\frac{\partial z}{\partial w} \Big _t\right)^{-2} \frac{\partial^2 [O_2]}{\partial w^2} \Big _t + D_{O_2} \left(\frac{\partial z}{\partial w} \Big _t\right)^{-2} \frac{\partial [O_2]}{\partial w} \Big _t \frac{A_{O_2}(v_{f0} - v_{f1})}{[M]_0 v_f^2} \frac{\partial [M]}{\partial w} \Big _t + R_{O_2}$ $- [O_2] \left(\frac{M_{HDDA}}{\rho_{HDDA}} D_M \left(\frac{\partial z}{\partial w} \Big _t\right)^{-2} \frac{\partial^2 [M]}{\partial w^2} \Big _t\right.$ $+ \frac{M_{HDDA}}{\rho_{HDDA}} \left(\frac{\partial z}{\partial w} \Big _t\right)^{-2} \left(\frac{\partial [M]}{\partial w} \Big _t\right)^2 \frac{A_M(v_{f0} - v_{f1})}{[M]_0 v_f^2} D_M$ $\left. - M_{HDDA} \left(\frac{1}{\rho_{HDDA}} - \frac{1}{\rho_{pol}}\right) R_M\right)$ <p>where:</p> $R_{O_2} = -k_{O_2,R}[O_2][R^{\bullet}] - k_{O_2,B}[O_2][B^{\bullet}] - k_{O_2,C}[O_2][C^{\bullet}] - k_{O_2,T}[O_2][T^{\bullet}] - k_{O_2,I}[O_2][I^{\bullet}]$ $- k_{O_2,I}[O_2][\tilde{I}^{\bullet}] - k_{O_2,IP}[O_2][I_P^{\bullet}] + \frac{1}{2}k_{t,OO}[O^{\bullet}][O^{\bullet}]$
---	--

9) Regular radical

<p>For $t = 0$ and $0 \leq w \leq 1$:</p> <p>$[R^{\bullet}] = 0$</p>	$\frac{\partial [R^{\bullet}]}{\partial t} \Big _w = R_{R^{\bullet}}$ $- [R^{\bullet}] \left(\frac{M_{HDDA}}{\rho_{HDDA}} D_M \left(\frac{\partial z}{\partial w} \Big _t\right)^{-2} \frac{\partial^2 [M]}{\partial w^2} \Big _t\right.$ $+ \frac{M_{HDDA}}{\rho_{HDDA}} \left(\frac{\partial z}{\partial w} \Big _t\right)^{-2} \left(\frac{\partial [M]}{\partial w} \Big _t\right)^2 \frac{A_M(v_{f0} - v_{f1})}{[M]_0 v_f^2} D_M$ $\left. - M_{HDDA} \left(\frac{1}{\rho_{HDDA}} - \frac{1}{\rho_{pol}}\right) R_M\right)$
---	---

where:

$$\begin{aligned}
 R_{R^{\bullet}} = & + 2k_{in,IM} [I^{\bullet}][M] + 2k_{in,\tilde{I}M} [\tilde{I}^{\bullet}][M] + 2k_{in,IPM} [I_P^{\bullet}][M] + 2k_{p,B} [B^{\bullet}][M] \\
 & + 2k_{p,C} [C^{\bullet}][M] + 2k_{p,T} [T^{\bullet}][M] + 2k_{p,O} [O^{\bullet}][M] - k_{b,R} [R^{\bullet}][V_P] \\
 & - k_C [R^{\bullet}] - k_{bb,R} [R^{\bullet}] - k_{t,RR} [R^{\bullet}][R^{\bullet}] - k_{t,RB} [R^{\bullet}][B^{\bullet}] \\
 & - k_{t,RC} [R^{\bullet}][C^{\bullet}] - k_{t,RT} [R^{\bullet}][T^{\bullet}] - k_{t,RO} [R^{\bullet}][O^{\bullet}] - k_{t,IR} [I^{\bullet}][R^{\bullet}] \\
 & - k_{t,\tilde{I}R} [\tilde{I}^{\bullet}][R^{\bullet}] - k_{t,IPR} [I_P^{\bullet}][R^{\bullet}] - k_{O_2,R} [R^{\bullet}][O_2]
 \end{aligned}$$

10) Branching radical

$$\left. \frac{\partial [B^{\bullet}]}{\partial t} \right|_w = R_{B^{\bullet}}$$

For $t = 0$ and $0 \leq w \leq 1$:
 $[B^{\bullet}] = 0$

$$\begin{aligned}
 & - [B^{\bullet}] \left(\frac{M_{HDDA}}{\rho_{HDDA}} D_M \left(\frac{\partial z}{\partial w} \right)_t \right)^{-2} \frac{\partial^2 [M]}{\partial w^2} \Big|_t \\
 & + \frac{M_{HDDA}}{\rho_{HDDA}} \left(\frac{\partial z}{\partial w} \right)_t^{-2} \left(\frac{\partial [M]}{\partial w} \right)_t^2 \frac{A_M (v_{f0} - v_{f1})}{[M]_0 v_f^2} D_M \\
 & - M_{HDDA} \left(\frac{1}{\rho_{HDDA}} - \frac{1}{\rho_{pol}} \right) R_M
 \end{aligned}$$

where:

$$\begin{aligned}
R_{B\cdot} = & + k_{in,IV_P} [I\cdot][V_P] + k_{in,\tilde{I}V_P} [\tilde{I}\cdot][V_P] + k_{in,I_P V_P} [I_P\cdot][V_P] + k_{b,R} [R^{\cdot\cdot}][V_P] \\
& + k_{b,C} [C\cdot][V_P] + k_{b,T} [T\cdot][V_P] + k_{b,O} [O\cdot][V_P] \\
& - 2 k_{p,B} [B\cdot][M] - k_{t,RB} [R^{\cdot\cdot}][B\cdot] - k_{t,BB} [B\cdot][B\cdot] - k_{t,BC} [[B\cdot]C\cdot] \\
& - k_{t,BT} [B\cdot][T\cdot] - k_{t,BO} [B\cdot][O\cdot] - k_{t,IB} [I\cdot][B\cdot] - k_{t,\tilde{I}B} [\tilde{I}\cdot][B\cdot] \\
& - k_{t,I_P B} [I_P\cdot][B\cdot] - k_{O_2,B} [B\cdot][O_2]
\end{aligned}$$

11) Cyclic radical

$$\begin{aligned}
\left. \frac{\partial [C\cdot]}{\partial t} \right|_w = & R_{C\cdot} - [C\cdot] \left(\frac{M_{HDDA}}{\rho_{HDDA}} D_M \left(\frac{\partial z}{\partial w} \right)_t \right)^{-2} \frac{\partial^2 [M]}{\partial w^2} \Big|_t \\
& + \frac{M_{HDDA}}{\rho_{HDDA}} \left(\frac{\partial z}{\partial w} \right)_t^{-2} \left(\frac{\partial [M]}{\partial w} \right)_t^2 \frac{A_M (v_{f0} - v_{f1})}{[M]_0 v_f^2} D_M \\
& - M_{HDDA} \left(\frac{1}{\rho_{HDDA}} - \frac{1}{\rho_{pol}} \right) R_M
\end{aligned}$$

For $t = 0$ and $0 \leq w \leq 1$:

$$[C\cdot] = 0$$

where:

$$\begin{aligned}
R_{C\cdot} = & + k_C [R^{\cdot\cdot}] - 2 k_{p,C} [C\cdot][M] - k_{b,C} [C\cdot][V_P] - k_{bb,R} [C\cdot] - k_{t,RC} [R^{\cdot\cdot}][C\cdot] \\
& - k_{t,BC} [B\cdot][C\cdot] - k_{t,CC} [C\cdot][C\cdot] - k_{t,CT} [C\cdot][T\cdot] - k_{t,CO} [C\cdot][O\cdot] \\
& - k_{t,IC} [I\cdot][C\cdot] - k_{t,\tilde{I}C} [\tilde{I}\cdot][C\cdot] - k_{t,I_P C} [I_P\cdot][C\cdot] - k_{O_2,C} [C\cdot][O_2]
\end{aligned}$$

12) Tertiary radical

<p>For $t = 0$ and $0 \leq w \leq 1$:</p> <p>$[T^\bullet] = 0$</p>	$\left. \frac{\partial [T^\bullet]}{\partial t} \right _w = R_{T^\bullet}$ $- [T^\bullet] \left(\frac{M_{HDDA}}{\rho_{HDDA}} D_M \left(\frac{\partial z}{\partial w} \right)_t \right)^{-2} \frac{\partial^2 [M]}{\partial w^2} \Big _t$ $+ \frac{M_{HDDA}}{\rho_{HDDA}} \left(\frac{\partial z}{\partial w} \right)_t^{-2} \left(\frac{\partial [M]}{\partial w} \right)_t^2 \frac{A_M (v_{f0} - v_{f1})}{[M]_0 v_f^2} D_M$ $- M_{HDDA} \left(\frac{1}{\rho_{HDDA}} - \frac{1}{\rho_{pol}} \right) R_M$ <p>where:</p> $R_{T^\bullet} = + k_{bb,R} [R^{\bullet}] + k_{bb,R} [C^\bullet] + k_{bb,O} [O^\bullet] - 2k_{p,T} [T^\bullet][M] - k_{b,T} [T^\bullet][V_P]$ $- k_{t,RT} [R^{\bullet}][T^\bullet] - k_{t,BT} [B^\bullet][T^\bullet] - k_{t,CT} [C^\bullet][T^\bullet] - k_{t,TT} [T^\bullet][T^\bullet]$ $- k_{t,TO} [T^\bullet][O^\bullet] - k_{t,IT} [I^\bullet][T^\bullet] - k_{t,\tilde{I}T} [\tilde{I}^\bullet][T^\bullet] - k_{t,I_P T} [I_P^\bullet][T^\bullet]$ $- k_{O_2,T} [T^\bullet][O_2]$
13) Peroxidic radical	
<p>For $t = 0$ and $0 \leq w \leq 1$:</p> <p>$[O^\bullet] = 0$</p>	$\left. \frac{\partial [O^\bullet]}{\partial t} \right _w = R_{O^\bullet}$ $- [O^\bullet] \left(\frac{M_{HDDA}}{\rho_{HDDA}} D_M \left(\frac{\partial z}{\partial w} \right)_t \right)^{-2} \frac{\partial^2 [M]}{\partial w^2} \Big _t$ $+ \frac{M_{HDDA}}{\rho_{HDDA}} \left(\frac{\partial z}{\partial w} \right)_t^{-2} \left(\frac{\partial [M]}{\partial w} \right)_t^2 \frac{A_M (v_{f0} - v_{f1})}{[M]_0 v_f^2} D_M$ $- M_{HDDA} \left(\frac{1}{\rho_{HDDA}} - \frac{1}{\rho_{pol}} \right) R_M$

where:

$$\begin{aligned}
 R_{O^\bullet} = & + k_{O_2,I}[I^\bullet][O_2] + k_{O_2,\tilde{I}}[\tilde{I}^\bullet][O_2] + k_{O_2,I_P}[I_P^\bullet][O_2] + k_{O_2,R}[R^{\bullet\bullet}][O_2] + k_{O_2,B}[B^\bullet][O_2] \\
 & + k_{O_2,C}[C^\bullet][O_2] + k_{O_2,T}[T^\bullet][O_2] - 2 k_{p,O} [O^\bullet][M] - k_{b,O} [O^\bullet][V_p] \\
 & - k_{bb,O}[O^\bullet] - k_{t,IO}[I^\bullet][O^\bullet] - k_{t,\tilde{I}O}[\tilde{I}^\bullet][O^\bullet] - k_{t,I_PCO}[I_P^\bullet][O^\bullet] \\
 & - k_{t,RO}[R^{\bullet\bullet}][O^\bullet] - k_{t,BO}[B^\bullet][O^\bullet] - k_{t,CO}[C^\bullet][O^\bullet] - k_{t,TO}[T^\bullet][O^\bullet] \\
 & - k_{t,OO}[O^\bullet][O^\bullet]
 \end{aligned}$$

14) Relationship between z and w

For $t = 0$ and $0 \leq w \leq 1$:

$$\left. \frac{\partial z}{\partial t} \right|_w = D_M \left. \frac{\partial [M]}{\partial w} \right|_t \left(\left. \frac{\partial z}{\partial w} \right|_t \right)^{-1} \frac{M_{HDDA}}{\rho_{HDDA}} - M_{HDDA} \left(\frac{1}{\rho_{HDDA}} - \frac{1}{\rho_{pol}} \right) Q$$

$$z = wz_{f0}$$

where:

For $t > 0$ and $w = 0$:

$$Q = \int_{w=0}^w R_M dz = \int_{z=0}^{z(w=0.4)} R_M dz$$

$$z = 0$$

where:

For $t = 0$ and $0 \leq w \leq 1$:

$$\begin{aligned}
 R_M = & 2k_{in,IM} [I^\bullet][M] + 2k_{in,\tilde{I}M} [\tilde{I}^\bullet][M] + 2k_{in,I_P M} [I_P^\bullet][M] + 2k_{p,R}[R^{\bullet\bullet}][M] \\
 & + 2k_{p,B} [B^\bullet][M] + 2k_{p,C} [C^\bullet][M] + 2k_{p,T} [T^\bullet][M] + 2 k_{p,O} [O^\bullet][M]
 \end{aligned}$$

$$Q = 0$$

For $t > 0$ and $w = 0$:

$$Q = 0$$

B3 Detailed derivation of model PDEs

B3.1 Relationship between z and w

This section describes the derivation of equation (3.6) in the manuscript. All symbols are described in Chapter 2 and in the nomenclature. Consider one of the 10 segments with height Δz and scaled height Δw during a short period of time Δt (s) as shown in figure S1.

A material balance on this segment gives:

$$\begin{aligned} \text{change in} &= \text{volume of material} - \text{volume of material} - \text{shrinkage within} \quad (\text{B.1}) \\ \text{volume} & \quad \text{diffusing in} \quad \quad \quad \text{diffusing out} \quad \quad \quad \text{the segment due to} \\ & \quad \quad \quad \quad \quad \quad \quad \quad \quad \quad \quad \quad \quad \quad \quad \text{polymerization} \end{aligned}$$

We assume that volume changes due to diffusion of initiator and oxygen are negligible. As a result, if the segment is the first (top) segment, the first term on the right-hand side is zero, because only oxygen diffuses through the top surface. In this situation equation (B.1) simplifies to:

$$\begin{aligned} \text{change in} &= - \text{volume of monomer} - \text{shrinkage within} \\ \text{volume} & \quad \text{diffusing out} \quad \quad \quad \text{the segment due to} \\ & \quad \quad \quad \quad \quad \quad \quad \quad \quad \quad \quad \quad \quad \quad \quad \text{polymerization} \end{aligned}$$

where:

$$\begin{aligned} \text{volume of monomer} & \\ \text{diffusing out} & = - D_M \frac{\partial [M]}{\partial z} \Big|_{t,w=0.1} \frac{M_{HDDA}}{\rho_{HDDA}} A \Delta t \end{aligned}$$

$$\begin{aligned} \text{shrinkage within} &= (\text{volume of 1 mol} - \text{volume of polymer}) * \text{mols of monomer} \\ \text{volume due to} & \quad \text{of monomer} \quad \text{made from 1 mol of} \quad \text{consumed} \\ \text{reaction} & \quad \quad \quad \text{monomer} \quad \quad \quad \text{during } \Delta t \end{aligned}$$

$$= A\Delta z_1 M_{HDDA} \left(\frac{1}{\rho_{HDDA}} - \frac{1}{\rho_{pol}} \right) \sum_X 2k_{p,X}[M][X] \Delta t$$

substituting these terms into equation (B.1) gives:

$$\begin{aligned} \Delta(A\Delta z_1) = & D_M \frac{\partial[M]}{\partial z} \Big|_{t,w=0.1} \frac{M_{HDDA}}{\rho_{HDDA}} A\Delta t \\ & - A\Delta z_1 \Delta t M_{HDDA} \left(\frac{1}{\rho_{HDDA}} - \frac{1}{\rho_{pol}} \right) \sum_X 2k_{p,X}[M][X] \end{aligned} \quad (B.2)$$

Substituting for R_M using equation (3.2) in the manuscript gives:

$$\Delta(A\Delta z_1) = D_M \frac{\partial[M]}{\partial z} \Big|_{t,w=0.1} \frac{M_{HDDA}}{\rho_{HDDA}} A\Delta t - A\Delta z_1 \Delta t M_{HDDA} \left(\frac{1}{\rho_{HDDA}} - \frac{1}{\rho_{pol}} \right) R_M \quad (B.3)$$

Similarly, a material balance on the i^{th} segment, for $i = 2 \dots 9$, is:

$$\begin{aligned} \Delta(A\Delta z_i) = & -D_M \frac{\partial[M]}{\partial z} \Big|_{t,w} \frac{M_{HDDA}}{\rho_{HDDA}} A\Delta t + D_M \frac{\partial[M]}{\partial z} \Big|_{t,w+\Delta w} \frac{M_{HDDA}}{\rho_{HDDA}} A\Delta t \\ & - A\Delta z_i \Delta t M_{HDDA} \left(\frac{1}{\rho_{HDDA}} - \frac{1}{\rho_{pol}} \right) R_M \end{aligned} \quad (B.4)$$

Because no monomer can diffuse through the bottom surface, the corresponding material balance

on the 10th segment is:

$$\Delta(A\Delta z_{10}) = -D_M \frac{\partial[M]}{\partial z} \Big|_{t,w=0.9} \frac{M_{HDDA}}{\rho_{HDDA}} A\Delta t - A\Delta z_{10} \Delta t M_{HDDA} \left(\frac{1}{\rho_{HDDA}} - \frac{1}{\rho_{pol}} \right) R_M \quad (B.5)$$

If we want to find the position z corresponding to a certain w , for example $w = 0.4$, which is the

bottom of the 4th segment from the top surface, we need to track the volume changes in the top 4

segments and add them together. At the bottom surface of the 4th segment, the change in position z during the period Δt is:

$$A\Delta \sum_{i=1}^4 (\Delta z_i) = D_M \left. \frac{\partial[M]}{\partial z} \right|_{t,w=0.4} \frac{M_{HDDA}}{\rho_{HDDA}} A\Delta t - A\Delta t M_{HDDA} \left(\frac{1}{\rho_{HDDA}} - \frac{1}{\rho_{pol}} \right) \sum_{i=1}^4 \Delta z_i R_M \quad (B.6)$$

Dividing both sides of equation (B.6) by $A\Delta t$ gives:

$$\frac{\Delta \sum_{i=1}^4 \Delta z_i}{\Delta t} = D_M \left. \frac{\partial[M]}{\partial z} \right|_{t,w=0.4} \frac{M_{HDDA}}{\rho_{HDDA}} - M_{HDDA} \left(\frac{1}{\rho_{HDDA}} - \frac{1}{\rho_{pol}} \right) \sum_{i=1}^4 \Delta z_i R_M \quad (B.7)$$

Taking the limit as $\Delta z \rightarrow 0$ while staying at $w = 0.4$ converts the summations into integrals:

$$\frac{\Delta \int_{w=0}^{w=0.4} 1 dz}{\Delta t} = D_M \left. \frac{\partial[M]}{\partial z} \right|_{t,w=0.4} \frac{M_{HDDA}}{\rho_{HDDA}} - M_{HDDA} \left(\frac{1}{\rho_{HDDA}} - \frac{1}{\rho_{pol}} \right) \int_{w=0}^{w=0.4} R_M dz \quad (B.8)$$

Because the integral of 1 with respect to z is z , equation (B.8) becomes:

$$\frac{\Delta z(w = 0.4)}{\Delta t} = D_M \left. \frac{\partial[M]}{\partial z} \right|_{t,w=0.4} \frac{M_{HDDA}}{\rho_{HDDA}} - M_{HDDA} \left(\frac{1}{\rho_{HDDA}} - \frac{1}{\rho_{pol}} \right) \int_{w=0}^{w=0.4} R_M dz \quad (B.9)$$

Let $Q = \int_{w=0}^{w=0.4} R_M dz = \int_{z=0}^{z(w=0.4)} R_M dz$, so that equation (B.9) becomes:

$$\frac{\Delta z(w = 0.4)}{\Delta t} = D_M \left. \frac{\partial[M]}{\partial z} \right|_{t,w=0.4} \frac{M_{HDDA}}{\rho_{HDDA}} - M_{HDDA} \left(\frac{1}{\rho_{HDDA}} - \frac{1}{\rho_{pol}} \right) Q \quad (B.10)$$

As $\Delta t \rightarrow 0$, equation (B.10) becomes:

$$\left. \frac{\partial z}{\partial t} \right|_{w=0.4} = D_M \left. \frac{\partial[M]}{\partial z} \right|_{t,w=0.4} \frac{M_{HDDA}}{\rho_{HDDA}} - M_{HDDA} \left(\frac{1}{\rho_{HDDA}} - \frac{1}{\rho_{pol}} \right) Q \quad (B.11)$$

In general, for any w , we can obtain the corresponding value of z by solving:

$$\left. \frac{\partial z}{\partial t} \right|_w = D_M \left. \frac{\partial [M]}{\partial z} \right|_t \frac{M_{HDDA}}{\rho_{HDDA}} - M_{HDDA} \left(\frac{1}{\rho_{HDDA}} - \frac{1}{\rho_{pol}} \right) Q \quad (\text{B.12})$$

In equation (B.12), $\left. \frac{\partial [M]}{\partial z} \right|_t$ is the spatial derivative of $[M]$ with respect to z . This derivative needs to be replaced by an expression involving w instead of z . We know that the monomer concentration is a function of z and t (i.e., $[M] = f_1(z, t)$) and, alternatively, a function of w and t (i.e., $[M] = f_2(w, t)$). Using the chain rule:

$$\left. \frac{\partial [M]}{\partial z} \right|_t = \left. \frac{\partial [M]}{\partial w} \right|_t \left. \frac{\partial w}{\partial z} \right|_t \quad (\text{B.13})$$

$$\therefore \left. \frac{\partial [M]}{\partial z} \right|_t = \left. \frac{\partial [M]}{\partial w} \right|_t \left(\left. \frac{\partial z}{\partial w} \right|_t \right)^{-1} \quad (\text{B.14})$$

Now substituting equation (B.14) in equation (B.12) leads to equation (3.6) in the manuscript:

$$\left. \frac{\partial z}{\partial t} \right|_w = D_M \left. \frac{\partial [M]}{\partial w} \right|_t \left(\left. \frac{\partial z}{\partial w} \right|_t \right)^{-1} \frac{M_{HDDA}}{\rho_{HDDA}} - M_{HDDA} \left(\frac{1}{\rho_{HDDA}} - \frac{1}{\rho_{pol}} \right) Q \quad (3.6)$$

where Q is:

$$Q = \int_{w=0}^w R_M dz = \int_{z=0}^{z(w)} R_M dz \quad (\text{B.15})$$

The initial condition (IC) for this PDE is $z(t = 0) = wz_{f,0}$. The boundary condition (BC) at the top surface of the film is $z(w = 0) = 0$. Since there is only a first derivative of z with respect to w on the right-hand side of equation (3.6), only one BC is needed.

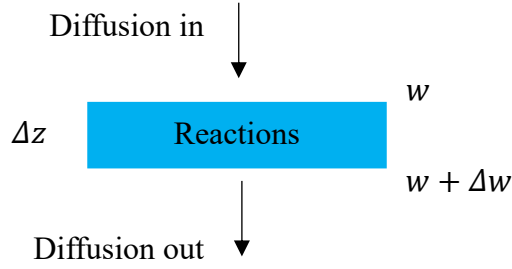


Fig. B.1: Schematic diagram of reactions and diffusion for a thin segment of height Δz and scaled height Δw during a short period of time Δt .

B3.2 Material Balance on Monomer PDE:

This section describes the derivation of equation (3.9) in the manuscript. Consider one of the 10 segments (see figure B.1) with height Δz and scaled height Δw during a short period of time Δt .

In this segment:

$$\begin{array}{l} \text{accumulation} \\ \text{of monomer} \end{array} = \begin{array}{l} \text{monomer} \\ \text{diffusing in} \end{array} - \begin{array}{l} \text{monomer} \\ \text{diffusing out} \end{array} - \begin{array}{l} \text{monomer consumed} \\ \text{by reaction} \end{array} \quad (\text{B.16})$$

The accumulation of monomer (in moles) in the segment is $\Delta([M]A\Delta z)$ where $[M]$ is the local HDDA monomer concentration in mol m^{-3} . The moles of monomer that diffuse in at the top of the segment is $-D_M \frac{\partial[M]}{\partial z} \Big|_{t,w} A\Delta t$ where D_M is the diffusivity of the monomer in $\text{m}^2 \text{s}^{-1}$. The moles of monomer that diffuse out at the bottom of the segment is $-D_M \frac{\partial[M]}{\partial z} \Big|_{t,w+\Delta w} A\Delta t$. The moles of monomer that get consumed due to polymerization is $A\Delta z\Delta t R_M$. Substituting into equation (B.16) gives:

$$\begin{aligned} \Delta([M]A\Delta z)|_w &= -D_M \frac{\partial[M]}{\partial z} \Big|_{t,w} A\Delta t + D_M \frac{\partial[M]}{\partial z} \Big|_{t,w+\Delta w} A\Delta t \\ &\quad - A\Delta z\Delta t \sum_X 2k_{p,x}[M][X] \end{aligned} \quad (\text{B.17})$$

Rearranging equation (B.17) and dividing both sides by $A\Delta t\Delta w$ gives:

$$\frac{\Delta\left([M] \frac{\Delta z}{\Delta w}\right) \Big|_w}{\Delta t} = \frac{D_M \frac{\partial[M]}{\partial z} \Big|_{t,w+\Delta w} - D_M \frac{\partial[M]}{\partial z} \Big|_{t,w}}{\Delta w} - \frac{\Delta z}{\Delta w} R_M \quad (\text{B.18})$$

Substituting for $\frac{\partial[M]}{\partial z} \Big|_t$ from equation (B.14) gives:

$$\begin{aligned} \frac{\Delta\left([M] \frac{\Delta z}{\Delta w}\right) \Big|_w}{\Delta t} &= \frac{D_M \frac{\partial[M]}{\partial w} \Big|_{t,w+\Delta w} \left(\frac{\partial z}{\partial w} \Big|_{t,w+\Delta w}\right)^{-1} - D_M \frac{\partial[M]}{\partial w} \Big|_{t,w} \left(\frac{\partial z}{\partial w} \Big|_{t,w}\right)^{-1}}{\Delta w} \\ &\quad - \frac{\Delta z}{\Delta w} R_M \end{aligned} \quad (\text{B.19})$$

As $\Delta z \rightarrow 0$ and $\Delta w \rightarrow 0$ equation (B.19) becomes:

$$\frac{\Delta\left([M] \frac{\partial z}{\partial w} \Big|_t\right) \Big|_w}{\Delta t} = \frac{\partial\left(D_M \frac{\partial[M]}{\partial w} \Big|_t \left(\frac{\partial z}{\partial w} \Big|_t\right)^{-1}\right) \Big|_t}{\partial w} - \frac{\partial z}{\partial w} \Big|_t R_M \quad (\text{B.20})$$

As $\Delta t \rightarrow 0$, equation (B.20) becomes:

$$\left. \frac{\partial \left([M] \frac{\partial z}{\partial w} \right)}{\partial t} \right|_w = \left. \frac{\partial \left(D_M \frac{\partial [M]}{\partial w} \left(\frac{\partial z}{\partial w} \right)^{-1} \right)}{\partial w} \right|_t - \left. \frac{\partial z}{\partial w} \right|_t R_M \quad (\text{B.21})$$

Applying the product rule for $\left. \frac{\partial \left([M] \frac{\partial z}{\partial w} \right)}{\partial t} \right|_w$ gives:

$$[M] \left. \frac{\partial \left(\frac{\partial z}{\partial w} \right)}{\partial t} \right|_w + \left. \frac{\partial z}{\partial w} \right|_t \left. \frac{\partial [M]}{\partial t} \right|_w = \left. \frac{\partial \left(D_M \frac{\partial [M]}{\partial w} \left(\frac{\partial z}{\partial w} \right)^{-1} \right)}{\partial w} \right|_t - \left. \frac{\partial z}{\partial w} \right|_t R_M \quad (\text{B.22})$$

Substituting $\left. \frac{\partial \left(\frac{\partial z}{\partial w} \right)}{\partial t} \right|_w = \frac{\partial^2 z}{\partial w \partial t}$ and rearranging gives:

$$\left. \frac{\partial z}{\partial w} \right|_t \left. \frac{\partial [M]}{\partial t} \right|_w = \left. \frac{\partial \left(D_M \frac{\partial [M]}{\partial w} \left(\frac{\partial z}{\partial w} \right)^{-1} \right)}{\partial w} \right|_t - \left. \frac{\partial z}{\partial w} \right|_t R_M - [M] \frac{\partial^2 z}{\partial w \partial t} \quad (\text{B.23})$$

Applying the product rule for $\left. \frac{\partial \left(D_M \frac{\partial [M]}{\partial w} \left(\frac{\partial z}{\partial w} \right)^{-1} \right)}{\partial w} \right|_t$ gives:

$$\begin{aligned} \left. \frac{\partial z}{\partial w} \right|_t \left. \frac{\partial [M]}{\partial t} \right|_w &= D_M \left. \frac{\partial [M]}{\partial w} \right|_t \left. \frac{\partial \left(\left(\frac{\partial z}{\partial w} \right)^{-1} \right)}{\partial w} \right|_t + D_M \left(\frac{\partial z}{\partial w} \right)^{-1} \left. \frac{\partial^2 [M]}{\partial w^2} \right|_t \\ &+ \left. \frac{\partial [M]}{\partial w} \right|_t \left(\frac{\partial z}{\partial w} \right)^{-1} \left. \frac{\partial D_M}{\partial w} \right|_t - \left. \frac{\partial z}{\partial w} \right|_t R_M - [M] \frac{\partial^2 z}{\partial w \partial t} \end{aligned} \quad (\text{B.24})$$

Taking D_M as a common factor from the first two terms on the right-hand side gives:

$$\begin{aligned} \left. \frac{\partial z}{\partial w} \right|_t \left. \frac{\partial [M]}{\partial t} \right|_w &= D_M \left(- \left. \frac{\partial [M]}{\partial w} \right|_t \left(\left. \frac{\partial z}{\partial w} \right|_t \right)^{-2} \left. \frac{\partial^2 z}{\partial w^2} \right|_t + \left(\left. \frac{\partial z}{\partial w} \right|_t \right)^{-1} \left. \frac{\partial^2 [M]}{\partial w^2} \right|_t \right) \\ &+ \left. \frac{\partial [M]}{\partial w} \right|_t \left(\left. \frac{\partial z}{\partial w} \right|_t \right)^{-1} \left. \frac{\partial D_M}{\partial w} \right|_t - \left. \frac{\partial z}{\partial w} \right|_t R_M - [M] \left. \frac{\partial^2 z}{\partial w \partial t} \right|_t \end{aligned} \quad (\text{B.25})$$

Rearranging so that $\left. \frac{\partial [M]}{\partial t} \right|_w$ appears by itself on the left-hand side gives:

$$\begin{aligned} \left. \frac{\partial [M]}{\partial t} \right|_w &= D_M \left(- \left. \frac{\partial [M]}{\partial w} \right|_t \left(\left. \frac{\partial z}{\partial w} \right|_t \right)^{-3} \left. \frac{\partial^2 z}{\partial w^2} \right|_t + \left(\left. \frac{\partial z}{\partial w} \right|_t \right)^{-2} \left. \frac{\partial^2 [M]}{\partial w^2} \right|_t \right) \\ &+ \left. \frac{\partial [M]}{\partial w} \right|_t \left(\left. \frac{\partial z}{\partial w} \right|_t \right)^{-2} \left. \frac{\partial D_M}{\partial w} \right|_t - R_M - [M] \left. \frac{\partial^2 z}{\partial w \partial t} \right|_t \left(\left. \frac{\partial z}{\partial w} \right|_t \right)^{-1} \end{aligned} \quad (\text{B.26})$$

Equation (B.26) can be simplified to get rid of the complicated $\left(\left. \frac{\partial z}{\partial w} \right|_t \right)^{-3} \left. \frac{\partial^2 z}{\partial w^2} \right|_t$ and $\left. \frac{\partial^2 z}{\partial w \partial t} \right|_t \left(\left. \frac{\partial z}{\partial w} \right|_t \right)^{-1}$ terms. First, consider $\left(\left. \frac{\partial z}{\partial w} \right|_t \right)^{-3} \left. \frac{\partial^2 z}{\partial w^2} \right|_t$, which is the limit as $\Delta z \rightarrow 0$ and $\Delta w \rightarrow 0$ of

$\left(\frac{\Delta z}{\Delta w} \right)^{-3} \frac{1}{\Delta w} \Delta \left(\frac{\Delta z}{\Delta w} \right) \Big|_t$. This expression in terms of Δw and Δz can be simplified using:

$$\begin{aligned} \left(\frac{\Delta z}{\Delta w} \right)^{-3} \frac{1}{\Delta w} \Delta \left(\frac{\Delta z}{\Delta w} \right) \Big|_t &= \frac{\Delta w^3}{\Delta z^3} \frac{1}{\Delta w} \Delta \left(\frac{\Delta z}{\Delta w} \right) \Big|_t = \frac{\Delta w^2}{\Delta z^3} \Delta \left(\frac{\Delta z}{\Delta w} \right) \Big|_t \\ \therefore \left(\frac{\Delta z}{\Delta w} \right)^{-3} \frac{1}{\Delta w} \Delta \left(\frac{\Delta z}{\Delta w} \right) \Big|_t &= \frac{\Delta w^2}{\Delta z^2} \frac{1}{\Delta z} \Delta \left(\frac{\Delta z}{\Delta w} \right) \Big|_t \end{aligned} \quad (\text{B.27})$$

As $\Delta z \rightarrow 0$ and $\Delta w \rightarrow 0$, equation (B.27) becomes:

$$\left(\left. \frac{\partial z}{\partial w} \right|_t \right)^{-3} \left. \frac{\partial^2 z}{\partial w^2} \right|_t = \left(\left. \frac{\partial w}{\partial z} \right|_t \right)^2 \left. \frac{\partial^2 z}{\partial z \partial w} \right|_t$$

Since the order of taking mixed second derivatives does not matter:

$$\therefore \left(\frac{\partial z}{\partial w}\right)_t^{-3} \frac{\partial^2 z}{\partial w^2}\bigg|_t = \left(\frac{\partial w}{\partial z}\right)^2 \frac{\partial}{\partial w} \left(\frac{\partial z}{\partial z}\right) = \left(\frac{\partial w}{\partial z}\right)^2 \frac{\partial(1)}{\partial w} = 0$$

In summary:

$$\left(\frac{\partial z}{\partial w}\right)_t^{-3} \frac{\partial^2 z}{\partial w^2}\bigg|_t = 0 \quad (\text{B.28})$$

Second, consider $\frac{\partial^2 z}{\partial w \partial t} \left(\frac{\partial z}{\partial w}\right)_t^{-1}$. Equation (3.6) provides an expression for $\frac{\partial z}{\partial t}\bigg|_w$ which can be differentiated with respect to w to give:

$$\frac{\partial^2 z}{\partial w \partial t} = \frac{\partial}{\partial w} \left(D_M \frac{\partial[M]}{\partial w}\bigg|_t \left(\frac{\partial z}{\partial w}\right)_t^{-1} \frac{M_{HDDA}}{\rho_{HDDA}} - M_{HDDA} \left(\frac{1}{\rho_{HDDA}} - \frac{1}{\rho_{pol}} \right) Q \right)\bigg|_t \quad (\text{B.29})$$

which becomes:

$$\begin{aligned} \therefore \frac{\partial^2 z}{\partial w \partial t} &= \frac{\partial}{\partial w} \left(D_M \frac{\partial[M]}{\partial w}\bigg|_t \left(\frac{\partial z}{\partial w}\right)_t^{-1} \frac{M_{HDDA}}{\rho_{HDDA}} \right)\bigg|_t \\ &\quad - \frac{\partial}{\partial w} \left(M_{HDDA} \left(\frac{1}{\rho_{HDDA}} - \frac{1}{\rho_{pol}} \right) Q \right)\bigg|_t \end{aligned} \quad (\text{B.30})$$

Factoring the constant molar masses and densities out of the derivatives gives:

$$\therefore \frac{\partial^2 z}{\partial w \partial t} = \frac{M_{HDDA}}{\rho_{HDDA}} \frac{\partial}{\partial w} \left(D_M \frac{\partial[M]}{\partial w}\bigg|_t \left(\frac{\partial z}{\partial w}\right)_t^{-1} \right)\bigg|_t - M_{HDDA} \left(\frac{1}{\rho_{HDDA}} - \frac{1}{\rho_{pol}} \right) \frac{\partial Q}{\partial w}\bigg|_t \quad (\text{B.31})$$

Differentiating equation (B.15) with respect to w gives:

$$\left. \frac{\partial Q}{\partial w} \right|_t = \left. \frac{\partial z}{\partial w} \right|_t R_M \quad (\text{B.32})$$

Applying product rule to $\left. \frac{\partial}{\partial w} \left(D_M \left. \frac{\partial[M]}{\partial w} \right|_t \left(\left. \frac{\partial z}{\partial w} \right|_t \right)^{-1} \right) \right|_t$ and substituting for $\left. \frac{\partial Q}{\partial w} \right|_t$ using equation (B.31)

gives:

$$\begin{aligned} \frac{\partial^2 z}{\partial w \partial t} &= \frac{M_{HDDA}}{\rho_{HDDA}} D_M \left(\left. \frac{\partial[M]}{\partial w} \right|_t \left. \frac{\partial}{\partial w} \left(\left(\left. \frac{\partial z}{\partial w} \right|_t \right)^{-1} \right) \right|_t + \left(\left. \frac{\partial z}{\partial w} \right|_t \right)^{-1} \left. \frac{\partial^2[M]}{\partial w^2} \right|_t \right) \\ &+ \frac{M_{HDDA}}{\rho_{HDDA}} \left. \frac{\partial[M]}{\partial w} \right|_t \left(\left. \frac{\partial z}{\partial w} \right|_t \right)^{-1} \left. \frac{\partial D_M}{\partial w} \right|_t - M_{HDDA} \left(\frac{1}{\rho_{HDDA}} - \frac{1}{\rho_{pol}} \right) \left. \frac{\partial z}{\partial w} \right|_t R_M \end{aligned} \quad (\text{B.33})$$

Using the chain rule to simplify $\left. \frac{\partial}{\partial w} \left(\left(\left. \frac{\partial z}{\partial w} \right|_t \right)^{-1} \right) \right|_t$ gives:

$$\begin{aligned} \frac{\partial^2 z}{\partial w \partial t} &= \frac{M_{HDDA}}{\rho_{HDDA}} D_M \left(- \left. \frac{\partial[M]}{\partial w} \right|_t \left(\left. \frac{\partial z}{\partial w} \right|_t \right)^{-2} \left. \frac{\partial^2 z}{\partial w^2} \right|_t + \left(\left. \frac{\partial z}{\partial w} \right|_t \right)^{-1} \left. \frac{\partial^2[M]}{\partial w^2} \right|_t \right) \\ &+ \frac{M_{HDDA}}{\rho_{HDDA}} \left. \frac{\partial[M]}{\partial w} \right|_t \left(\left. \frac{\partial z}{\partial w} \right|_t \right)^{-1} \left. \frac{\partial D_M}{\partial w} \right|_t - M_{HDDA} \left(\frac{1}{\rho_{HDDA}} - \frac{1}{\rho_{pol}} \right) \left. \frac{\partial z}{\partial w} \right|_t R_M \end{aligned} \quad (\text{B.34})$$

As a result, the ugly expression of interest $\left. \frac{\partial^2 z}{\partial w \partial t} \left(\left. \frac{\partial z}{\partial w} \right|_t \right)^{-1} \right|_t$ becomes:

$$\begin{aligned}
& \frac{\partial^2 z}{\partial w \partial t} \left(\frac{\partial z}{\partial w} \Big|_t \right)^{-1} \\
&= \frac{M_{HDDA}}{\rho_{HDDA}} D_M \left(- \frac{\partial[M]}{\partial w} \Big|_t \left(\frac{\partial z}{\partial w} \Big|_t \right)^{-2} \frac{\partial^2 z}{\partial w^2} \Big|_t \right. \\
&+ \left. \left(\frac{\partial z}{\partial w} \Big|_t \right)^{-1} \frac{\partial^2[M]}{\partial w^2} \Big|_t \right) \left(\frac{\partial z}{\partial w} \Big|_t \right)^{-1} + \frac{M_{HDDA}}{\rho_{HDDA}} \frac{\partial[M]}{\partial w} \Big|_t \left(\frac{\partial z}{\partial w} \Big|_t \right)^{-2} \frac{\partial D_M}{\partial w} \Big|_t \\
&- M_{HDDA} \left(\frac{1}{\rho_{HDDA}} - \frac{1}{\rho_{pol}} \right) R_M
\end{aligned} \tag{B.35}$$

which simplifies to:

$$\begin{aligned}
& \frac{\partial^2 z}{\partial w \partial t} \left(\frac{\partial z}{\partial w} \Big|_t \right)^{-1} \\
&= \frac{M_{HDDA}}{\rho_{HDDA}} D_M \left(- \frac{\partial[M]}{\partial w} \Big|_t \left(\frac{\partial z}{\partial w} \Big|_t \right)^{-3} \frac{\partial^2 z}{\partial w^2} \Big|_t + \left(\frac{\partial z}{\partial w} \Big|_t \right)^{-2} \frac{\partial^2[M]}{\partial w^2} \Big|_t \right) \\
&+ \frac{M_{HDDA}}{\rho_{HDDA}} \frac{\partial[M]}{\partial w} \Big|_t \left(\frac{\partial z}{\partial w} \Big|_t \right)^{-2} \frac{\partial D_M}{\partial w} \Big|_t - M_{HDDA} \left(\frac{1}{\rho_{HDDA}} - \frac{1}{\rho_{pol}} \right) R_M
\end{aligned} \tag{B.36}$$

Substituting for $\left(\frac{\partial z}{\partial w} \Big|_t \right)^{-3} \frac{\partial^2 z}{\partial w^2} \Big|_t = 0$ using equation (B.36) gives:

$$\begin{aligned}
& \frac{\partial^2 z}{\partial w \partial t} \left(\frac{\partial z}{\partial w} \Big|_t \right)^{-1} \\
&= \frac{M_{HDDA}}{\rho_{HDDA}} D_M \left(\frac{\partial z}{\partial w} \Big|_t \right)^{-2} \frac{\partial^2[M]}{\partial w^2} \Big|_t + \frac{M_{HDDA}}{\rho_{HDDA}} \frac{\partial[M]}{\partial w} \Big|_t \left(\frac{\partial z}{\partial w} \Big|_t \right)^{-2} \frac{\partial D_M}{\partial w} \Big|_t \\
&- M_{HDDA} \left(\frac{1}{\rho_{HDDA}} - \frac{1}{\rho_{pol}} \right) R_M
\end{aligned} \tag{B.37}$$

Substituting equations (B.28) and (B.37) into equation (B.26) gives:

$$\begin{aligned}
\left. \frac{\partial [M]}{\partial t} \right|_w &= D_M \left(\left. \frac{\partial z}{\partial w} \right|_t \right)^{-2} \left. \frac{\partial^2 [M]}{\partial w^2} \right|_t + \left. \frac{\partial [M]}{\partial w} \right|_t \left(\left. \frac{\partial z}{\partial w} \right|_t \right)^{-2} \left. \frac{\partial D_M}{\partial w} \right|_t - R_M \\
&- [M] \left(\frac{M_{HDDA}}{\rho_{HDDA}} D_M \left(\left. \frac{\partial z}{\partial w} \right|_t \right)^{-2} \left. \frac{\partial^2 [M]}{\partial w^2} \right|_t \right. \\
&\left. + \frac{M_{HDDA}}{\rho_{HDDA}} \left. \frac{\partial [M]}{\partial w} \right|_t \left(\left. \frac{\partial z}{\partial w} \right|_t \right)^{-2} \left. \frac{\partial D_M}{\partial w} \right|_t - M_{HDDA} \left(\frac{1}{\rho_{HDDA}} - \frac{1}{\rho_{pol}} \right) R_M \right)
\end{aligned} \tag{B.38}$$

Notice that there are no mixed second derivatives in this PDE. To get an appropriate expression for $\left. \frac{\partial D_M}{\partial w} \right|_t$, we acknowledge that D_M is a function of position because it depends on the local monomer concentration as indicated by equation B.4.13 in Table B.3.

$$D_M = D_{M_HDDA} \exp \left[-A_M \left(\frac{1}{v_{f1} + \frac{[M]}{[M]_0} (v_{f0} - v_{f1})} - \frac{1}{v_{f0}} \right) \right] \tag{B.39}$$

Differentiating equation (B.39) with respect to w gives:

$$\left. \frac{\partial D_M}{\partial w} \right|_t = D_M \frac{A_M (v_{f0} - v_{f1})}{[M]_0 (v_f)^2} \left. \frac{\partial [M]}{\partial w} \right|_t \tag{B.40}$$

Substituting equation (B.40) into equation (B.38) gives:

$$\begin{aligned}
\left. \frac{\partial [M]}{\partial t} \right|_w &= D_M \left(\left. \frac{\partial z}{\partial w} \right|_t \right)^{-2} \left. \frac{\partial^2 [M]}{\partial w^2} \right|_t + \left(\left. \frac{\partial [M]}{\partial w} \right|_t \right)^2 \left(\left. \frac{\partial z}{\partial w} \right|_t \right)^{-2} \frac{A_M (v_{f0} - v_{f1})}{[M]_0 (v_f)^2} D_M - R_M \\
&- [M] \left(\frac{M_{HDDA}}{\rho_{HDDA}} D_M \left(\left. \frac{\partial z}{\partial w} \right|_t \right)^{-2} \left. \frac{\partial^2 [M]}{\partial w^2} \right|_t \right. \\
&+ \frac{M_{HDDA}}{\rho_{HDDA}} \left(\left. \frac{\partial [M]}{\partial w} \right|_t \right)^2 \left(\left. \frac{\partial z}{\partial w} \right|_t \right)^{-2} \frac{A_M (v_{f0} - v_{f1})}{[M]_0 (v_f)^2} D_M \\
&\left. - M_{HDDA} \left(\frac{1}{\rho_{HDDA}} - \frac{1}{\rho_{pol}} \right) R_M \right)
\end{aligned} \tag{B.41}$$

The corresponding IC is $[M] = [M]_0 = 4.75 \left(\frac{mol}{L} \right)$ at $t = 0$. The BCs at $w = 0$ and $w = 1$ are both $\left. \frac{\partial [M]}{\partial w} \right|_t = 0$ because monomer cannot diffuse through either the top or bottom surface of the film. Notice that equation (B.41) contains the spatial derivative of z with respect to w at various locations on the right-hand side. Fortunately, z appears as a state variable in the model (see equation (3.6)) so this is not a problem.

B3.3 Material Balance PDE for R^{\bullet} Radical End Group

Consider a thin segment of scaled height Δw during a short period of time Δt as shown in figure B.1. No polymeric species diffuse in or out of this segment (See Assumption B.2.1 in Table B.2).

As a result, the material balance on polymeric radicals of type R^{\bullet} is:

$$\begin{aligned}
\text{accumulation} &= R^{\bullet} \text{ generated} - R^{\bullet} \text{ consumed} \\
\text{of } R^{\bullet} &\quad \text{by reactions} \quad \quad \quad \text{by reactions}
\end{aligned} \tag{B.42}$$

Moles of R^{\bullet} that accumulate in the segment are $\Delta([R^{\bullet}]A\Delta z)$. The net moles of R^{\bullet} that are generated is $A\Delta z\Delta t R_{R^{\bullet}}$ where:

$$\begin{aligned}
R_{R^{\bullet}} = & 2k_{in,IM} [I^{\bullet}][M] + 2k_{in,\tilde{I}M} [\tilde{I}^{\bullet}][M] + 2k_{in,IPM} [I_P^{\bullet}][M] + 2k_{p,B} [B^{\bullet}][M] \\
& + 2k_{p,C} [C^{\bullet}][M] + 2k_{p,T} [T^{\bullet}][M] + 2k_{p,O} [O^{\bullet}][M] - k_{b,R} [R^{\bullet}][V_P] \\
& - k_C [R^{\bullet}] - k_{bb,R} [R^{\bullet}] - k_{t,RR} [R^{\bullet}][R^{\bullet}] - k_{t,RB} [R^{\bullet}][B^{\bullet}] \\
& - k_{t,RC} [R^{\bullet}][C^{\bullet}] - k_{t,RT} [R^{\bullet}][T^{\bullet}] - k_{t,RO} [R^{\bullet}][O^{\bullet}] - k_{t,IR} [I^{\bullet}][R^{\bullet}] \quad (B.43) \\
& - k_{t,\tilde{I}R} [\tilde{I}^{\bullet}][R^{\bullet}] - k_{t,IPR} [I_P^{\bullet}][R^{\bullet}] - k_{O_2,R} [R^{\bullet}][O_2]
\end{aligned}$$

Substituting into equation (B.42) without substituting the messy expression for $R_{R^{\bullet}}$ gives:

$$\Delta([R^{\bullet}]A\Delta z)|_w = A\Delta z\Delta t R_{R^{\bullet}} \quad (B.44)$$

Dividing both sides of equation (B.44) by $A\Delta t\Delta w$ gives:

$$\left. \frac{\Delta \left([R^{\bullet}] \frac{\Delta z}{\Delta w} \right)}{\Delta t} \right|_w = \frac{\Delta z}{\Delta w} R_{R^{\bullet}} \quad (B.45)$$

As $\Delta z \rightarrow 0$ and $\Delta w \rightarrow 0$, equation (B.45) becomes:

$$\left. \frac{\Delta \left([R^{\bullet}] \frac{\partial z}{\partial w} \Big|_t \right)}{\Delta t} \right|_w = \frac{\partial z}{\partial w} \Big|_t R_{R^{\bullet}} \quad (B.46)$$

As $\Delta t \rightarrow 0$, equation (B.46) becomes:

$$\left. \frac{\partial \left([R^{\bullet}] \frac{\partial z}{\partial w} \Big|_t \right)}{\partial t} \right|_w = \frac{\partial z}{\partial w} \Big|_t R_{R^{\bullet}} \quad (B.47)$$

Applying product rule for $\left. \frac{\partial \left([R^{\bullet}] \frac{\partial z}{\partial w} \Big|_t \right)}{\partial t} \right|_w$ gives:

$$[R^{=\bullet}] \frac{\partial \left(\frac{\partial z}{\partial w} \Big|_t \right)}{\partial t} \Big|_w + \frac{\partial z}{\partial w} \Big|_t \frac{\partial [R^{=\bullet}]}{\partial t} \Big|_w = \frac{\partial z}{\partial w} \Big|_t R_{R^{=\bullet}} \quad (\text{B.48})$$

Rearranging to isolate $\frac{\partial [R^{=\bullet}]}{\partial t} \Big|_w$ on the left-hand side gives:

$$\frac{\partial [R^{=\bullet}]}{\partial t} \Big|_w = R_{R^{=\bullet}} - [R^{=\bullet}] \frac{\partial^2 z}{\partial w \partial t} \left(\frac{\partial z}{\partial w} \Big|_t \right)^{-1} \quad (\text{B.49})$$

Substituting for $\frac{\partial^2 z}{\partial w \partial t} \left(\frac{\partial z}{\partial w} \Big|_t \right)^{-1}$ from equation (B.37) gives:

$$\begin{aligned} \frac{\partial [R^{=\bullet}]}{\partial t} \Big|_w &= R_{R^{=\bullet}} \\ &- [R^{=\bullet}] \left(\frac{M_{HDDA}}{\rho_{HDDA}} D_M \left(\frac{\partial z}{\partial w} \Big|_t \right)^{-2} \frac{\partial^2 [M]}{\partial w^2} \Big|_t \right. \\ &\left. + \frac{M_{HDDA}}{\rho_{HDDA}} \frac{\partial [M]}{\partial w} \Big|_t \left(\frac{\partial z}{\partial w} \Big|_t \right)^{-2} \frac{\partial D_M}{\partial w} \Big|_t - M_{HDDA} \left(\frac{1}{\rho_{HDDA}} - \frac{1}{\rho_{pol}} \right) R_M \right) \end{aligned} \quad (\text{B.50})$$

Substituting for $\frac{\partial D_M}{\partial w} \Big|_t$ from equation (B.40) gives:

$$\begin{aligned}
\left. \frac{\partial [R^{\bullet}]}{\partial t} \right|_w &= R_{R^{\bullet}} \\
&- [R^{\bullet}] \left(\frac{M_{HDDA}}{\rho_{HDDA}} D_M \left(\frac{\partial z}{\partial w} \right)_t \right)^{-2} \frac{\partial^2 [M]}{\partial w^2} \Big|_t \\
&+ \frac{M_{HDDA}}{\rho_{HDDA}} \left(\frac{\partial z}{\partial w} \right)_t^{-2} \left(\frac{\partial [M]}{\partial w} \right)_t^2 \frac{A_M (v_{f0} - v_{f1})}{[M]_0 v_f^2} D_M \\
&- M_{HDDA} \left(\frac{1}{\rho_{HDDA}} - \frac{1}{\rho_{pol}} \right) R_M
\end{aligned} \tag{B.51}$$

The corresponding IC is $[R^{\bullet}] = 0$ at $t = 0$. No BCs are required because there is no diffusion term for R^{\bullet} on the right-hand side.

B3.4 Material Balance on Oxygen PDE

Consider the thin segment in figure B.1 with height Δz and scaled height Δw during a short period of time Δt . A material balance on oxygen dissolved in this segment is:

$$\begin{aligned}
\text{accumulation} &= \text{oxygen} - \text{oxygen} + \text{oxygen changes} \\
\text{of oxygen} &\quad \text{diffusing in} \quad \text{diffusing out} \quad \text{by reactions}
\end{aligned} \tag{B.52}$$

The moles of oxygen accumulating in the segment is $\Delta([O_2]A\Delta z)$. The moles of oxygen that diffuse in at the top of the segment is $-D_{O_2} \frac{\partial [O_2]}{\partial z} \Big|_{t,w} A\Delta t$. The moles of oxygen that diffuse out at the bottom of the segment is $-D_{O_2} \frac{\partial [O_2]}{\partial z} \Big|_{t,w+\Delta w} A\Delta t$. The moles of oxygen that get consumed due to reactions is $A\Delta z\Delta t R_{O_2}$. Substituting into equation (B.52) gives:

$$\Delta([O_2]A\Delta z) \Big|_w = -D_{O_2} \frac{\partial [O_2]}{\partial z} \Big|_{t,w} A\Delta t + D_{O_2} \frac{\partial [O_2]}{\partial z} \Big|_{t,w+\Delta w} A\Delta t + A\Delta z\Delta t R_{O_2} \tag{B.53}$$

where R_{O_2} is the net rate of oxygen consumption:

$$\begin{aligned}
R_{O_2} = & -k_{O_2,R}[O_2][R^{\bullet}] - k_{O_2,B}[O_2][B^{\bullet}] - k_{O_2,C}[O_2][C^{\bullet}] - k_{O_2,T}[O_2][T^{\bullet}] \\
& - k_{O_2,I}[O_2][I^{\bullet}] - k_{O_2,\tilde{I}}[O_2][\tilde{I}^{\bullet}] - k_{O_2,I_P}[O_2][I_P^{\bullet}] + \frac{1}{2}k_{t,OO}[O^{\bullet}]^2
\end{aligned} \tag{B.54}$$

Dividing both sides of equation (B.53) by $A\Delta t\Delta w$ and rearranging gives:

$$\frac{\Delta\left([O_2]\frac{\Delta z}{\Delta w}\right)}{\Delta t}\bigg|_w = \frac{D_{O_2}\frac{\partial[O_2]}{\partial z}\big|_{t,w+\Delta w} - D_{O_2}\frac{\partial[O_2]}{\partial z}\big|_{t,w}}{\Delta w} + \frac{\Delta z}{\Delta w}R_{O_2} \tag{B.55}$$

Using the chain rule for $\frac{\partial[O_2]}{\partial z}\big|_t$ gives:

$$\frac{\Delta\left([O_2]\frac{\Delta z}{\Delta w}\right)}{\Delta t}\bigg|_w = \frac{D_{O_2}\frac{\partial[O_2]}{\partial w}\big|_{t,w+\Delta w}\left(\frac{\partial z}{\partial w}\big|_{t,w+\Delta w}\right)^{-1} - D_{O_2}\frac{\partial[O_2]}{\partial w}\big|_{t,w}\left(\frac{\partial z}{\partial w}\big|_{t,w}\right)^{-1}}{\Delta w} + \frac{\Delta z}{\Delta w}R_{O_2} \tag{B.56}$$

As $\Delta z \rightarrow 0$ and $\Delta w \rightarrow 0$ equation (B.56) becomes:

$$\frac{\Delta\left([O_2]\frac{\partial z}{\partial w}\big|_t\right)}{\Delta t}\bigg|_w = \frac{\partial\left(D_{O_2}\frac{\partial[O_2]}{\partial w}\big|_t\left(\frac{\partial z}{\partial w}\big|_t\right)^{-1}\right)}{\partial w}\bigg|_t + \frac{\partial z}{\partial w}\bigg|_t R_{O_2} \tag{B.57}$$

As $\Delta t \rightarrow 0$, equation (B.57) becomes:

$$\frac{\partial\left([O_2]\frac{\partial z}{\partial w}\big|_t\right)}{\partial t}\bigg|_w = \frac{\partial\left(D_{O_2}\frac{\partial[O_2]}{\partial w}\big|_t\left(\frac{\partial z}{\partial w}\big|_t\right)^{-1}\right)}{\partial w}\bigg|_t + \frac{\partial z}{\partial w}\bigg|_t R_{O_2} \tag{B.58}$$

Applying product rule for $\frac{\partial([O_2]\frac{\partial z}{\partial w}|_t)}{\partial t}\Big|_w$, equation (B.58) becomes:

$$[O_2]\frac{\partial\left(\frac{\partial z}{\partial w}\Big|_t\right)}{\partial t}\Big|_w + \frac{\partial z}{\partial w}\Big|_t \frac{\partial[O_2]}{\partial t}\Big|_w = \frac{\partial\left(D_{O_2}\frac{\partial[O_2]}{\partial w}\Big|_t\left(\frac{\partial z}{\partial w}\Big|_t\right)^{-1}\right)}{\partial w}\Big|_t + \frac{\partial z}{\partial w}\Big|_t R_{O_2} \quad (\text{B.59})$$

Rearranging to isolate for $\frac{\partial z}{\partial w}\Big|_t \frac{\partial[O_2]}{\partial t}\Big|_w$ on the left-hand side gives:

$$\frac{\partial z}{\partial w}\Big|_t \frac{\partial[O_2]}{\partial t}\Big|_w = \frac{\partial\left(D_{O_2}\frac{\partial[O_2]}{\partial w}\Big|_t\left(\frac{\partial z}{\partial w}\Big|_t\right)^{-1}\right)}{\partial w}\Big|_t + \frac{\partial z}{\partial w}\Big|_t R_{O_2} - [O_2]\frac{\partial^2 z}{\partial w \partial t} \quad (\text{B.60})$$

Applying product rule for $\frac{\partial\left(D_{O_2}\frac{\partial[O_2]}{\partial w}\Big|_t\left(\frac{\partial z}{\partial w}\Big|_t\right)^{-1}\right)}{\partial w}\Big|_t$ gives:

$$\begin{aligned} \frac{\partial z}{\partial w}\Big|_t \frac{\partial[O_2]}{\partial t}\Big|_w &= D_{O_2}\frac{\partial[O_2]}{\partial w}\Big|_t \frac{\partial}{\partial w}\left(\left(\frac{\partial z}{\partial w}\Big|_t\right)^{-1}\right)\Big|_t + D_{O_2}\left(\frac{\partial z}{\partial w}\Big|_t\right)^{-1} \frac{\partial^2[O_2]}{\partial w^2}\Big|_t \\ &\quad + \frac{\partial[O_2]}{\partial w}\Big|_t \left(\frac{\partial z}{\partial w}\Big|_t\right)^{-1} \frac{\partial D_{O_2}}{\partial w}\Big|_t + \frac{\partial z}{\partial w}\Big|_t R_{O_2} - [O_2]\frac{\partial^2 z}{\partial w \partial t} \end{aligned} \quad (\text{B.61})$$

Rearranging to solve for $\frac{\partial[O_2]}{\partial t}\Big|_w$ gives:

$$\begin{aligned} \frac{\partial[O_2]}{\partial t}\Big|_w &= D_{O_2}\left(-\frac{\partial[O_2]}{\partial w}\Big|_t \left(\frac{\partial z}{\partial w}\Big|_t\right)^{-3} \frac{\partial^2 z}{\partial w^2}\Big|_t + \left(\frac{\partial z}{\partial w}\Big|_t\right)^{-2} \frac{\partial^2[O_2]}{\partial w^2}\Big|_t\right) \\ &\quad + \frac{\partial[O_2]}{\partial w}\Big|_t \left(\frac{\partial z}{\partial w}\Big|_t\right)^{-2} \frac{\partial D_{O_2}}{\partial w}\Big|_t + R_{O_2} - [O_2]\frac{\partial^2 z}{\partial w \partial t} \left(\frac{\partial z}{\partial w}\Big|_t\right)^{-1} \end{aligned} \quad (\text{B.62})$$

Substituting for $\left(\frac{\partial z}{\partial w}\right)_t^{-3} \frac{\partial^2 z}{\partial w^2}\bigg|_t$ from equation (B.28) and for $\frac{\partial^2 z}{\partial w \partial t} \left(\frac{\partial z}{\partial w}\right)_t^{-1}$ from equation (B.37)

gives:

$$\begin{aligned} \frac{\partial [O_2]}{\partial t}\bigg|_w &= D_{O_2} \left(\frac{\partial z}{\partial w}\right)_t^{-2} \frac{\partial^2 [O_2]}{\partial w^2}\bigg|_t + \frac{\partial [O_2]}{\partial w}\bigg|_t \left(\frac{\partial z}{\partial w}\right)_t^{-2} \frac{\partial D_{O_2}}{\partial w}\bigg|_t + R_{O_2} \\ &\quad - [O_2] \left(\frac{M_{HDDA}}{\rho_{HDDA}} D_M \left(\frac{\partial z}{\partial w}\right)_t^{-2} \frac{\partial^2 [M]}{\partial w^2}\bigg|_t \right. \\ &\quad \left. + \frac{M_{HDDA}}{\rho_{HDDA}} \frac{\partial [M]}{\partial w}\bigg|_t \left(\frac{\partial z}{\partial w}\right)_t^{-2} \frac{\partial D_M}{\partial w}\bigg|_t - M_{HDDA} \left(\frac{1}{\rho_{HDDA}} - \frac{1}{\rho_{pol}}\right) R_M \right) \end{aligned} \quad (B.63)$$

We know that D_{O_2} is a function of conversion and monomer (see equation (B.3.13) in Table B.3):

$$D_{O_2} = D_{O_2,HDDA} \exp \left[-A_{O_2} \left(\frac{1}{v_{f1} + \frac{[M]}{[M]_0} (v_{f0} - v_{f1})} - \frac{1}{v_{f0}} \right) \right] \quad (B.64)$$

Differentiating equation (B.64) with respect to w gives:

$$\frac{\partial D_{O_2}}{\partial w}\bigg|_t = D_{O_2} \frac{A_{O_2} (v_{f0} - v_{f1})}{[M]_0 v_f^2} \frac{\partial [M]}{\partial w}\bigg|_t \quad (B.65)$$

Substituting for $\frac{\partial D_{O_2}}{\partial w}\bigg|_t$ from equation (B.65) and for $\frac{\partial D_M}{\partial w}\bigg|_t$ from equation (B.40) in equation (B.63)

gives the final PDE describing the oxygen concentration as a function of time and transformed position coordinate w :

$$\begin{aligned}
\left. \frac{\partial [O_2]}{\partial t} \right|_w &= D_{O_2} \left(\left. \frac{\partial z}{\partial w} \right|_t \right)^{-2} \left. \frac{\partial^2 [O_2]}{\partial w^2} \right|_t + \left. \frac{\partial [O_2]}{\partial w} \right|_t \left(\left. \frac{\partial z}{\partial w} \right|_t \right)^{-2} D_{O_2} \frac{A_{O_2} (v_{f0} - v_{f1})}{[M]_0 v_f^2} \left. \frac{\partial [M]}{\partial w} \right|_t \\
&+ R_{O_2} \\
&- [O_2] \left(\frac{M_{HDDA}}{\rho_{HDDA}} D_M \left(\left. \frac{\partial z}{\partial w} \right|_t \right)^{-2} \left. \frac{\partial^2 [M]}{\partial w^2} \right|_t \right. \\
&+ \frac{M_{HDDA}}{\rho_{HDDA}} \left(\left. \frac{\partial [M]}{\partial w} \right|_t \right)^2 \left(\left. \frac{\partial z}{\partial w} \right|_t \right)^{-2} \frac{A_M (v_{f0} - v_{f1})}{[M]_0 (v_f)^2} D_M \\
&\left. - M_{HDDA} \left(\frac{1}{\rho_{HDDA}} - \frac{1}{\rho_{pol}} \right) R_M \right)
\end{aligned} \tag{B.66}$$

The corresponding IC is $[O_2] = [O_2]^* = 2.5 \times 10^{-3} \left(\frac{mol}{L} \right)$ which is the concentration in equilibrium with air [17]. The BC at the top surface of the film is $[O_2] = [O_2]^*$ because the top surface is always in equilibrium with the air (Assumption B.2.27). The BC at the bottom of the film is $\left. \frac{\partial [O_2]}{\partial w} \right|_{w=1} = 0$, because oxygen cannot diffuse through the bottom surface of the film.

See Table S5 for PDE balances for initiator species I and \tilde{I} , pendant vinyl groups V_p and all other radical species (i.e., B^* , C^* , T^* and O^*). These balance equations are analogous to equation (B.51) because diffusion of these species between segments is neglected (Assumption B.2.1).

B4 Detailed Algebraic Modifications Required to Solve the PDEs using MATLAB “pdepe”

Unfortunately, the PDEs in Table B.55 cannot be solved directly using MATLAB’s PDE solver “pdepe”. The “pdepe” solver requires that PDEs be written in a specific format. For example, “pdepe” requires that second derivatives be isolated on the right-hand side. The resulting rearranged PDEs are provided in Table B.5. Unfortunately, “pdepe” is unable to solve PDEs that

have second derivatives of variables other than the main state variable for each PDE (i.e., the variable that has a time derivative). Notice, for example, that the PDE for R^{\bullet} in equation (B.51) contains the second derivative $\left. \frac{\partial^2 [M]}{\partial w^2} \right|_t$ on the right-hand side. To overcome this problem, we introduce a new state variable G defined as:

$$G = \left. \frac{\partial [M]}{\partial w} \right|_t \quad (\text{B.67})$$

Differentiating equation (B.67) with respect to w yields:

$$\left. \frac{\partial G}{\partial w} \right|_t = \left. \frac{\partial^2 [M]}{\partial w^2} \right|_t \quad (\text{B.68})$$

We use equation (B.68) substitute for all undesirable $\left. \frac{\partial^2 [M]}{\partial w^2} \right|_t$ terms in the PDEs in Table B.4 to obtain the PDEs in Table B.5. A consequence of using this approach is that equation (B.67) appears as an additional differential equation in the model.

Table B.5: List of restructured PDEs for MATLAB's PDE solver "pdepe".

<p>B.5.1 - Initiator:</p> $\left. \frac{\partial [I]}{\partial t} \right _w = R_I - [I] \left(\frac{M_{HDDA}}{\rho_{HDDA}} D_M \left(\left. \frac{\partial z}{\partial w} \right _t \right)^{-2} \left. \frac{\partial G}{\partial w} \right _t + \frac{M_{HDDA}}{\rho_{HDDA}} \left(\left. \frac{\partial z}{\partial w} \right _t \right)^{-2} \left(\left. \frac{\partial [M]}{\partial w} \right _t \right)^2 \frac{A_M (v_{f0} - v_{f1})}{[M]_0 v_f^2} D_M - M_{HDDA} \left(\frac{1}{\rho_{HDDA}} - \frac{1}{\rho_{pol}} \right) R_M \right)$ <p>where:</p> $R_I = -2k_d [I]$
<p>B.5.2 – Initiator fragment:</p>

$$\frac{\partial[\tilde{I}]}{\partial t}\Big|_w = R_{\tilde{I}} - [\tilde{I}] \left(\frac{M_{HDDA}}{\rho_{HDDA}} D_M \left(\frac{\partial z}{\partial w} \Big|_t \right)^{-2} \frac{\partial G}{\partial w} \Big|_t + \frac{M_{HDDA}}{\rho_{HDDA}} \left(\frac{\partial z}{\partial w} \Big|_t \right)^{-2} \left(\frac{\partial[M]}{\partial w} \Big|_t \right)^2 \frac{A_M(v_{f0}-v_{f1})}{[M]_0 v_f^2} D_M - M_{HDDA} \left(\frac{1}{\rho_{HDDA}} - \frac{1}{\rho_{pol}} \right) R_M \right)$$

where:

$$R_{\tilde{I}} = -k_{\tilde{d}}[\tilde{I}] + 2k_{in,\tilde{I}M}[\tilde{I}^{\bullet}][M] + k_{in,\tilde{I}V_p}[\tilde{I}^{\bullet}][V_p] + k_{t,\tilde{I}R}[\tilde{I}^{\bullet}][R^{\bullet}] + k_{t,\tilde{I}B}[\tilde{I}^{\bullet}][B^{\bullet}] + k_{t,\tilde{I}C}[\tilde{I}^{\bullet}][C^{\bullet}] + k_{t,\tilde{I}T}[\tilde{I}^{\bullet}][T^{\bullet}] + k_{t,\tilde{I}O}[\tilde{I}^{\bullet}][O^{\bullet}] + k_{t,\tilde{I}I}[\tilde{I}^{\bullet}][I^{\bullet}] + k_{t,\tilde{I}I}[\tilde{I}^{\bullet}][\tilde{I}^{\bullet}] + k_{t,\tilde{I}I_p}[\tilde{I}^{\bullet}][I_p^{\bullet}] + k_{O_2,\tilde{I}}[\tilde{I}^{\bullet}][O_2]$$

B.5.3 – Monomer:

$$\frac{1}{D_M} \left(\frac{\partial z}{\partial w} \Big|_t \right)^2 \frac{\partial[M]}{\partial t} \Big|_w = \frac{\partial^2[M]}{\partial w^2} \Big|_t + \left(\frac{\partial[M]}{\partial w} \Big|_t \right)^2 \frac{A_M(v_{f0}-v_{f1})}{[M]_0 (v_f)^2} - \frac{1}{D_M} \left(\frac{\partial z}{\partial w} \Big|_t \right)^2 R_M - [M] \left(\frac{M_{HDDA}}{\rho_{HDDA}} \frac{\partial G}{\partial w} \Big|_t + \frac{M_{HDDA}}{\rho_{HDDA}} \left(\frac{\partial z}{\partial w} \Big|_t \right)^2 \frac{A_M(v_{f0}-v_{f1})}{[M]_0 (v_f)^2} - M_{HDDA} \left(\frac{1}{\rho_{HDDA}} - \frac{1}{\rho_{pol}} \right) R_M \frac{1}{D_M} \left(\frac{\partial z}{\partial w} \Big|_t \right)^2 \right)$$

Where:

$$R_M = +2k_{in,IM} [I^{\bullet}][M] + 2k_{in,\tilde{I}M} [\tilde{I}^{\bullet}][M] + 2k_{in,I_pM} [I_p^{\bullet}][M] + 2k_{p,R} [R^{\bullet}][M] + 2k_{p,B} [B^{\bullet}][M] + 2k_{p,C} [C^{\bullet}][M] + 2k_{p,T} [T^{\bullet}][M] + 2k_{p,O} [O^{\bullet}][M]$$

B.5.4 – Pendant vinyl group:

$$\frac{\partial[V_p]}{\partial t}\Big|_w = R_{V_p} - [V_p] \left(\frac{M_{HDDA}}{\rho_{HDDA}} D_M \left(\frac{\partial z}{\partial w} \Big|_t \right)^{-2} \frac{\partial G}{\partial w} \Big|_t + \frac{M_{HDDA}}{\rho_{HDDA}} \left(\frac{\partial z}{\partial w} \Big|_t \right)^{-2} \left(\frac{\partial[M]}{\partial w} \Big|_t \right)^2 \frac{A_M(v_{f0}-v_{f1})}{[M]_0 v_f^2} D_M - M_{HDDA} \left(\frac{1}{\rho_{HDDA}} - \frac{1}{\rho_{pol}} \right) R_M \right)$$

where:

$$\begin{aligned}
R_{V_P} = & + 2k_{p,R} [R^{\bullet\bullet}][M] + k_{bb,R} [R^{\bullet\bullet}] + k_{t,RR} [R^{\bullet\bullet}][R^{\bullet\bullet}] + k_{t,RB} [R^{\bullet\bullet}][B^{\bullet}] + k_{t,RC} [R^{\bullet\bullet}][C^{\bullet}] \\
& + 2k_{t,RT} [R^{\bullet\bullet}][T^{\bullet}] + k_{t,RO} [R^{\bullet\bullet}][O^{\bullet}] + k_{t,IR} [I^{\bullet}][R^{\bullet\bullet}] + k_{t,\tilde{I}R} [\tilde{I}^{\bullet}][R^{\bullet\bullet}] \\
& + k_{t,I_P R} [I_P^{\bullet}][R^{\bullet\bullet}] + k_{t,BT} [B^{\bullet}][T^{\bullet}] + k_{t,CT} [C^{\bullet}][T^{\bullet}] + k_{t,TT} [T^{\bullet}][T^{\bullet}] \\
& + k_{t,TO} [O^{\bullet}][T^{\bullet}] + k_{t,IT} [I^{\bullet}][T^{\bullet}] + k_{t,\tilde{I}T} [\tilde{I}^{\bullet}][T^{\bullet}] + k_{t,I_P T} [I_P^{\bullet}][T^{\bullet}] \\
& - k_{in,IV_P} [I^{\bullet}][V_P] - k_{in,\tilde{I}V_P} [\tilde{I}^{\bullet}][V_P] - k_{in,I_P V_P} [I_P^{\bullet}][V_P] - k_{b,B} [B^{\bullet}][V_P] \\
& - k_{b,C} [C^{\bullet}][V_P] - k_{b,T} [T^{\bullet}][V_P] - k_{b,O} [O^{\bullet}][V_P] + k_{O_2,R} [R^{\bullet\bullet}][O_2]
\end{aligned}$$

B.5.5 – Oxygen:

$$\begin{aligned}
\frac{1}{D_{O_2}} \left(\frac{\partial z}{\partial w} \Big|_t \right)^2 \frac{\partial [O_2]}{\partial t} \Big|_w = & \frac{\partial^2 [O_2]}{\partial w^2} \Big|_t + \frac{\partial [O_2]}{\partial w} \Big|_t \frac{A_{O_2}(v_{f0}-v_{f1})}{[M]_0 v_f^2} \frac{\partial [M]}{\partial w} \Big|_t + \frac{1}{D_{O_2}} \left(\frac{\partial z}{\partial w} \Big|_t \right)^2 R_{O_2} - \\
[O_2] \left(\frac{M_{HDDA}}{\rho_{HDDA}} \frac{D_M}{D_{O_2}} \frac{\partial G}{\partial w} \Big|_t + \frac{M_{HDDA}}{\rho_{HDDA}} \frac{D_M}{D_{O_2}} \left(\frac{\partial [M]}{\partial w} \Big|_t \right)^2 \frac{A_{O_2}(v_{f0}-v_{f1})}{[M]_0 v_f^2} - M_{HDDA} \left(\frac{1}{\rho_{HDDA}} - \right. \right. \\
\left. \left. \frac{1}{\rho_{pol}} \right) R_M \frac{1}{D_{O_2}} \left(\frac{\partial z}{\partial w} \Big|_t \right)^2 \right)
\end{aligned}$$

where:

$$\begin{aligned}
R_{O_2} = & -k_{O_2,R} [O_2][R^{\bullet\bullet}] - k_{O_2,B} [O_2][B^{\bullet}] - k_{O_2,C} [O_2][C^{\bullet}] - k_{O_2,T} [O_2][T^{\bullet}] - k_{O_2,I} [O_2][I^{\bullet}] \\
& - k_{O_2,\tilde{I}} [O_2][\tilde{I}^{\bullet}] - k_{O_2,I_P} [O_2][I_P^{\bullet}] + \frac{1}{2} k_{t,O_2} [O^{\bullet}][O^{\bullet}]
\end{aligned}$$

B.5.6 – Regular radical:

$$\begin{aligned}
\frac{\partial [R^{\bullet\bullet}]}{\partial t} \Big|_w = & R_{R^{\bullet\bullet}} - [R^{\bullet\bullet}] \left(\frac{M_{HDDA}}{\rho_{HDDA}} D_M \left(\frac{\partial z}{\partial w} \Big|_t \right)^{-2} \frac{\partial G}{\partial w} \Big|_t + \right. \\
\left. \frac{M_{HDDA}}{\rho_{HDDA}} \left(\frac{\partial z}{\partial w} \Big|_t \right)^{-2} \left(\frac{\partial [M]}{\partial w} \Big|_t \right)^2 \frac{A_M(v_{f0}-v_{f1})}{[M]_0 v_f^2} D_M - M_{HDDA} \left(\frac{1}{\rho_{HDDA}} - \frac{1}{\rho_{pol}} \right) R_M \right)
\end{aligned}$$

where:

$$\begin{aligned}
 R_{R^{\bullet}} = & + 2k_{in,IM} [I^{\bullet}][M] + 2k_{in,\tilde{I}M} [\tilde{I}^{\bullet}][M] + 2k_{in,I_P M} [I_P^{\bullet}][M] + 2k_{p,B} [B^{\bullet}][M] \\
 & + 2k_{p,C} [C^{\bullet}][M] + 2k_{p,T} [T^{\bullet}][M] + 2k_{p,O} [O^{\bullet}][M] - k_{b,R} [R^{\bullet}][V_P] \\
 & - k_C [R^{\bullet}] - k_{bb,R} [R^{\bullet}] - k_{t,RR} [R^{\bullet}][R^{\bullet}] - k_{t,RB} [R^{\bullet}][B^{\bullet}] \\
 & - k_{t,RC} [R^{\bullet}][C^{\bullet}] - k_{t,RT} [R^{\bullet}][T^{\bullet}] - k_{t,RO} [R^{\bullet}][O^{\bullet}] - k_{t,IR} [I^{\bullet}][R^{\bullet}] \\
 & - k_{t,\tilde{I}R} [\tilde{I}^{\bullet}][R^{\bullet}] - k_{t,I_P R} [I_P^{\bullet}][R^{\bullet}] - k_{O_2,R} [R^{\bullet}][O_2]
 \end{aligned}$$

B.5.7 – Crosslinking radical:

$$\begin{aligned}
 \left. \frac{\partial [B^{\bullet}]}{\partial t} \right|_w = & R_{B^{\bullet}} - [B^{\bullet}] \left(\frac{M_{HDDA}}{\rho_{HDDA}} D_M \left(\frac{\partial z}{\partial w} \right)_t \right)^{-2} \frac{\partial G}{\partial w} \Big|_t + \frac{M_{HDDA}}{\rho_{HDDA}} \left(\frac{\partial z}{\partial w} \right)_t^{-2} \left(\frac{\partial [M]}{\partial w} \right)_t^2 \frac{A_M (v_{f0} - v_{f1})}{[M]_0 v_{f2}} D_M - \\
 & M_{HDDA} \left(\frac{1}{\rho_{HDDA}} - \frac{1}{\rho_{pol}} \right) R_M
 \end{aligned}$$

where:

$$\begin{aligned}
 R_{B^{\bullet}} = & + k_{in,IV_P} [I^{\bullet}][V_P] + k_{in,\tilde{I}V_P} [\tilde{I}^{\bullet}][V_P] + k_{in,I_P V_P} [I_P^{\bullet}][V_P] + k_{b,R} [R^{\bullet}][V_P] \\
 & + k_{b,C} [C^{\bullet}][V_P] + k_{b,T} [T^{\bullet}][V_P] + k_{b,O} [O^{\bullet}][V_P] \\
 & - 2k_{p,B} [B^{\bullet}][M] - k_{t,RB} [R^{\bullet}][B^{\bullet}] - k_{t,BB} [B^{\bullet}][B^{\bullet}] - k_{t,BC} [B^{\bullet}][C^{\bullet}] \\
 & - k_{t,BT} [B^{\bullet}][T^{\bullet}] - k_{t,BO} [B^{\bullet}][O^{\bullet}] - k_{t,IB} [I^{\bullet}][B^{\bullet}] - k_{t,\tilde{I}B} [\tilde{I}^{\bullet}][B^{\bullet}] \\
 & - k_{t,I_P B} [I_P^{\bullet}][B^{\bullet}] - k_{O_2,B} [B^{\bullet}][O_2]
 \end{aligned}$$

B.5.8 – Cyclic radical:

$$\left. \frac{\partial [C^\bullet]}{\partial t} \right|_w = R_{C^\bullet} - [C^\bullet] \left(\frac{M_{HDDA}}{\rho_{HDDA}} D_M \left(\frac{\partial z}{\partial w} \right)_t \right)^{-2} \frac{\partial G}{\partial w} \Big|_t + \frac{M_{HDDA}}{\rho_{HDDA}} \left(\frac{\partial z}{\partial w} \right)_t^{-2} \left(\frac{\partial [M]}{\partial w} \Big|_t \right)^2 \frac{A_M(v_{f0}-v_{f1})}{[M]_0 v_f^2} D_M -$$

$$M_{HDDA} \left(\frac{1}{\rho_{HDDA}} - \frac{1}{\rho_{pol}} \right) R_M$$

where:

$$R_{C^\bullet} = + k_C [R^{\bullet}] - 2 k_{p,C} [C^\bullet][M] - k_{b,C} [C^\bullet][V_P] - k_{bb,R} [C^\bullet] - k_{t,RC} [R^{\bullet}][C^\bullet]$$

$$- k_{t,BC} [B^\bullet][C^\bullet] - k_{t,CC} [C^\bullet][C^\bullet] - k_{t,CT} [C^\bullet][T^\bullet] - k_{t,CO} [C^\bullet][O^\bullet]$$

$$- k_{t,IC} [I^\bullet][C^\bullet] - k_{t,\tilde{I}C} [\tilde{I}^\bullet][C^\bullet] - k_{t,IP} [I_P^\bullet][C^\bullet] - k_{O_2,C} [C^\bullet][O_2]$$

B.5.9 – Tertiary radical:

$$\left. \frac{\partial [T^\bullet]}{\partial t} \right|_w = R_{T^\bullet} - [T^\bullet] \left(\frac{M_{HDDA}}{\rho_{HDDA}} D_M \left(\frac{\partial z}{\partial w} \right)_t \right)^{-2} \frac{\partial G}{\partial w} \Big|_t + \frac{M_{HDDA}}{\rho_{HDDA}} \left(\frac{\partial z}{\partial w} \right)_t^{-2} \left(\frac{\partial [M]}{\partial w} \Big|_t \right)^2 \frac{A_M(v_{f0}-v_{f1})}{[M]_0 v_f^2} D_M -$$

$$M_{HDDA} \left(\frac{1}{\rho_{HDDA}} - \frac{1}{\rho_{pol}} \right) R_M$$

where:

$$R_{T^\bullet} = + k_{bb,R} [R^{\bullet}] + k_{bb,R} [C^\bullet] + k_{bb,O} [O^\bullet] - 2 k_{p,T} [T^\bullet][M] - k_{b,T} [T^\bullet][V_P]$$

$$- k_{t,RT} [R^{\bullet}][T^\bullet] - k_{t,BT} [B^\bullet][T^\bullet] - k_{t,CT} [C^\bullet][T^\bullet] - k_{t,TT} [T^\bullet][T^\bullet]$$

$$- k_{t,TO} [T^\bullet][O^\bullet] - k_{t,IT} [I^\bullet][T^\bullet] - k_{t,\tilde{I}T} [\tilde{I}^\bullet][T^\bullet] - k_{t,IP} [I_P^\bullet][T^\bullet]$$

$$- k_{O_2,T} [T^\bullet][O_2]$$

B.5.10 – Peroxidic radical:

$$\left. \frac{\partial [O^*]}{\partial t} \right|_w = R_{O^*} - [O^*] \left(\frac{M_{HDDA}}{\rho_{HDDA}} D_M \left(\frac{\partial z}{\partial w} \right)_t^{-2} \frac{\partial G}{\partial w} \right)_t + \frac{M_{HDDA}}{\rho_{HDDA}} \left(\frac{\partial z}{\partial w} \right)_t^{-2} \left(\frac{\partial [M]}{\partial w} \right)_t^2 \frac{A_M (v_{f0} - v_{f1})}{[M]_0 v_f^2} D_M - M_{HDDA} \left(\frac{1}{\rho_{HDDA}} - \frac{1}{\rho_{pol}} \right) R_M$$

where:

$$\begin{aligned} R_{O^*} = & + k_{O_2, I} [I^*] [O_2] + k_{O_2, \tilde{I}} [\tilde{I}^*] [O_2] + k_{O_2, I_P} [I_P^*] [O_2] + k_{O_2, R} [R^{*\cdot}] [O_2] + k_{O_2, B} [B^*] [O_2] \\ & + k_{O_2, C} [C^*] [O_2] + k_{O_2, T} [T^*] [O_2] - 2 k_{p, O} [O^*] [M] - k_{b, O} [O^*] [V_p] \\ & - k_{bb, O} [O^*] - k_{t, IO} [I^*] [O^*] - k_{t, \tilde{I}O} [\tilde{I}^*] [O^*] - k_{t, I_P CO} [I_P^*] [O^*] \\ & - k_{t, RO} [R^{*\cdot}] [O^*] - k_{t, BO} [B^*] [O^*] - k_{t, CO} [C^*] [O^*] - k_{t, TO} [T^*] [O^*] \\ & - k_{t, OO} [O^*] [O^*] \end{aligned}$$

B.5.11 – Relationship between z and w:

$$\left. \frac{\partial z}{\partial t} \right|_w = D_M \left. \frac{\partial [M]}{\partial w} \right|_t \left(\frac{\partial z}{\partial w} \right)_t^{-1} \frac{M_{HDDA}}{\rho_{HDDA}} - M_{HDDA} \left(\frac{1}{\rho_{HDDA}} - \frac{1}{\rho_{pol}} \right) Q$$

where:

$$Q = \int_{w=0}^w R_M dz = \int_{z=0}^{z(w=0.4)} R_M dz$$

where:

$$\begin{aligned} R_M = & + 2k_{in, IM} [I^*] [M] + 2k_{in, \tilde{I}M} [\tilde{I}^*] [M] + 2k_{in, I_P M} [I_P^*] [M] + 2k_{p, R} [R^{*\cdot}] [M] \\ & + 2k_{p, B} [B^*] [M] + 2k_{p, C} [C^*] [M] + 2k_{p, T} [T^*] [M] + 2k_{p, O} [O^*] [M] \end{aligned}$$

B.5.12 – Monomer gradient:

$$0 = \frac{\partial[M]}{\partial w} \Big|_t - G$$